Design, characterization, and implementation of lower-limb exoskeletons for performance augmentation during walking and running

Submitted in partial fulfillment of the requirements for
the degree of
Doctor of Philosophy
in
Mechanical Engineering

Kirby A. Witte
B.S., Mechanical Engineering, University of New Mexico
M.S., Mechanical Engineering, Carnegie Mellon University

Carnegie Mellon University
Pittsburgh, PA
December, 2018

Acknowledgements

First, thank you to my adviser, Steve Collins. I had not considered pursuing a PhD before participating in your course and likely would never have discovered my love of research without you. Thank you for providing world-class tools to complete my research.

Thank you to my committee, Greg Sawicki, Aaron Johnson and Jessica Hodgins for our discussions of research and academia both serious and fanciful over the past several years.

Thank you to everyone in the Experimental Biomechatronics Lab. Particularly Rachel, JJ, Josh and Myunghee for welcoming me and showing me the ropes (sometimes literally). Thank you Pieter for all of your hard work on the running project. Thank you, Stuart, for going through this together from beginning to end and checking in on me in the lab under the stairs. Thanks, Katie, for all the support through experiments and quick responses to questions. Thanks, Kyle, for being my copilot early on. Thanks, Andreas and Kevin, for being my guinea pigs and sticking with me through piloting.

Thank you, John, Jim, and Ed, for making the shop my home and helping me out of my most impossible predicaments.

Thank you, Hartmut, Nitish and Eni, for sharing your lab spaces and treadmills. It would have been impossible to do my research without your generosity.

Thanks to Chris Atkeson for providing additional mentorship and support as part of your lab in the last few months of my PhD.

Thanks to Mikey, Lucy, Sean, Natalie, Stephanie, and all my students for the odds and ends you contributed. I hope you enjoyed research as much I enjoyed sharing it with you.

Thank you, Padraig, for being my ground truth through it all. For being my first test subject, my best friend and my husband. Thank you for loving our kids enough for both of us while I completed this thesis.

Thank you, Mom and Dad, for encouraging me to keep doing tough things and for providing much needed support in its many forms.

Thanks to Nike and to the NSF for funding my work under Grant No. DGE-1252522.

Abstract

Lower-limb exoskeletons have potential to increase endurance, reduce incidence of injury, aid rehabilitation and prolong independence. Progress in exoskeleton research is slowed by the complex nature of exoskeleton design and by the complexity of the humans they are supposed to assist. Developing highly versatile tools to address these issues will accelerate research and bring exoskeletons closer to becoming life changing products.

This thesis details an approach to exoskeleton development that leverages both universal exoskeleton emulators and human-in-the-loop optimization to enable accurate comparisons of qualitatively different exoskeleton assistance strategies. Instead of building new or adjusting old hardware to test a given exoskeleton design, we developed highly capable, lightweight, tethered exoskeletons that were used to emulate the behavior of a wide variety of possible exoskeleton designs. The development of these exoskeleton emulators revealed guiding principles of lower-limb exoskeleton design that will aid in the creation of future exoskeletons. Experimental comparisons of exoskeleton control architectures for walking and running were performed to determine the most promising strategies to pursue. Passive, spring-like assistance was compared to powered assistance for running. Three qualitatively different assistance strategies were explored for assisting walking. Included among the walking assistance strategies was a first look at an EMG-based muscle-tendon controller. This controller applied a muscle-tendon model to measured EMG activity to produce exoskeleton assistance in a manner similar to human muscle. In both the walking and running experiments, human-in-the-loop optimization was performed to provide customization of exoskeleton settings to fit the needs of individual subjects. This enabled a more accurate comparison of candidate assistance strategies. We expect our findings to influence the design of portable, untethered ankle exoskeletons and to proliferate the use of emulator systems in combination with human-in-the-loop optimization to perform side-by-side comparisons of assistance strategies.

Contents

List of Figures

List of Tables

Chapter 1

Introduction

1.1 Motivation

Lower-limb exoskeletons promise to assist people with a diverse range of needs by acting in parallel with a user to augment or replace joint function. Lower-limb exoskeletons show promise for generally improving performance for work or for pleasure and aiding in rehabilitation. Exoskeletons have been used to reduce the energetic cost of walking [1, 2, 3, 4] and running [5, 6]. Reducing the energetic cost of walking could improve quality of life and prolong the independence of populations with a high cost of transport such as stroke patients or the elderly. The importance of these outcomes is highlighted by changing demographics. The percentage of the U.S. population over 65 years of age is projected to increase to levels above 20% in 2050, up significantly from 9.8% in the 1970s and 15% today [7].

Reducing the energetic cost of walking and running can not only improve endurance, but also reduce incidence of injury for soldiers and others who walk or run long distances for work [8]. Exoskeletons may also improve participation in physical activity by reducing the intensity of sports for entry level athletes, potentially leading to better overall health [9, 10, 11, 12]. In the extreme long term, exoskeletons may even be used to enable bionic sports in which both engineers and athletes take the center stage.

Outside of enhancing general performance, exoskeletons can be used as tools for rehabilitation. They can provide consistent, high intensity rehabilitation by offloading the physical work typically applied by physical therapists [13, 14]. This may result in cheaper, more frequent therapy in sessions of longer duration.

Though exoskeletons are not commonplace today, they are a rapidly growing area of research with some projections placing the exoskeleton market value between 2.5 [15] and 5 billion dollars in annual revenue by 2025 [16]. Many new companies have begun selling exoskeletons for medical, industrial, and military applications and recognizable brands are becoming involved in development such as Samsung [3], Honda [17], Hyundai [18], and Panasonic [19].

This kind of industry engagement makes it seem like exoskeletons are well developed, but much is left to be understood and progress is slow. Exoskeletons have been in development for over a hundred years and the first demonstrable benefits were achieved in 2013 [1]. Since then moderate progress has been made in improving the magnitude of these benefits, but large questions still remain that, until answered, reduce the usefulness of exoskeletons in generalized circumstances. In particular, effectively controlling exoskeletons to interact usefully with people is a surprisingly difficult task. Not only is it important to develop controllers that result in useful behaviors from exoskeletons, but it is also important to facilitate adaptation in the user to enable beneficial human-robot interactions. Very little work has been done in these areas and there is much to learn before exoskeletons can truly reach their potential.

1.1.1 Prior work in lower-limb exoskeleton assistance

Exoskeleton control

Time-based strategies dominate the field of exoskeletons [20, 21, 4, 3]. The first metabolic reductions achieved with exoskeleton assistance were produced using a time-based controller on an ankle exoskeleton [1], and this same method remains the most effective overall strat-

egy to date [2]. In general, time-based control involves first detecting some important indicator of gait phase, such as heel strike [1] or maximum hip flexion [22], and applying assistance accordingly as a function of time as a percentage of the anticipated duration of the step. This approach may depend on a single event for timing, or may apply assistance as a piece-wise function according to several gait events. It is very simple, but requires clever implementation to operate well under non-steady state conditions where estimation of step duration is not accurately achieved by a slow moving average.

The long term efficacy of time-based control is in question as accomplishing diverse tasks requires prediction of user intent through classifiers. Incorrect classification of intent could have disastrous results. For example, mistaking stair descent for stair ascent could be life threatening. Progress has been made in this area [23, 24, 25], but more work is needed to generalize time-based control.

In contrast to time-based control, electromyographic (EMG) control is thought to be beneficial as it should be highly responsive to inter-step variability and user intent. Surface electrodes adhered to skin are used to measure electrical activity in underlying muscles. This electrical activity is indicative of muscle recruitment and should encode user intent. Using EMG signals to drive exoskeleton assistance should allow seamless transitions between different activities with little need for classifiers. Proportional EMG control [26] and variants involving adaptive gains [27] have been shown to significantly reduce metabolic cost during walking. Strategies that leverage measurement of antagonistic muscle activity to inhibit exoskeleton assistance have resulted in more natural kinematics than methods that utilize activity from a single muscle [28]. Time based assistance currently outperforms EMG control, but this is possibly a result of the fact that time-based control has existed longer and more groups have been focused on it.

Neuromuscular control implemented on robotic prostheses has resulted in metabolic reductions for amputees [29], but it has not been evaluated for use on exoskeletons by healthy individuals. Neuromuscular control involves running a simulation of muscle-tendon dy-

namics and a positive-force feedback reflex scheme to calculate joint torque to be applied by the prosthesis. This method is currently under investigation for use in exoskeletons with healthy users by Georgia Tech's PoWeR lab, but metabolic data is currently unavailable.

Passive strategies that utilize springs and clutches also show potential and are appealing as they can operate without the need for motors or power. Some success has been demonstrated with passive ankle exoskeletons for walking [30], and a passive hip exoskeleton has been successful in assisting running [6].

1.1.2 Challenges

Two major challenges inhibit progress in lower-limb exoskeleton development: the complexity of exoskeleton design and the complexity of humans. The physical structures of exoskeletons innately apply metabolic penalties to their users by adding mass and volume to legs [31, 32, 33]. Exoskeletons must first be capable of offsetting these innate penalties before any assistance can be demonstrated. As a result, exoskeletons must be lightweight and low profile to be effective. Fitting power supplies, motors, transmissions, and control hardware in a package that fits on the leg without impeding motion often requires expensive custom parts and results in structures that are difficult to reconfigure. Such designs often require complete redesigns when an adjustment needs to be made which is expensive and time consuming.

The complexity of biological joints can complicate the design of exoskeletons. Human joints are often not well approximated by simple pivot joints and some degrees of freedom are mechanically constrained to one another. For example, the human knee joint exhibits a moving center of rotation and has a "screw-home" mechanism which results in rotation of the femur with respect to the tibia in the later stages of extension [34]. Exoskeletons that cross human joints must accommodate for this complexity in some way as misalignment between the biological joint and the mechanical joint can result in greater internal joint forces.

The variability of humans presents a significant problem in the development of exoskeletons. Not only do people exhibit different sizes and morphologies that make fitting exoskeletons difficult, but they also often demonstrate different responses to the exact same exoskeleton assistance. In addition, individuals can exhibit significant variations in behavior over the course of time due to adaption, learning and fatigue. It is difficult to develop assistance strategies that are effective across people and can adjust to the changing needs of the user.

1.2 Approach

1.2.1 Simplifying design: universal exoskeleton emulators

Universal exoskeleton emulators can vastly simplify design of prototype hardware without sacrificing performance [35]. Power supplies, motors, transmissions, and control hardware make up the heaviest, and most complex portions of exoskeletons. The problem of exoskeleton design can be largely simplified by decoupling these components from the worn portion of an exoskeleton. Exoskeleton emulators consist of off-board control hardware and motors placed on a separate structure behind a treadmill. The worn portion of the emulator system is called an exoskeleton end-effector. Mechanical power is transmitted from the off-board motors to the end-effector via a flexible Bowden cable. This enables the worn portion of exoskeletons to be limited to the frame, sensors, physical user interfaces, and terminations for the Bowden cable housing and inner cable. The resulting worn exoskeleton is extremely lightweight compared to fully portable systems, and the design time required is drastically reduced.

The motors used in such a configuration can be large and powerful, enabling greater performance than could otherwise be achieved with such a lightweight exoskeleton. Higher peak torques and torque bandwidths can be achieved using exoskeleton emulators than are possible in portable systems. High available torque, mechanical power, and torque band-

width enable exoskeleton emulators to mimic (or emulate) the behavior of a variety of candidate designs. In this way, a single system can be used to quickly evaluate a variety of candidate exoskeleton behaviors without building new hardware. This general concept is not novel [36, 37], and the off-board components utilized in experiments presented in this thesis were originally developed for the evaluation of prostheses [35]. The exoskeleton end-effectors presented in this work present new approaches to exoskeleton design.

1.2.2 Addressing human complexity

Human-in-the-loop optimization (HILO) can be used to systematically customize exoskeleton assistance to fit the needs of individuals [2]. Exoskeleton users benefit from the customization of device settings, but adjusting settings by hand tuning is a lengthy process that is not guaranteed to result in optimal performance. Performing a parameter sweep of possible settings does not always yield useful observations as the user learns and adapts to exoskeleton assistance over time. This means that settings tested at the beginning of the sweep may appear to have poorer performance than they would if tested towards the end. For this reason, HILO was used to aid in the customization of exoskeleton settings for individual subjects in each of the experiments presented here. The optimization strategy applied is called a covariance matrix adaptation evolutionary strategy (CMA-ES) [38]. HILO utilizing CMA-ES was first used in the customization of ankle exoskeleton assistance resulting in the greatest metabolic reductions demonstrated during walking to date [2]. It is thought that HILO utilizing CMA-ES as the optimization strategy is robust to noisy measurements of metabolic cost and the changing behavior of exoskeleton users.

1.3 Scope

1.3.1 Developing tools for enabling performance augmentation

The goal of this thesis is to enable performance augmentation during walking and running as measured by metabolic cost. Exoskeleton end-effectors were designed to be lightweight and capable of replacing the joint torques normally produced by muscles during walking. This enabled a wide range of possible assistance strategies to be emulated and tested on a single device. The exoskeletons developed included bilateral ankle exoskeletons and two variations of knee exoskeletons.

The performance of the ankle exoskeletons exceeded the performance of all similar systems. The ankle exoskeletons are lightweight, 0.835 kg each, capable of applying 120 Nm of torque during walking, and have phase limited force bandwidth of at least 17.7 Hz. This high performance is largely enabled by leveraging powerful off-board motors.

I developed a five-degree-of-freedom knee exoskeleton for assisting walking. It assisted both extension and flexion of the knee while also providing four unassisted degrees of freedom. A pure-moment joint mechanism allowed application of high knee torques without significantly increasing internal joint forces within the human knee. The four additional degrees of freedom allowed the device to accommodate users of a surprising range of sizes and shapes. Unfortunately, this end-effector had several design flaws that limited its utility. The design and testing of this knee exoskeleton revealed design principles that inspired the design of a new knee exoskeleton with a simple pivot joint. The performance of the knee exoskeleton was similar to that of the ankle exoskeletons with a mass of 0.76 kg, torque bandwidth of 23 Hz, and torque capability of 120 Nm in extension and 75 Nm in flexion.

Developing these three different end-effectors helped me to develop general principles of exoskeleton design that are applicable to most lower-limb exoskeletons. I also demonstrated a preferred method of bandwidth testing that more accurately characterizes the torque bandwidth of lower-limb exoskeletons than the standard methods previously applied.

1.3.2 Comparison by emulation of qualitatively different hardware configurations for assisting running

Developing devices to assist running could improve participation in running for exercise and improve safety and endurance for those who run for work such as soldiers or emergency responders. It is unclear what the best strategies for assisting running with portable exoskeletons may be. It would be convenient if a passive, spring-loaded ankle exoskeleton could effectively assist running without the need for motors and power supply. Specialized shoes with embedded carbon fiber plates that store and return energy [39] and passive hip exoskeletons [6] have demonstrated that passive strategies can be effective during running. The ankle produces higher peak torque and power than the hip or knee during running and may be a more effective location to apply assistance. Both passive and powered strategies have been successful at the ankle for assisting walking and these benefits may translate to running.

Understanding the relative benefits produced by spring-like and powered assistance strategies could have significant implications for the design of portable systems. To this end, an experiment was performed using an ankle exoskeleton emulator to compare passive and powered assistance strategies for running. Human-in-the-loop optimization was performed to enable a more accurate comparison between controllers by customizing device settings to fit the needs of individuals for both passive and powered conditions.

1.3.3 Understanding the relative benefits of qualitatively different ankle exoskeleton assistance strategies for walking

While ankle exoskeleton assistance with time-based control has demonstrated higher metabolic benefits than any other method [2], it is unclear whether time-based control outperforms other methods fundamentally. Too many confounding factors exist between studies to make objective comparisons. Most specifically, human-in-the-loop optimization of other controllers

has not been performed. EMG control has also demonstrated metabolic benefits [27, 40, 26, 28] and a virtual muscle-tendon based controller with EMG input may better capture user intent by simulating muscle-dynamics. We performed an experimental comparison of time, simple EMG, and muscle-tendon based controllers to demonstrate the relative benefits between qualitatively different approaches. The muscle-tendon based controller represents a novel attempt created by reducing the scope of a neuromuscular controller [41] to a simulation of only muscle-tendon dynamics with EMG as an input. Human-in-the-loop optimization was performed to enable a more accurate comparison by customizing the settings of each controller to best suit the needs of each individual.

1.4 Thesis overview

This thesis presents the approach I have taken to develop strategies for assisting walking and running using lower-limb exoskeletons. In Chapter 2, I present an introduction to the state-of-the-art of exoskeleton emulator testbeds and describe the general principles I have developed for the design of lower limb exoskeletons through the experience of designing three qualitatively different end-effectors. Chapter 3, presents the design and characterization of the ankle end-effectors that enabled experimental comparisons of qualitatively different assistance strategies using the emulator test-bed. In Chapter 4, I present the design and characterization of two knee exoskeletons that were designed for future experimental work. In Chapter 5, I compare the relative benefits of powered and passive spring-like ankle exoskeletons for assisting running performance. Chapter 6, describes an experiment performed to compare the relative metabolic benefits of three fundamentally different high level controllers as implemented on bilateral ankle exoskeletons.

Chapter 2

Lower-limb exoskeletons and emulator systems: principles of design

Abstract

This chapter provides guiding principles for design and case studies of effective approaches to help developers begin the process of designing their own lower-limb exoskeletons. This is discussed mainly in the context of exoskeleton emulator systems which are used to emulate existing exoskeletons or to test candidate control strategies and hardware designs before they are prototyped. Topics include the pros and cons of exoskeleton testbeds, selection of actuators, development of free body diagrams for evaluating loading and stresses, comfort and safety measures, tips for frame and joint design, sensor selection, materials and manufacturing, series elasticity for improved torque tracking, and a brief description of low-level control strategies.

A text book chapter presenting this chapter is in press [42].

2.1 Introduction

Designing lower-limb exoskeletons is a difficult process with many inherent challenges. All exoskeletons add mass and inertia to their user, which makes locomotion more energetically costly. Exoskeletons also restrict natural movement by increasing the overall volume of the leg and by resisting or completely inhibiting motion in some directions. The assistance provided by exoskeletons must effectively offset these innate costs before the userâĂŹs performance can be improved. This requires exoskeletons to be lightweight and compact while ensuring safety and conforming to constraints such as desired degree of adjustability.

Designs range from soft to rigid and single jointed to full body, but all exoskeletons have the same key components: frames, actuators, sensors, control hardware, and physical interfaces that connect to the user. These features can be distributed in various ways, from a fully untethered system with all components mounted on the user to an emulator testbed with many components located off-board.

This chapter provides guiding principles for design and case studies of effective approaches to help developers begin the process of designing their own lower-limb exoskeletons. Topics include the pros and cons of exoskeleton testbeds, selection of actuators, development of free body diagrams for evaluating loading and stresses, comfort and safety measures, tips for frame and joint design, sensor selection, materials and manufacturing, series elasticity for improved torque tracking, and a brief description of low-level control strategies.

2.2 Exoskeleton emulator testbeds

Exoskeleton hardware is often complicated and expensive. Exoskeletons are usually built as an untethered system with onboard power supply, control hardware, and actuation. Fitting all of this into a compact package that fits on a user without impeding movement often requires complex custom parts. Researchers build exoskeletons and discover unsatisfac-

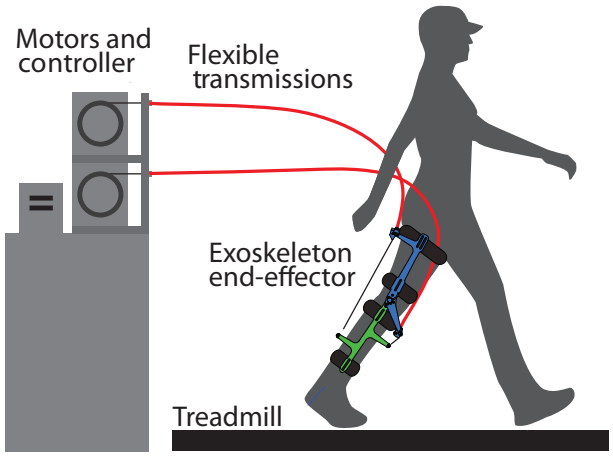

Figure 2.1: Example of an emulator system with a knee exoskeleton end-effector. Powerful off-board motors transmit mechanical power to the exoskeleton end-effector via flexible transmissions known as Bowden cables. Power is supplied by a three-phase wall outlet and control is managed by off-board control hardware. Any number of end-effectors can be used on a single emulator system.

tory details, resulting in the need for adjustments that require substantial redesign. This is discouraging, time consuming and expensive, and can be largely avoided by beginning development with an exoskeleton emulator system.

Exoskeleton emulators are laboratory testbeds that are used to emulate existing systems or to test candidate exoskeleton designs before they are developed. The key components of an exoskeleton emulator include an exoskeleton end-effector worn by a user and off-board components, including actuation, control hardware, and power supply (Fig. 2.1). Placing these components off-board makes the exoskeleton simpler, which reduces design time and expense, while simultaneously improving performance.

Several research groups have adopted emulator testbeds with success. The Details of their exoskeleton design vary widely while still using the same general approach (Fig. 2.2).

Most testbed systems are used to test general strategies or candidate designs for untethered systems before prototyping them, but sometimes testbeds are used with the intent of remaining testbeds forever. For example, the MIT Anklebot is intended to be used in a clinical setting to characterize the stiffness and impedance of ankles [43], and it has been used to identify the active, passive and dissipative behavior of the ankle joint during walking [44].

Emulator testbeds can be affordable and efficient tools for both researchers and clin-

icians. Developing a testbed can deliver benefits for years, but not without some minor drawbacks.

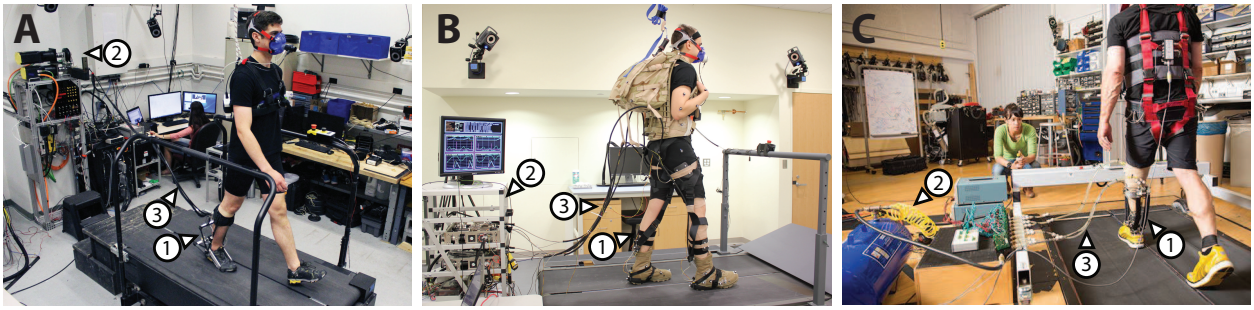

Figure 2.2: Testbeds keep devices simple and lightweight by placing heavy high-power components off-board and enable timely walking experiments on a treadmill. **A** [2] Carnegie Mellon University's Emulator testbed includes (1) a rigid ankle exoskeleton actuated by (2) an off-board electric motor with (3) a flexible Bowden cable transmission [45, 46, 47, 2, 48]. **B** The Harvard Biodesign Lab [49] actuates their (1) soft exoskeleton end-effector with (2) off-board motors and (3) Bowden cable transmission. **C** The Human Neuromechanics laboratory [50] at the University of Michigan tests (1) a rigid carbon fiber ankle-foot orthosis actuated by pneumatic artificial muscles with (2) an air compressor located off-board and mechanical power transmitted through (3) pneumatic tubes.

2.2.1 Emulator pros and cons

Exoskeleton emulators are fast, inexpensive, and flexible, but restricted to a laboratory setting. Emulators are fast to design, manufacture and adjust. Placing the motor, power and control hardware off-board removes the problem of designing mounts and mechanical transmissions on the leg, which eliminates the most complex elements of the design. Without these components the number of parts on the end-effector is drastically reduced, which reduces both design time and the cost of manufacturing. The greatest time saving feature is that any device behavior can be programed in without changing hardware. Let's say we think a passive clutch and spring system, such as that developed by North Carolina State and Carnegie Mellon Universities [51], could be beneficial. The proposed system can be emulated by programming in the expected torque profiles. Changing the virtual spring stiffness or clutch timing is done with a keystroke rather than replacing parts, tuning finicky components, or building an entire exoskeleton. In this way a single end-effector can be used to test any number of candidate mechanical systems.

Emulators are cost-effective largely because the most expensive components are off-board, which allows them to be used and reused for any number of end-effectors over the course of years. Batteries and motors that are small and light enough to mount on a user, but powerful enough to get the job done are expensive, while wall power and reusable motors that sit on a shelf are much cheaper with greater capability. Lastly, precise design requirements can be determined based on experimental results before designing complex untethered systems, so mass, space and money are not wasted building in too much capability, or worse: too little.

The only major con is that the tether to power and actuation restricts exoskeletons to treadmill walking. While this seems like a major limitation, exoskeletons have been under development for more than 120 years, yet the first measurable benefits were recorded using a pneumatic emulator in 2013 [1]. While some research groups may be ready to step out into the world to address behaviors not easily captured on a treadmill, substantial basic research remains to be done in the laboratory.

2.2.2 Off-board components: power, actuation and control hardware

Selecting off-board components with more capability than required by the current application has the benefit of keeping additional strategies available for future endeavors. The cost of overdesigning off-board components is very low as they can be used for years to come.

Common actuators include pneumatic artificial muscles [1, 52], Bowden cable transmissions connected to powerful off-board electric motors [35], and linear actuators [53]. In this chapter, we will focus mainly on Bowden cable systems. Regardless of the actuator you select, there is a trade-off between joint torque and velocity. The actuator must produce the required torques at velocities that can match or exceed the demands of the assisted biological joints.

Bowden cables attached to large electric motors are a common option for actuation be-

cause they are simple to implement and require little maintenance. An example of a Bowden cable is a bicycle brake cable. It is a thin cable that travels through a tough, flexible outer housing. Forces acting on the ends of the housing are equal and opposite to the tension on the inner cable. These equal and opposite forces result in no net force, meaning the brakes are not pulled towards the handle bars and exoskeleton end-effectors will not be pulled towards off-board motors. The exoskeleton just needs a small clamp for the housing to attach to and a lever or drum onto which to tie the inner cable. Another benefit of Bowden cable actuation is that it is extremely backdrivable. The motor can simply let the cable go slack for the exoskeleton to switch to a zero-torque mode.

Overdesigning off-board components allows for a highly responsive system. Off-board actuators can often provide higher peak torque than the exoskeleton frame can withstand, but that torque can be used to accelerate the rotor quickly. This allows for higher force bandwidth and greater disturbance rejection. The more bandwidth you have, the more types of assistance you can accurately apply. Disturbance rejection is important as torque can be developed in two ways: the motor can turn, or the user can disturb the system by flexing a joint to tighten the Bowden cable. This means your motor will need to get out of the way quickly to achieve accurate torque tracking.

2.3 Untethered systems

While testbeds give researchers a high degree of flexibility, untethered systems are needed for overground walking and are often the end goal of research performed on a testbed. Many untethered systems are currently in use and several have been shown to reduce the metabolic cost of walking. An untethered ankle exoskeleton from MIT effectively reduced the metabolic cost of walking during load carriage [4]. This exoskeleton is likely successful because it allows the ankle to maintain mobility in uncontrolled directions and its mass is kept to a minimum by eliminating explicit joints and taking advantage of lightweight

materials such as fiberglass leaf springs and cord. Researchers at Samsung developed a sleek product-like hip exoskeleton that reduced the metabolic cost of walking by 20% with maximum torque as small as 10 Nm [54].

Some untethered exoskeletons have particularly unique designs. North Carolina and Carnegie Mellon Universities collaborated on a passive ankle exoskeleton with a mechanical clutch and spring that stored and released energy during walking resulting in a metabolic energy reduction of about 7% [51]. The Harvard Biodesign Lab has untethered versions of their soft exoskeletons with power and actuation located in a backpack. These untethered soft exoskeletons have been used to reduce the metabolic cost of walking during load carriage by 7% compared to walking without the mass of the exoskeleton and 14% compared to an unpowered mode [55]. The physical structure of the soft exoskeleton is unique and impressive as it can be worn under clothing, is lightweight, and the materials of the exoskeleton are exceptionally inexpensive to manufacture. Lastly, Simon Fraser University and Bionic Power have produced an energy harvesting knee exoskeleton that generates electricity while decelerating the knee at the end of the swing phase [56]. This is similar to regenerative braking in a hybrid vehicle. The negative work performed by the exoskeleton, which powers the generator, replaces positive work in human muscle, so the additional metabolic cost of wearing the device is small. This energy harvesting knee exoskeleton may provide power to medical devices or allow charging in remote areas.

Several position-controlled exoskeletons are currently available for assisting individuals with spinal cord injuries. One such device is the ReWalk which senses the tilt of the torso and commands a predetermined hip and knee trajectory that results in a step when the user leans forward [57]. The user can also use a remote to command the exoskeleton to aid with several tasks such as sit-to-stand transitions.

Some exoskeletons have been well designed, but have not produced measurable benefits for the user. The Achilles exoskeleton developed at Delft University of Technology is cleverly designed with an efficient leaf spring and linear actuator drive system [58]. However, it did

not reduce the metabolic cost of walking, likely due to the weight of the hardware and details of its current control scheme [59].

2.4 Mechanical design of onboard components

Regardless of whether an exoskeleton is untethered or part of an emulator system, the same principles of exoskeleton design apply. Exoskeleton design requires balancing competing design goals and constraints. In general, we would like to minimize mass, inertia and volume while maintaining safety, comfort, mechanical strength, and peak torque and power capabilities. In this section we will discuss general approaches for ensuring comfort and safety, frame design, joint design, sensing, series elasticity and materials and manufacturing.

2.4.1 Loading analysis: free body diagrams

Free body diagrams enable designers to understand the forces applied to the user and stresses in the exoskeleton. This allows designers to make better decisions to produce lightweight designs while ensuring comfort and safety. Free body diagrams will reveal whether or not a design will operate as intended. They can also reveal the relationships between design parameters and outcomes such as the magnitude of forces applied to users and mechanical stresses in components. This chapter assumes a basic understanding of free body diagrams. If some background is needed, we recommend referring to a textbook on Engineering Statics or Physics such as Introduction to Statics and Dynamics available online [60].

Here are some helpful techniques for generating free body diagrams of exoskeletons:

1. Simplify free body diagrams of the exoskeleton and user by including only a portion of the user. It is acceptable to make a “cut” and include only the user’s leg, but you must include internal forces and moments at the “cut.” Make certain that any other forces applied at the boundaries of your free body are also included.

2. The mass of exoskeletons and the accelerations experienced during walking and running are often small compared to the driving forces and moments, so the gravitational and dynamic loads can usually be safely neglected. Complexity can be added as the design takes shape.

3. Assumptions that are in line with design goals can simplify analysis and verify that the exoskeleton will operate as expected. For example, if you do not want straps to apply shear force to your user, assume straps only apply forces normal to the user. If you cannot achieve static equilibrium with this assumption in place, you know your design will not function as intended.

Once free body diagrams are composed, you can solve the static equilibrium equations for outcomes of interest. This allows you to see the effect of changing design parameters such as component lengths on outcomes like the magnitude of force applied to a user. If static equilibrium cannot be achieved, you will need to make adjustments to your assumptions or change the overall design of your system.

Comparing candidate architectures and identifying issues early in the design process can greatly impact performance and avoid costly alterations later. After load analysis is performed, dimensions can be selected to minimize forces and stresses, which allows for a mass-efficient design.

See the case study in section 2.4.2 for an example of free body diagrams and how they were used to develop an ankle exoskeleton.

2.4.2 Safety stops and physical interfaces

An exoskeleton has limited usefulness if it is unsafe or too uncomfortable to be worn. We can ensure safety by preventing the user's natural range of motion from being exceeded, and we can improve comfort by placing physical interfaces far apart, keeping forces acting normal to the user, and restricting natural motion as little as possible.

Safety stops

Hard stops should prevent an exoskeleton from applying force to the user outside their natural range of motion. Placing hard stops far away from the assisted joint will reduce the magnitude of force applied to the hard stop. A singularity may be an acceptable replacement for a hard stop in some cases. A singularity works by aligning the inner Bowden cable with the joint center. In this configuration, tension in the rope can be very high and still apply zero torque to the user's leg at the maximum allowable angle. This approach is less desirable than the hard stop. A large portion of the exoskeleton frame still experiences large forces and stresses, and the user is not protected against hyperextension of joints due to other causes such as trips or the momentum of the leg itself.

Other safety measures such as mechanical fuses and in-software safeties should be in place. A breakaway cable can be tied in line with the inner Bowden cable at the motor. If tension in the cable rises higher than expected, the breakaway cable will break and separate the end-effector from the motor. Software safeties can command zero torque when certain limits are exceeded, but software safeties should never be relied on completely as sensor malfunctions or wiring problems can render them ineffective.

Case study: knee exoskeleton end-effector utilizes hard stops

The Carnegie Mellon University (CMU) knee exoskeleton end-effector utilizes safety hard stops to prevent flexing or extending the knee beyond acceptable limits (Fig. 2.3). The Bowden cable housing termination and the inner cable termination press against each other to counteract the tension in the cable. This type of hard stop is preferable compared to a singularity because all the force is reacted through these two components and the rest of the exoskeleton remains unloaded.

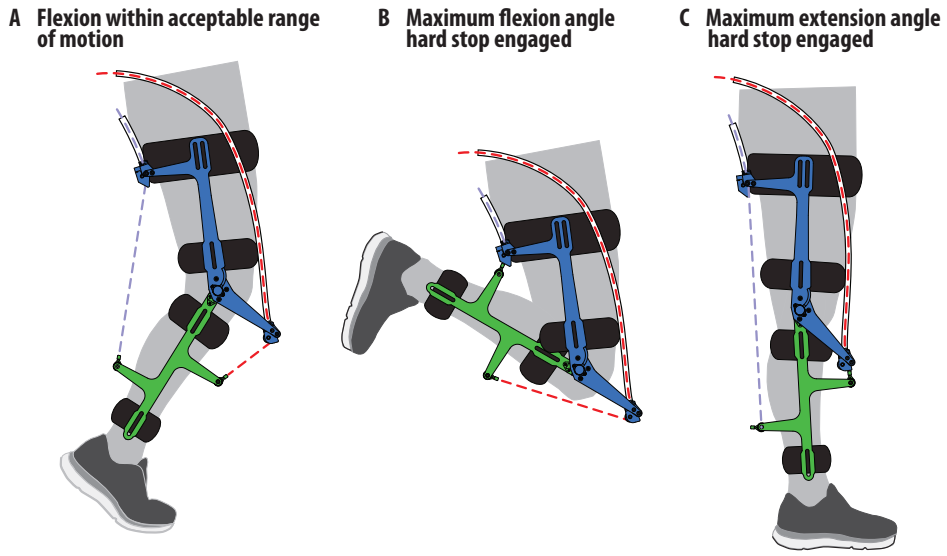

Figure 2.3: **A** The exoskeleton experiences a flexion angle within the acceptable range. **B** The exoskeleton has reached its maximum allowable flexion angle. The Bowden cable housing termination collides with the inner cable termination thus preventing the exoskeleton from flexing any further. **C** The exoskeleton is in its straight leg configuration and will not allow further extension of the knee.

2.4.3 Straps

Placing interfaces far apart maximizes lever arm lengths and minimizes forces applied to the user. It is also more comfortable for force to be applied directly towards the leg (normal to) than along its surface (in shear). Not only do shear forces cause rubbing and pain, but skin does not support them well [61]. This can be demonstrated by gripping your wrist and pressing directly toward the bone. There is little movement between your hand and wrist. Now grip your left forearm tightly and force your right hand alternatingly towards the left elbow and hand. Your hands slide with respect to each other with little resistance as your soft tissues deform. This motion is undesirable and will be worse in very fleshy areas like the thigh. For these reasons exoskeletons should apply forces mainly normal to the user whenever possible.

Straps are key to the success of exoskeletons and should be prototyped early in the development process. The best strapping locations have a shape conducive to preventing downward migration, experience little change in muscle volume, and are bony. One of the best strapping locations is at the top of the calf. The large size of the gastrocnemius muscle

prevents a calf strap from sliding down the leg. The top of the calf also sees very little change in volume allowing for inextensible straps. The shin is bony and an excellent location for applying force without losing mechanical power to the deformation of soft tissues. The thigh is less convenient and requires more thoughtful design as it is shaped like an inverted cone and thigh straps tend to slide down.

Some mechanical power loss is experienced at all human-exoskeleton interfaces due to movement of the device relative to the user, deformation of soft tissues and compliance in the straps themselves. Some measures of power loss at interfaces are as high as 55% [62]. While some of this power is returned viscoelastically, the timing of its return is difficult to anticipate.

Applying forces to the user at bony locations and making straps out of inextensible material can help avoid relative motion between the exoskeleton, mitigate rubbing, and reduce mechanical power loss, but the changing shape of the user may require some elasticity at locations that experience large volume changes. For example, a strap above the knee may be comfortable for walking, but uncomfortably tight for running or squats.

Straps must be able to resist gravity and dynamic loads. These loads are often neglected during component design as they are small and cause low stress, but will cause exoskeletons to migrate with respect to the user over time. Legs experience high rotational velocity during locomotion which acts along with gravity to force exoskeletons down the leg. This problem can be mitigated by reducing mass. Additional suspension straps may also help. Knee exoskeletons often utilize a strap to the waist to prevent downward migration. The distribution of mass is important as laterally offset mass can cause the exoskeleton to spin around the leg as the user walks. The coefficient of friction between the user and straps can be improved using self-adhering sport wrap such as Coban or prosthesis socket liner. Developing straps is often a matter of trial and error, as mechanical engineers, clinicians, and biomechanists are not typically expert in apparel design. Comfort may be best maintained by adapting straps already well-developed for sports, weight lifting, or safety equipment.

2.4.4 Case study: ankle exoskeleton designed for low forces and safety

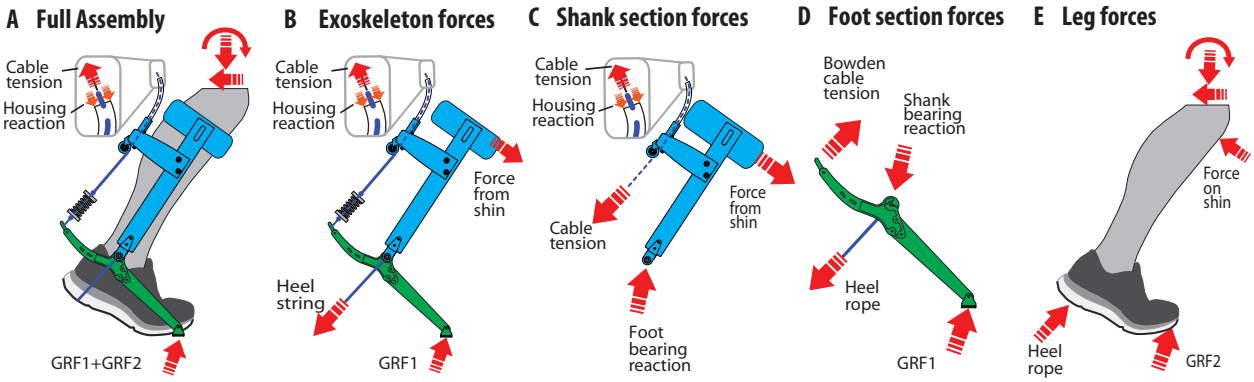

Figure 2.4: Free body diagrams of an ankle exoskeleton **A** The full system including the exoskeleton and user's leg. Forces in the Bowden cable housing act equal and opposite to tension in the cable resulting in zero net force on the exoskeleton. **B** The exoskeleton interfaces with the user in three locations: a strap at the shin, a rope embedded in the heel of the shoe and a plate in the toe of the shoe. **C** The shank section experiences force from the calf strap, force at the Bowden cable housing termination that is equal and opposite to the tension in the inner Bowden cable, and a reaction force at the bearing. Note that the force from the redirection of the inner Bowden cable around a pulley is not included as it is internal to the free body. If the inner Bowden cable were not included then the redirection force would be needed. **D** Forces acting on the foot section of the exoskeleton. **E** Forces acting on the user.

In the first stages of designing the ankle exoskeleton, we used free body diagrams to select among architectures, set major geometric parameters, and estimate loads on the device and the body (Fig. 2.4). The exoskeleton interfaces with the user at three locations: a strap above the calf, a rope under the heel of the shoe and a plate embedded in the toe of the shoe. These diagrams adhere to the recommendations listed in section 2.4.1.

It is assumed that the force applied by the calf strap acts normal to the user's shin (Fig. 2.4B). This assumption ensures that it is physically possible for the exoskeleton to work as intended and makes solving the force balance equations easier. If force balance could not be achieved with this assumption in place, it would be understood that the exoskeleton must apply undesirable shear force to the shin and calf. The no-shear assumption is reasonable as the straps and soft tissues have low stiffness in shear loading and disallow the development of large forces except in the case of large displacements.

The interfaces at the calf, heel and toe are placed as far apart as possible to reduce forces on the user. For example, if a moment balance is taken about the bearing in Figure 2.4C, the force in the calf strap is inversely proportional to the distance between the strap and the bearing. Placing the strap half way down the shin would decrease the overall size of the exoskeleton, but would also double the force on the user's leg for the same applied torque.

Free body diagrams can be used to answer many design questions. For example, why is the heel rope included? If we start with known tension in the Bowden cable, the joint reaction force between the shank and foot section can be solved for using Figure 2.4C and static balance equations. This joint force can then be used in Figure 22.4D to solve for the three unknowns: tension in the heel rope, the ground reaction force, and the direction of the ground reaction force. Three static balance equations (sum of the forces in the x and y directions along with a moment balance) can be used to solve for our three unknowns. If the heel rope was not included, the problem would be under constrained with two unknowns and three equations. Static balance would not be possible without additional forces, such as a shear force on the shank.

The ankle exoskeleton features a singularity (Fig. 2.5) to prevent the exoskeleton from applying torque to the user outside their normal range of motion. As the ankle approaches its maximum allowable plantarflexion angle, the inner Bowden cable aligns with the joint center, ensuring that zero torque is applied at this maximum angle. Furthermore, if the plantarflexion angle exceeds this maximum angle, a restoring dorsiflexion torque will be applied. However, a large portion of the frame is loaded when the singularity is reached. This means that the frame must be reinforced to a greater degree when using the singularity as a safety instead of a hard stop.

2.4.5 Frame and joint design

We would like to minimize mass, inertia and volume while allowing the device to fit many different users comfortably without inhibiting gait. The energy cost of carrying mass increases drastically as the location of the added weight becomes more distal [31]. Compo-

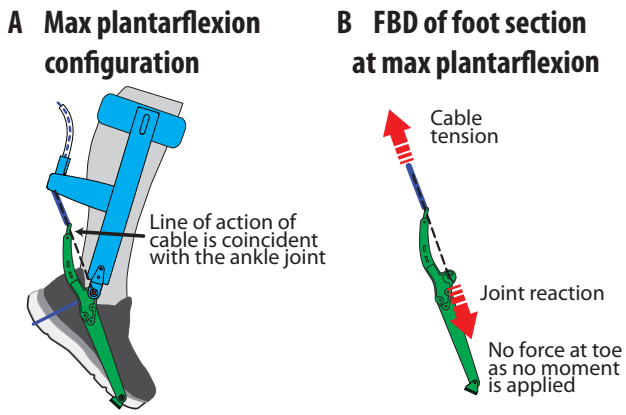

Figure 2.5: Singularity on an ankle exoskeleton. **A** As the ankle approaches its maximum allowable plantarflexion angle, the inner Bowden cable aligns with the joint center. **B** A Free body diagram of the foot section demonstrates that zero torque is applied at this maximum angle.

nents should be mass efficient and heavier components should be as close to the torso as possible. Adding an exoskeleton also increases the overall volume of the leg, which requires the user to increase circumduction (swing their legs further to the side) to avoid collisions between legs during walking. This is very tiresome as the net rate of energy expenditure during walking increases with the square of circumduction amplitude [63]. With this in mind, protrusions from the leg on the medial aspect should be kept to a minimum.

Frame design

Attaching to people is difficult. Not only are people squishy and oddly shaped, but there is wide variability in the shape of individuals. Variation in leg length, leg diameter, shoe size, levels of valgus or varus alignment in the knee (knock-kneed or bow-legged), and external rotation of the toe, among other things can make fitting multiple individuals with one exoskeleton difficult. Developing an exoskeleton that is one-size-fits-all is likely impossible without including some amount of adjustability, modularity, or compliance.

Adjustability can be a time saver when running lots of experiments. Sliders can extend or shorten struts to fit legs of different lengths, but add weight and complexity to the design. Users of different sizes can be accommodated through modularity by making multiple sizes of select components. Addressing fit with modularity is simple, but can be time consuming

to adjust as connective hardware needs to be removed and replaced and wires might need to be rerouted.

In some cases, sizing can be addressed through compliance in select directions. Frames with built-in flexibility can flex in or out to accommodate users of different leg sizes. Selective compliance can also be used to provide passive degrees of freedom to a joint. This is desirable as biological joints usually have many degrees of freedom, but an exoskeleton may be designed to only assist only one or two. Allowing some motion in the unassisted directions through compliance keeps locomotion relatively uninhibited while maintaining a simple design.

Case study: Carnegie Mellon University's ankle exoskeleton

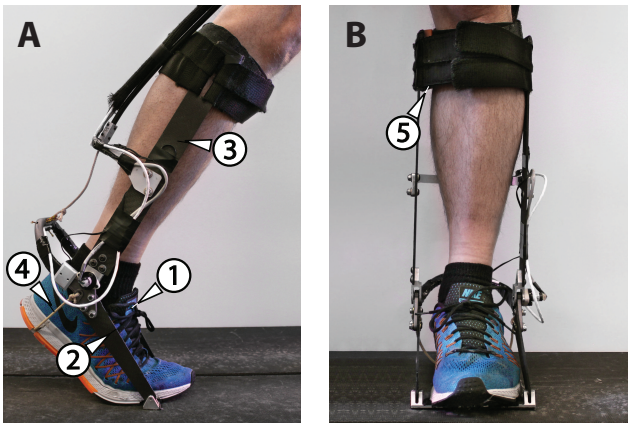

Figure 2.6: Modularity ensures a good fit on different users. **A** The shoe (1), toe struts (2), calf struts (3), and heel rope (4) can be exchanged to fit users of different foot and calf lengths, while the rest of the components are one-size-fits-all. **B** This subject requires a wide spacer (5) under the strap on the medial aspect of the calf to ensure that the ankle is centered in the exoskeleton. Other subjects may require spacers on the lateral aspect, or none at all.

- **Modularity**: The shoe, toe strut and calf strut of the CMU ankle exoskeleton (Fig. 2.6) can be exchanged to fit different users, but the joints, Bowden cable termination and heel spur are one-size-fits-all. The exoskeleton can be shifted by adding spacers of unequal size to the top of the calf. Often the calf is not symmetric around the center of the leg. More muscle mass can be located on the lateral side of the leg, which shifts the exoskeleton towards the lateral side. This is a problem if the medial malleolus of

the biological ankle joint contacts the frame. This can be fixed by adding a wide spacer to the medial side and a thin (or no) spacer to the lateral side.

- **Selective compliance for fit:** The tops of the calf struts on this ankle exoskeleton can flex towards and away from the leg to accommodate legs of differing diameter. The struts are thin in the frontal plane to allow flexing, but wide in the sagittal plane to ensure that they are rigid in the directions in which large forces are applied.

- **Selective compliance for passive degrees of freedom:** The biological ankle acts mainly in the plantarflexion/dorsiflexion direction, but is also capable of rotation and roll. The CMU ankle exoskeleton only assists plantarflexion and uses a simple pivot joint, but still allows freedom for the ankle to roll through compliance in the shoe, heel rope, strap, and struts (Fig. 2.7). Low compliance in the heel rope is particularly useful for allowing inversion and eversion of the ankle, although ankle rotation is still limited.

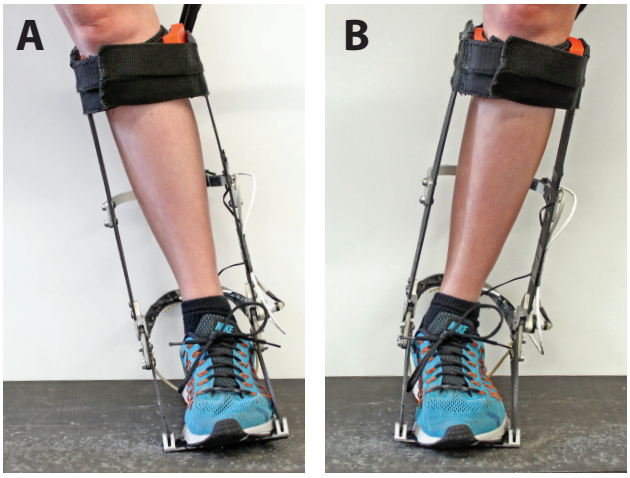

Figure 2.7: Selective compliance allows freedom of motion in several degrees of freedom without complex joint design. Flexibility in the shoe, straps, struts and heel rope allow for comfortable inversion **(A)** and eversion **(B)** of the ankle.

Joint design

Simple pivot joints are lightweight and functional as they simplify attachment and sensing. For example, a knee exoskeleton can depend largely on the calf strap to prevent the entire structure from sliding down the leg if the joint has only one degree of freedom. However, if translation between the thigh and calf sections of the exoskeleton is allowed by a more complex joint, the calf strap cannot support the thigh portion. More degrees of freedom require better strapping. Additionally, many control strategies require real-time measurement of joint angle. This is most easily accomplished by attaching an encoder to a pivot joint.

Deliberately designing for structural compliance in unassisted directions allows simple joint designs to be effective. Biological joints are complex and have multiple degrees of freedom, but each of these may not need to be explicitly addressed by the mechanical joint if there is sufficient compliance in soft tissues, straps and the exoskeleton structure. However, small natural movements in the unassisted degrees of freedom of biological joints will result in undesirable large forces if the exoskeleton and its interface with the user are both very stiff.

Several successful exoskeletons have been developed without explicit joints. A jointless autonomous ankle exoskeleton has reduced the metabolic cost of walking [4]. Soft exoskeletons typically lack explicit joints and are extremely lightweight and allow freedom of motion [21]. However, the magnitude of torque applied can be limited using this strategy as some shear forces must be applied by straps, which can be uncomfortable. The range of available control strategies can also be limited as the measurement of joint angle is more difficult without an explicit joint.

Case study: Five-degree-of-freedom knee exoskeleton

Complex designs to address multiple degrees of freedom and fitting issues can be time consuming to design, expensive to manufacture and heavy, while a simpler, lighter design may suffice. Consider the five-degree-of-freedom knee exoskeleton developed by Carnegie Mellon

University in collaboration with Boston Dynamics shown in Figure 2.8.

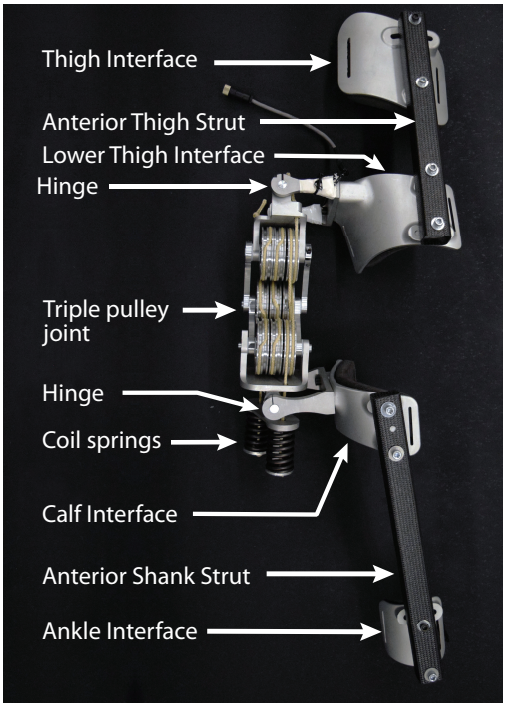

Figure 2.8: A five-degree-of-freedom exoskeleton designed to provide a pure moment to the knee joint. The exoskeleton consists of four aluminum strap interfaces at the upper thigh, lower thigh, calf, and ankle. These interfaces are connected by anterior struts formed of rectangular carbon fiber tubes. The joint is composed of two hinges and three sets of triple pulleys, which allow for five degrees of freedom.

Five degrees of freedom were selected so the center of rotation of the exoskeleton could match the center of rotation of the biological joint and accommodate all natural degrees of freedom other than knee rotation. Internal/external knee rotation was omitted to prevent torque application in unintended directions.

The joint of the knee exoskeleton was comprised of three sets of triple pulleys: one for extension torque, one for flexion, and one for a safety hard stop to prevent hyperextension. Straps at four physical interfaces attached at the top of the thigh, above the knee, calf, and above the ankle.

This exoskeleton had many desirable traits, but failed to be useful in walking experiments. It featured no rigid components on the medial aspect of the leg, which avoided increased circumduction during walking. It could fit a wide range of adults easily regardless of leg-length, degree of varus or valgus alignment of the knee or leg diameter without

the need for modularity. Similar to another exoskeleton developed by Boston Dynamics [64], it also delivered a near pure moment (limited by friction at the bearings) to the biological knee, meaning internal joint forces were not increased due to the use of the exoskeleton. Unfortunately, the weight and bulk of the complex joint limited the utility of the device. The offset mass caused it to gradually rotate around the leg during walking, and the long length of the hard stop cable reduced its stiffness and effectiveness. A simpler knee exoskeleton was developed as a replacement (Fig. 2.9).

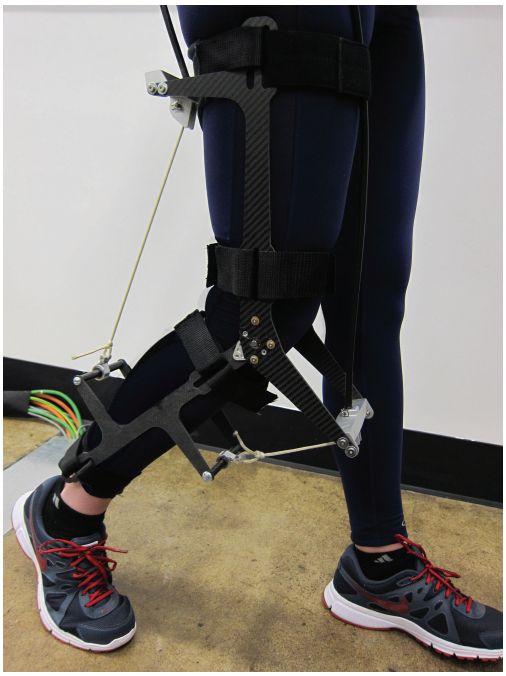

Figure 2.9: Knee exoskeleton featuring a simple pivot joint and plate carbon fiber frame.

Our second knee exoskeleton (Fig. 2.9) was developed using simple pivot joints and planar struts on the medial and lateral aspects of the leg. We found the single degree of freedom to be adequate as compliance allowed for comfortable use. The rigid components on the medial aspect of the leg are not desirable, but the exoskeleton has enabled walking experiments and was relatively simple to design and build. Information gained from this simple exoskeleton can be applied to more complex designs with more desirable form factors later.

2.4.6 Sensing

Emulator systems should include enough sensors to allow flexibility in the design of control strategies. Including sensors for joint angle, torque measurement, and heel contact keep most control strategies available for testing. For example, joint angle may not be needed to implement proportional electromyographic control, but it would be necessary to emulate the behavior of a spring-loaded passive device or to detect different phases of gait.

Joint encoders make measurement of joint angle simple. Magnetic encoders are recommended as they can be found in very small sizes and are relatively robust to misalignment compared to optical encoders.

Torque can be measured directly by lightweight strain gauges. Strain gauges can be configured in a Wheatstone bridge to improve sensitivity. The arrangement of the strain gauges can be designed to measure strain from specific types of loading while rejecting others. Torque can also be calculated by measuring tension in the Bowden cable with a load cell and multiplying by the effective lever arm which is calculated considering geometry and joint angle. Placing the load cell on the motor side of the Bowden cable in order to reuse the load cell across end-effectors is not recommended. Friction between the Bowden cable housing and the inner cable can result in lower (or higher) tension in the cable on the end-effector side compared to the motor side, resulting in inaccurate torque measurements [65].

A switch in the heel and/or toe of the shoe can provide information on the userâĂŹs place in the gait cycle. A pressure sensor may be more desirable than a simple on/off switch as it would open up more assistance strategies.

Sensors can often be moved off-board. For example, pressure sensors may be replaced by ground reaction forces as measured by an instrumented treadmill. Joint angle can be sensed by motion capture cameras. However, moving sensors off-board may involve delays or additional setup time for experiments.

If electromyographic (EMG) sensors are required for control strategies such as proportional EMG control [66] or for locomotion mode identification [23], then extra space is needed

between the user's leg and the exoskeleton frame near the instrumented muscles. Contact between EMG sensors and the exoskeleton can cause spikes in measured EMG data.

Wiring problems can be hard to diagnose and can result in large development delays. Wiring problems can be largely mitigated by making plans early in the design process. Routing wires over or near the axis of joints to avoid sharp repeated bends will reduce fatigue and prevent internal breaks in the cable that are hard to find. Buying cable with high flexibility will reduce the chances of failure due to fatigue. Including snaps or guides for cables will reduce the need for tape or cable ties. Routing all the cables for sensors into a single connector rigidly mounted on the exoskeleton frame will allow for a single cable extending from the exoskeleton to power and the controller. This reduces mass and makes unplugging the exoskeleton easy and reduces dangling cables which get in the way during maintenance and adjustments. Wireless sensors may be an option, but larger latencies are likely.

2.4.7 Series elasticity for improved torque tracking

Placing an elastic element like a spring in series with an actuator creates a series-elastic actuator [67]. This can improve torque tracking by improving disturbance rejection, but may also reduce bandwidth [68]. It is easiest to think of disturbance rejection in extremes. Consider the following scenario: the motor is being held still, the inner Bowden cable is taught and the user suddenly flexes the exoskeleton. If the Bowden cable has high stiffness, a large increase in force is generated quickly. If the Bowden cable has extremely low stiffness, like a rubber band, the user can quickly flex their joint without developing a large change in force. However, greater compliance in the transmission also reduces force bandwidth. If the transmission is very stiff, the Bowden cable is taught and there is a step increase in desired torque, the motor turns a tiny amount to create tension in the cable and a large force is quickly generated. If the transmission has very low stiffness, the motor must turn much further to generate the same amount of force, as force is equal to the stiffness of the transmission multiplied by displacement. Because the motor must turn more when

the transmission is less stiff, it takes more time to develop torque and lag is experienced between the desired and measured torque, which limits force bandwidth.

There is some intermediate stiffness that supplies some disturbance rejection without reducing bandwidth below acceptable levels. The optimal stiffness depends on the frequency content of the desired torque and the magnitude and frequency of disturbances. The best stiffness for an ankle exoskeleton was shown to be the one that most closely approximated desired torque patterns while holding the motor in a fixed position during walking [69]. Additionally, the stiffness of the entire transmission - the cable, the added spring, the straps, the structure of the exoskeleton and the soft tissues of the user - needs to be considered. In some cases, the user's soft tissues may reduce the stiffness of the exoskeleton/user system below the ideal stiffness for torque tracking. When this occurs, adding a spring cannot improve torque tracking.

2.4.8 Materials and manufacturing

Components for end-effectors can be machined, 3D printed, or made by carbon fiber layup. Most other manufacturing techniques are too expensive, as these devices are made in batches of only one or two. Each of these manufacturing techniques has pros and cons that should be considered.

CNC machining is widely available and somewhat complex shapes can be achieved affordably, allowing for a more closely fitting exoskeleton than that possible with a few simple planar parts. CNC machining is a highly repeatable method and the material properties of CNC machined metals, such as aluminum, are well understood. It is helpful as a designer to have a good understanding of material properties and expected fatigue life.

3D printing is attractive for exoskeleton design as very complex geometry can be easily achieved. Flowing 3D shapes can be made to wrap elegantly around the leg and small details for attachment to other components are simple to create. Complex or hollow cross-sections can be created to achieve mass efficient designs. However, 3D printed materials

have less predictable bulk material properties as the strength of the material is higher within a printed layer and lower between layers.

An exoskeleton's life likely involves more than a million steps, so fatigue becomes a real concern and predicting the fatigue life of 3D printed materials is currently extremely difficult. Little information is available on the performance of 3D printed materials in high cycle applications. Fatigue life of parts depends on surface finish and the size and quantity of internal defects. Printed materials are porous by nature and high residual stresses are created as a result of the additive manufacturing process. This makes printed materials more susceptible to fatigue than similar conventionally machined materials [70].

When small loads are expected, and fatigue is not an issue, inexpensive plastic 3D printed parts can be lightweight and convenient. Spacers, sensor protectors, cable guides and bump guards can all be produced easily and relatively cheaply using 3D printing processes such as fused deposition modeling (FDM) or stereolithography (SLA).

Carbon fiber is an attractive material for exoskeletons as it has a high strength to weight ratio. Carbon fiber is expensive both in terms of raw material and manufacturing costs. The complexity of 3D parts made by carbon fiber layup is limited by how fine the weave is. Carbon fiber does not lay flat in sharp bends and cannot achieve small complex geometry. Custom carbon fiber layups can result in very nice form-fitting exoskeletons, but care needs to be taken in their design. The orientation of the fibers needs to be considered and the bulk properties stated for the epoxy or carbon fiber material should be considered rough estimates as they depend on the quality of the layup itself. Additionally, carbon fiber is extremely susceptible to wear through abrasion and care should be taken to avoid any rubbing between carbon fiber components and other parts.

Sheets of carbon fiber, fiberglass, metals and plastics can all be interesting materials if planar parts are being considered. Planar parts are very quick and cheap to form by a variety of processes including waterjet cutting, plasma cutting, and laser cutting. Waterjet cutting of carbon fiber is particularly attractive because it is very inexpensive and the

hazardous dust is captured in the cutting fluid. The cost effectiveness of parts becomes especially important when addressing sizing and fit through modularity. Making the majority of a frame out of planar parts makes having three or more sizes more affordable than if utilizing complex three-dimensional parts. In addition to being affordable, planar parts also have very predictable beam stiffness, which allows compliance in select directions for fit and freedom of motion.

In general, 3D printing is advantageous where extremely complex geometry is necessary, CNC machining is appropriate for moderately complex parts, and waterjet cutting of carbon fiber plates is effective for large parts that will be replicated in multiple sizes or where compliance in select directions is needed.

Case study: the evolution of the CMU ankle exoskeleton

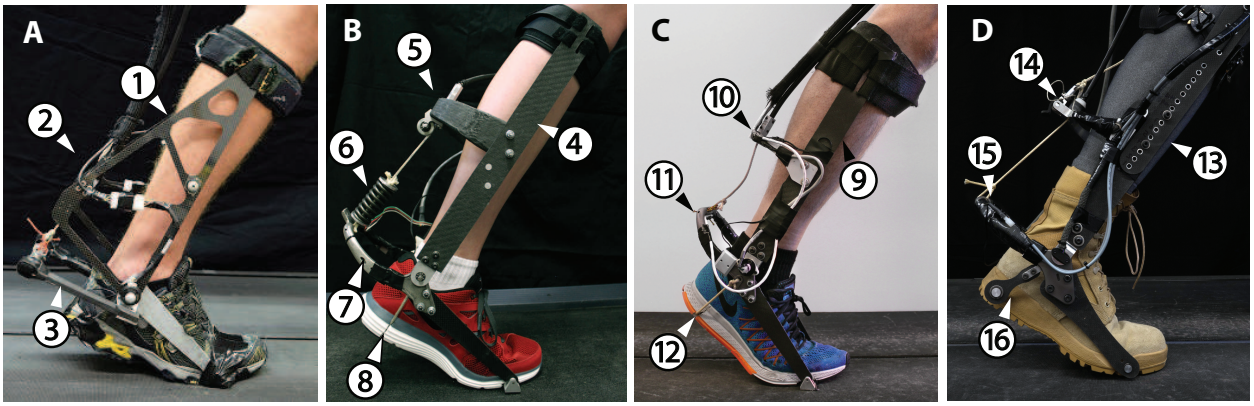

Figure 2.10: Evolution of ankle exoskeleton end-effectors **A** The original ankle exoskeleton is comprised almost entirely of (1) planar carbon fiber parts with (2) a rectangular Bowden cable termination connecting the medial and lateral aspects of the frame. (3) Fiberglass leaf springs provide series elasticity and leverage. **B** A more recent iteration of the ankle exoskeleton featuring (4) rectangular carbon fiber frame, (5) a hollow carbon fiber Bowden cable termination, (6) a steel coil spring, (7) a hollow titanium heel spur, and (8) a heel rope. **C** (9) The rectangular carbon fiber frame was reused and the Bowden cable termination was replaced with (10) a CNC aluminum component. (11) The titanium heel spur and (12) heel rope were also reused. The coil spring was removed as elasticity in the inner Bowden cable itself was found to be sufficient. **D** This ankle exoskeleton is a small part of a Bilateral Lower Limb Exoskeleton Emulator (BiLLEE). Discrete adjustability was added to the (13) frame. (14) The Bowden cable termination and (15) titanium heel spur remain mostly unchanged. The heel rope was replaced with (16) a carbon fiber link attached to a rod extending through the heel of the shoe to allow compressive loads to be carried.

The frame of the first iteration of the ankle exoskeleton was composed of planar carbon fiber parts to allow for high compliance in the frontal plane and to reduce cost (Fig. 2.10 A). The next three iterations use simple rectangular carbon fiber struts ((Fig. 2.10 B, C and D). These shapes have lower compliance, but are well suited to the expected loading, make manufacturing multiple sizes inexpensive, and provide compliance at the tops of the struts to fit calves of different diameters. Adjustability was added for the fourth iteration (Fig. 2.10 D). The fourth ankle exoskeleton is part of a larger Bilateral Lower Limb Exoskeleton Emulator (BiLLEE) capable of assisting the ankles, knees, and hips.

A heel rope is used in three of the ankle exoskeleton iterations (Fig. 2.10A, B and C). It is strong and stiff in tension, but allows for free motion of the ankle in rotation and inversion and eversion, which would be difficult to match with other more conventional materials. The heel rope was replaced with a carbon fiber link in the fourth iteration (Fig. 2.10 D) to

allow loading in compression, as part of the BiLLEE system.

The Bowden cable housing termination connects the medial and lateral aspects of the shank portion of the frame. The frame of the first iteration had to be large and extend far behind the calf to allow a rectangular shaped termination to work along with the fiberglass leaf springs (Fig. 2.10A). This configuration was easy to produce, but created a large boxy device envelope. The envelope was too large to allow for bilateral testing as frequent collisions occurred between the left and right exoskeletons. For this reason, we changed to a sweeping, U-shaped Bowden cable housing termination that fit the leg more closely (Fig. 2.10 B, C, and D). The first U shaped termination was made out of hollow carbon fiber (Fig. 2.10 B). This part was formed by casting a wax mold of the component, performing a carbon fiber layup around the wax form, and melting the wax out by submerging the part in warm water. While this produced a lightweight component, it was very time consuming to manufacture. For ease of manufacturing, the Bowden cable housing termination was changed to a machined aluminum component (Fig. 2.10 C and D).

Series elasticity was originally supplied by fiberglass leaf springs (Fig. 2.10 A). It was believed that this design would be lightweight as the leaf springs could act as both springs and as a lever. But bulky connective hardware was needed to allow for robust attachment that prevented cracks from developing in the leaf springs. A coil spring was later used to provide series elasticity. The spring was heavy and torque tracking was acceptable without it. So the spring was removed in subsequent iterations (Fig. 2.10 C and D).

The lever supplied by the leaf springs was replaced with a 3D printed titanium heel spur (Fig. 2.10 B C and D)). The complex loading experienced in the part was well addressed by a complex flowing shape easily produced by additive manufacturing. Torsion experienced in the middle of the horseshoe shape is well addressed by a hollow tube while bending stresses at the tips of the horseshoe can be reduced by using an I-beam cross-section. The majority of the heel spur is hollow, which would not be possible with conventional machining. The first iteration of the titanium spur experienced failure due to fatigue after two years of use

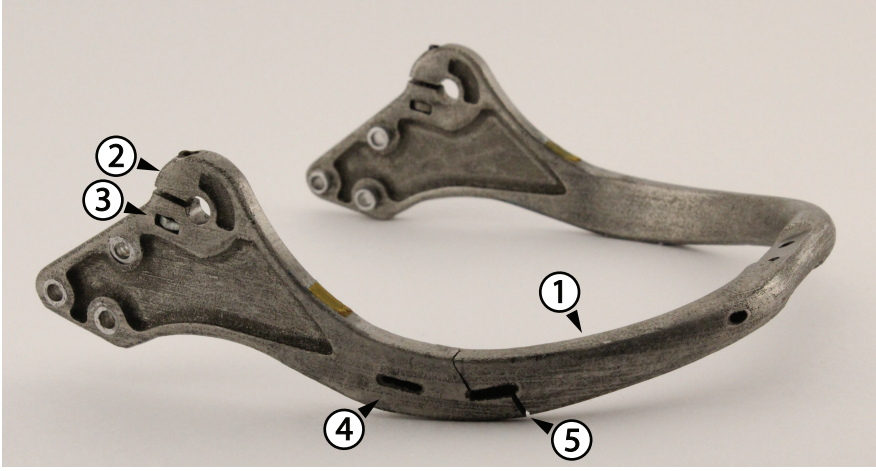

Figure 2.11: Titanium heel spur created by electron beam melting (EBM). Additive manufacturing allows for simple manufacturing of (1) sweeping shapes with hollow cross-sections and small complex geometry such as the (2) split hub clamp. However, this manufacturing process has some drawbacks. The printed material cannot be reliably threaded, so (3) a slot was required for capturing a nut for tightening the clamp. Hollow cross sections are filled with partially sintered titanium dust which require (4) vents to be included. The vent holes must be large enough to allow a small pick access to the hollow area to forcibly remove the dust. These vents limit the strength of the part and reduce the usefulness of the hollow cross-sections. Other additive manufacturing techniques such as selective laser sintering require smaller holes and the dust can be simply blown out with compressed air. Material made through additive manufacturing is especially susceptible to fatigue failure due to its porosity and poor surface finish. (5) Fatigue cracking began at the bottom of the part, propagated up to the vent hole and continued to the top of the component after two years of consistent use.

(Fig. 2.11). It is likely the next iteration of the heel spur will be conventionally machined because the fatigue life of conventional materials can be better predicted. This change will be made at the cost of added mass as hollow cross sections will not be possible using conventional machining.

2.5 Control

Control of robotic systems can be split into high-level control of behaviors and low-level control of positions or torques. High-level control determines what you want your device to do while low-level control is how your device achieves it. The high level controller determines the desired torque or position, and the low-level control attempts to track the desired signal as closely as possible. Emulator systems are most often used to give the user the experience of using a candidate device, and so the low-level controller typically aims to match the

torques that would have been produced by that device.

The simplest form of closed-loop low-level control is proportional control. The measured torque is subtracted from the desired torque to calculate the torque error which is then multiplied by a gain. This value then becomes the motor velocity command. In this way, the motor turns to take up slack when torque is too low and spins the other direction to let out slack when torque is too high. The speed that the motor turns is proportional to the error, so the bigger the error, the faster the motor turns.

Stability can be added to proportional control by adding damping injection. A damping gain is applied to the measured motor velocity and the product is subtracted from the motor velocity command such that there is resistance to further speeding up the motor when the motor is already moving very rapidly.

An iterative learning term can be added to the motor command to correct for error that is consistent across multiple consecutive steps. Iterative learning takes advantage of the repetitive nature of walking to create a feed-forward term based on past torque tracking error [69].

If a series elastic actuator is being used, other methods of improving disturbance rejection include disturbance observers [71], acceleration feedback [72], and model based environment-adaptive control [73].

Most exoskeletons have used high-level controllers that command either a prescribed torque or position as a function of time. However, many other types of high-level control have been shown to be beneficial such as proportional EMG [40, 27], and neuromuscular models [74, 75]. Impedance control does not rely on determining the intent of the user and can make an exoskeleton behave as if it has negative mass, damping or stiffness properties [76, 77]. Admittance control can render low inertia, while also achieving stability and excellent disturbance rejection [78]. There are an infinite number of high-level control strategies and testing many of them rapidly is made possible by easily programmable emulator systems.

2.5.1 Case study: control of any CMU emulator end-efffector

In the case of the CMU ankle and knee exoskeletons, the low level torque controller consists of proportional control plus damping injection and iterative learning as described in Eq. 2.1.

$$\dot{\theta}_{des}(i,n) = K_p * e_\tau(i,n) - K_d * \dot{\theta}_m(i,n) + \dot{\theta}_{learn}(i+d,n) \quad (2.1)$$

There are two indices in Eq. 2.1. i indicates the time step, which is set to zero at the moment of heel strike and is updated at a rate of 500Hz. n refers to the number of the current stride which is updated at every heel strike of the same foot. d is a delay equal to the number of time steps required for a change in motor velocity to be reflected in applied torque. $\dot{\theta}_{des}$ refers to the desired motor velocity. K_p is the proportional gain applied to e_τ, the error in torque tracking. K_d is the damping gain applied to $\dot{\theta}_m$, motor velocity. $\dot{\theta}_{learn}$ is a learning term calculated in Eq. 2.2.

$$\dot{\theta}_{learn}(i,n) = \beta * \dot{\theta}_{des}(i,n-1) - K_l * e_{\tau filt}(i,n-1) \quad (2.2)$$

Where β is a "forgetting" term that acts as a weight on the learned trajectory and K_l is a gain applied to the filtered torque error, $e_{\tau filt}$, which is calculated in Eq. 2.3.

$$e_{\tau filt}(i,n) = (1-\gamma) * e_{\tau filt}(i,n-1) + \gamma * e_\tau(i,n) \quad (2.3)$$

Where λ is a weighting term on the learned error.

Many other control strategies have been tried on the CMU emulator system, but proportional control with damping injection and iterative learning have proven to be the most effective. It is important to note that iterative learning, as implemented on the CMU emulator, has limited utility during non-steady state behavior as the cyclic nature of walking cannot be exploited. Other low-level control strategies may be required for accurate torque or position tracking during non-steady state behaviors.

Time based control has been used extensively on the ankle exoskeleton. After performing individualized optimization of control parameters, the time-based controller has delivered a 23% reduction in metabolic energy on average with some subjects experiencing reductions as high as 37% [2]. Proportional electromyographic (EMG) control and an EMG controller with a virtual muscle-tendon model have also been evaluated with mixed results. See chapter 6 for a comparison of time-based, proportional EMG, and virtual muscle control.

2.6 Making strides in the future

Emulator testbeds are accelerating exoskeleton development and will help researchers and industry partners to quickly develop viable commercial products that improve lives. Emulators allow more rapid progress than that possible using complex untethered systems based mainly on intuition without experimental data to guide design.

Whether designing exoskeletons as emulator end-effectors or as standalone untethered devices, many of the same guiding principles apply: keep designs simple, allow for natural motion, and minimize weight while maintaining safety and comfort.

While some researchers may develop untethered product-like devices to address problems like non-steady state locomotion and uneven terrain, there are more questions we can answer in the lab before making the leap to mobile systems. How can exoskeletons best improve stability and prevent falls? Which joints should we assist to improve maximum running speed? How does exoskeleton use affect muscle-tendon dynamics? How can we best facilitate user adaptation to assistive devices? Is there a single control strategy that is effective for multiple gaits? Can we use exoskeletons to teach novel skills such as dancing or football punting? How do the answers to these questions affect the design of our devices? It is our hope that researchers will tackle these questions and more by applying our guidelines for design and taking on the testbed strategy to help their exoskeletons evolve into effective tools efficiently and affordably.

Chapter 3

Design and characterization of ankle exoskeletons

Abstract

Lower-limb exoskeletons capable of high torques controlled at high bandwidth can be used to probe the neuromuscular system and assist or impede gait during rehabilitation. We developed two tethered ankle exoskeletons with strong lightweight frames, comfortable three-point contact, and series elasticity for improved torque control. Both devices are lightweight (0.88 kg), compliant in select directions, actuated by off-board motors and instrumented to measure joint angle, torque and heel contact. Torque is controlled using proportional feedback, damping injection, and iterative learning. We tested closed-loop torque control by commanding 20 N·m and 50 N·m chirps in desired torque while exoskeletons were worn by users or rigidly fixed, and measured bandwidths of up to 24 Hz. Separate tests demonstrated a peak power of 1 kW. In walking trials, we measured 120 N·m peak torque and 2 N·m RMS torque tracking error. These performance measures compare favorably with existing devices and ankle musculature. Our results validate a high-performance testbed that

A manuscript presenting this chapter is in preparation. Portions of this chapter were presented in the proceedings of ICRA 2015 [47].

can be used to explore a range of control techniques and robotic assistance paradigms.

3.1 Introduction

Exoskeletons have been used successfully to reduce the metabolic cost of normal [1] and heavily loaded walking [4]. They may be useful for aiding in rehabilitation of those with gait impairments [14], and for improving stability in the elderly. As these devices become more capable, we can imagine rescue workers using them to kick down barriers and carry victims to safety from disaster areas, or to aid military personnel.

While many possibilities exist for these devices, the best approaches to mechanical design, actuation and control are unknown. Human locomotion is a versatile and complex behavior that remains poorly understood, and designing devices to interact usefully with humans during walking is a difficult task.

Developing flexible testbeds in which actuation and control are located off-board can simplify the process of designing, manufacturing and testing exoskeletons, which allows for rapid and inexpensive iteration of both design and control strategies. Such 'emulator' systems typically involve off-board power transmitted either by flexible Bowden cable [79] [45] or pneumatics [80]. Off-board power and actuation make it relatively easy to meet or exceed the peak torque, velocity and power naturally produced in lower limb joints, which broadens the available experimental space without adding complexity to the exoskeleton design. For example, augmenting both walking and jumping might require a lower-limb exoskeleton to produce a large range of torque, velocity and power [81]. In addition to having high peak torque and power, exoskeleton emulators should also be highly responsive. High bandwidth allows desired torque trajectories to be realized with high fidelity despite unexpected changes in user behavior. Torque control is desirable, as opposed to position or velocity control, because these systems are used to provide wearers with the physical experience of interacting with an emulated device. This is best achieved if the forces experienced by the

user are rendered with the highest possible fidelity to those that would be experienced when using the emulated device.

Including a series elastic element, such as a spring, decouples the human from the inertia of the motor and gearbox and improves torque control [67]. The stiffness of the spring also determines the nominal behavior of the device, or the torque profile produced when the motor position is fixed while joint angle changes. The optimal stiffness is not known *a priori* as it may vary across subjects and applications, but it may be advantageous for the nominal behavior to approximately match desired torque trajectories [82]. As such, selectable stiffness may be desirable for better performance in different tasks.

Because exoskeletons act in parallel with a user, the overall compliance of the exoskeleton-human system likely affects its useful torque-control bandwidth. While an exoskeleton may have high torque and bandwidth capabilities on a test stand, results may change when a human is included in the system. For this reason, it may be best for the bandwidth of exoskeletons to be measured on the exoskeleton-human system, but this idea has yet to be tested empirically.

The ankle may be an effective location for applying assistance because it produces large peak torques and positive work during walking [83]. This is supported by the fact that increasing amounts of net work applied to the ankle can correspond to reductions in metabolic energy cost during walking [84, 85]. Even energetically passive ankle assistance can yield a benefit [30] Additionally, applying assistive torques to the ankle and the hip have been shown to be more effective than assisting the hip alone during load carriage [86]. Understanding how to assist the ankle joint with an exoskeleton will likely lead to better methods of designing and controlling exoskeletons for the entire lower-limb.

The effects of increased mass, constraint of natural motion and increased volume of the leg-exoskeleton system should be considered during the design process as they all have an effect on walking performance. Adding distal mass to the leg incurs a metabolic penalty [31, 87]. Additionally, the physical structure of exoskeletons can interfere with normal kinemat-

ics by inhibiting natural motions. Reducing the overall device envelope, especially medial and posterior protrusions, decreases additional metabolic energy costs associated with increased step width and circumduction [56]. For these reasons, it may be best for ankle exoskeletons to be mass efficient, have minimal protrusions from the leg, and restrict motion in uncontrolled directions as little as possible.

Even if an exoskeleton has high performance capabilities, its usefulness may be limited if it is not comfortable. Forces should be applied normal to the skin because shear forces cause discomfort, pain and increased risk of injury [61]. Applying forces normal to the user over a large surface area allows for greater magnitudes of applied force while maintaining comfort.

Interfacing with the user in areas with little soft tissue such as the shin can be more comfortable and may result in better efficiency of mechanical energy transfer between the exoskeleton and the user. By some estimates, as much as 50% of mechanical power supplied by exoskeletons can be dissipated in compression of soft tissues [88]. The most common attachment methods usually feature either padded straps or a padded rigid shell that clamps around the limb. It is not clear which attachment methods best limit migration, transmit power and provide comfort. New attachment methods [89] may soon provide improved load bearing capacity.

A good fit is important to comfort. Users vary in size and shape, such as leg length and calf circumference. Designing a new device for each user can result in a comfortable fit [90], but adds time and expense. Adjustability or modularity [91] provide freedom to fit a range of users, but adjustability often adds mass by requiring additional components, and modularity often requires bulky connective hardware to allow robust assembly and disassembly.

Our goal was to develop and characterize an ankle exoskeleton that fits a wide range of subjects and is capable of applying large torques at high power and bandwidth. Two candidate designs, Alpha and Beta, were developed as ankle exoskeleton end-effectors for a

tethered emulator system. The Alpha device was designed mainly to provide high compliance in selected directions in order to allow relatively uninhibited motion. The Beta device was designed to have reduced overall envelope with small medial protrusions. We then conducted experiments aimed at characterizing critical aspects of performance, including device mass, torque measurement accuracy, peak torque, closed-loop torque control bandwidth, peak joint velocity and peak mechanical power. We also sought to determine whether these performance measured differed when the device was worn on a person's leg compared to when it was held rigidly by a fixture on the benchtop. A final aim was to characterize device performance under practical conditions, considering torque tracking quality during walking, the effects of device envelope on step width and leg circumduction, and comfort and usability.

We presented preliminary findings from this study at the 2015 International Conference on Robotics and Automation. We have since collected improved data, particularly on force bandwidth, compared bandwidth as measured on a person's leg to that measured on a rigid test stand, performed tests of peak power, and measured average circumduction during walking.

3.2 Methods

We designed, built and tested two ankle exoskeletons to be used as end-effectors in a tethered emulator system (Fig. 3.1A). The prototypes, Alpha and Beta, were designed with different goals in mind. They have several similar features, such as series elastic elements and lightweight carbon fiber components. The Alpha exoskeleton was designed to provide compliance in selected directions, while the Beta exoskeleton was designed to reduce overall envelope while still accomodating a range of subject sizes. There is often a trade-off between these two goals and future designs may be influenced by whether or not performance differs greatly between the two exoskeletons.

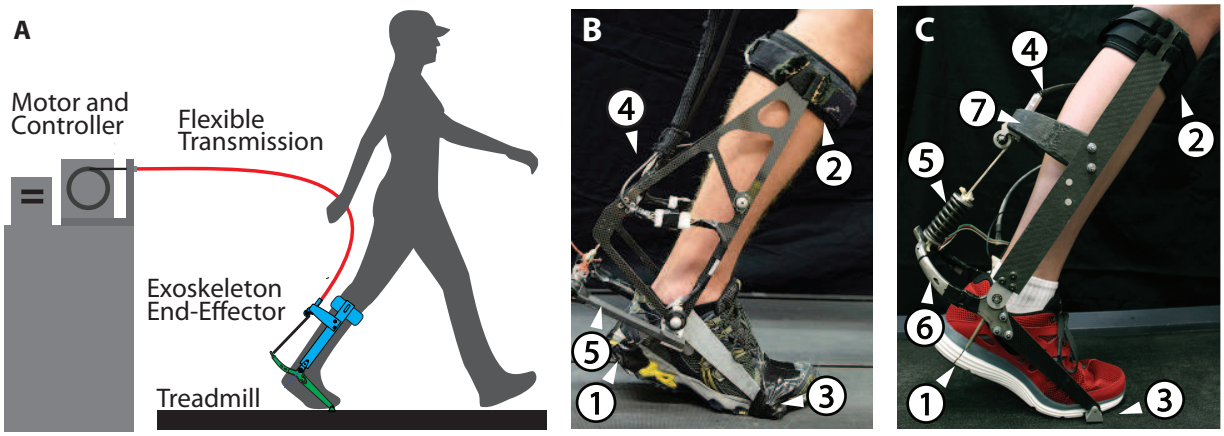

Figure 3.1: Emulator system and exoskeleton end-effectors. **A** The testbed comprises a powerful off-board motor and controller, a flexible Bowden cable transmission, and an ankle exoskeleton end-effector. **B** The Alpha design contacted (1) the heel using a string, (2) the shin using a strap, and (3) the ground using a hinged plate embedded in the shoe. The Bowden cable conduit attached to (4) the shank frame, while the Bowden cable rope terminated at (5) the leaf springs. **C** The Beta design. In addition to (1–4), this prototype has (5) a coil spring, (6) a titanium ankle lever wrapping behind the heel and (7) a hollow carbon fiber Bowden cable support.

Benchtop tests were used to determine characteristics such as closed-loop torque bandwidth, both while the device was worn by a user and while fixed in a rigid test stand. Walking trials were used to quantify outcomes such as torque tracking error, while also testing whether or not large torques could be comfortably applied.

3.2.1 Mechanical design

The ankle exoskeleton end-effectors were actuated by a powerful off-board motor and real-time controller, with mechanical power transmitted through a flexible Bowden cable tether. The motor, controller and tether are described in detail in [35].

Both ankle exoskeletons interface with the user in three locations: the foot under the heel, the shin below the knee, and the ground beneath the toe. The exoskeleton frames include rotational joints on either side of the ankle, with axes of rotation approximately collinear with that of the human joint (Fig. 3.1 B,C).

Each exoskeleton frame can be separated into foot and shank sections. The foot section has a lever arm posterior to the ankle that wraps around the heel. The Bowden cable pulls up on this lever while the Bowden cable conduit presses down on the shank section. This

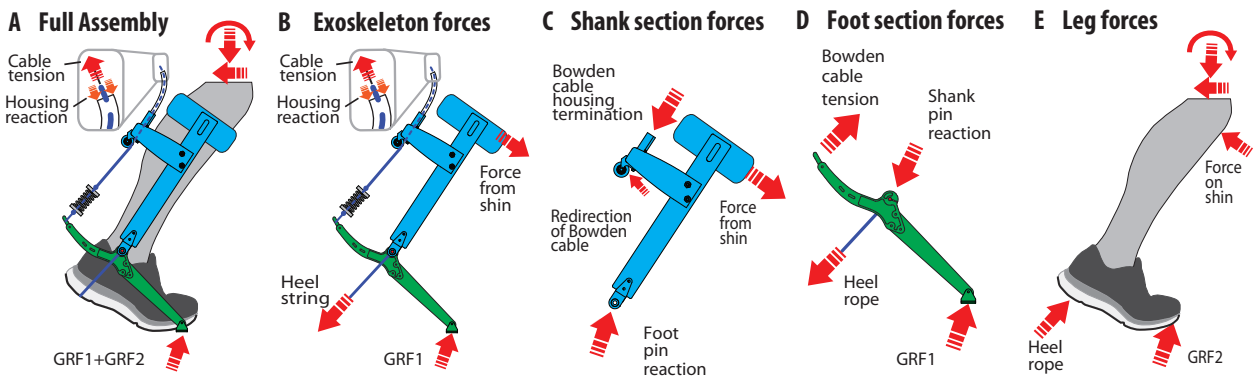

Figure 3.2: Free body diagrams of the exoskeleton structure. **A** The exoskeleton experiences a ground reaction force, GRF1 and the user experiences a ground reaction force, GRF2 on the bottom of the shoe. Forces in the Bowden cable conduit and inner rope (inset) are equal and opposite, producing no net external load on the leg. **B** The complete exoskeleton experiences external loads at the three attachment points, which together create an ankle plantarflexion torque. Forces at the conduit and inner rope are equal and opposite. **C** Shank section forces. **D** Foot section forces. **E** Forces acting on the user's leg.

results in an upward force beneath the user's heel, a rearward force on the top of the shin, and a downward force on the ground, generating a plantarflexion torque (Fig. 4.3).

The toe and shin attachment points are located far from the ankle joint, maximizing their leverage about the ankle and minimizing forces applied to the user for a given plantarflexion torque. Forces are comfortably transmitted to the shin via a padded strap, which is situated above the calf muscle to prevent the device from migrating downwards. Forces are transmitted to the user's heel via a lightweight synthetic rope placed in a groove in the sole of a running shoe.

The exoskeletons were designed to provide greater peak torque, peak velocity and range of motion than observed at the ankle during unaided fast walking. The Alpha and Beta devices were designed to withstand torques of 120 N·m and 150 N·m, respectively, limited by frame strength.

Both exoskeletons are modular to accommodate a range of subject sizes. Toe struts, calf struts, and heel strings can be exchanged to fit different foot and shank sizes. We designed and fabricated components that fit users with shank lengths ranging from 0.42 to 0.50 m and shoe sizes ranging from a women's size 7 to a men's size 12 (US). Slots in the calf struts allow an additional 0.04 m of continuous adjustability in the Beta device.

Series elasticity was provided by a pair of leaf springs in the Alpha design. The custom leaf springs were fiberglass (GC-67-UB, Gordon Composites, Montrose, CO, USA), which has a mass per unit strain-energy storage, $\rho E \sigma_y^{-2}$, one eighth that of spring steel [35], but mass savings were limited by additional hardware required for robust attachment. The leaf springs also functioned as the ankle lever in the Alpha exoskeleton, thereby reducing the number of components required. A stock coil spring (DWC-225M-13, Diamond Wire Spring Co., Pittsburgh, PA, USA) was used in the Beta design. The lever arm and joint assembly of the Alpha device were lighter by 0.059 kg compared to the Beta design (Table 3.1), but this comparison is confounded by factors such as different maximum expected loads and spring stiffnesses.

Spring type strongly affected overall exoskeleton envelope. The structure of the Alpha device extends substantially into space medial and posterior to the ankle joint (Fig. 3.3) and required an increase in user step width. The average maximal ankle external rotation during walking for healthy subjects is approximately 18° [92], and the average step width is only 0.1 m [93]. For this reason, the Beta exoskeleton was designed to reduce medial and posterior protrusions to prevent collisions between the device and the contralateral limb and excessive increases in step width during bilateral use. The maximum protrusion length measured from the center of the human ankle joint is 24% smaller than that of the Alpha design.

The plate-like components of the Alpha design were easily machined, while more complex Beta components were suited to additive manufacturing and lost-wax carbon fiber molding. The ankle lever experienced large bending and torsion loads, well addressed by I-beam and tubular structures. The ankle lever also required small, precise features for connection to the ankle shaft and toe hardware. Additive manufacturing using electron beam melting of titanium allowed these disparate design requirements to be addressed by a single component in the Beta device. The titanium component weighed 40% less than an equivalent structure from an earlier prototype comprised of a carbon fiber ankle lever, two

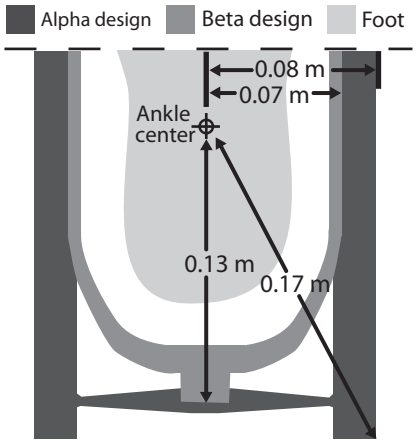

Figure 3.3: Comparison of envelopes of the two devices and human heel, depicted from above. The Beta device was slimmer in terms of mediolateral protrusion and maximum protrusion from the joint center.

aluminum joint components and connective hardware. The Beta Bowden cable termination support is subjected to similar loading as the ankle lever, but has less complex connection geometry, making a hollow carbon fiber structure appropriate.

The hollow carbon fiber Bowden cable support was manufactured using a lost wax molding method. A wax form with a threaded aluminum insert was cast using a fused deposition ABS shell-mold. A composite layup was performed on the wax form using braided carbon fiber sleeves. The wax was melted out by submerging the component in hot water. An alternative method of fabrication includes a hollow plastic mold instead of a wax casting. The plastic mold cannot be removed after the layup and adds a significant amount of mass as it must have sufficient structural strength to withstand the vacuum bagging process. For example, an earlier prototype utilized a permanent plastic mold that added 0.048 kg to the component.

Both exoskeleton designs provide structural compliance in directions that are not actively controlled. Thin plate-like shank struts act as flexures, allowing the calf strap to move medially and laterally and fit snugly around a wide range of calf sizes. This flexural compliance, in concert with sliding of the calf strap on the struts, sliding of the rope beneath the heel, and compliance in the shoe, allows ankle rotation in both roll and yaw during walking. The Bowden cable support connecting the medial and lateral shank struts is located

lower and further back from the leg in the Alpha design, allowing more deflection at the top of the struts. The Bowden cable support is located higher in the Beta design to allow space for the in-line coil spring, which reduces compliance near the calf strap and makes additional spacers necessary to appropriately fit smaller calves.

3.2.2 Sensing and control

Both devices sense ankle angle with optical encoders (E4P and E5, respectively, US Digital Corp., Vancouver, WA, USA) and foot contact with switches (7692K3, McMaster-Carr, Cleveland, Ohio, USA) in the heel of the shoe. The Alpha exoskeleton uses a load cell (LC201, Omega Engineering Inc., Stamford, CT, USA) to measure Bowden cable tension. The Beta exoskeleton uses four strain gauges (MMF003129, Micro Measurements, Wendell, NC, USA) in a Wheatstone-bridge configuration on the ankle lever to measure torque directly. Bridge voltage was sampled at 5000 Hz and low-pass filtered at 200 Hz to reduce the effects of electromagnetic interference. A combination of classical feedback control and iterative learning was used to control exoskeleton torque during walking [94]. Proportional control with damping injection was used in closed-loop torque controlled bandwidth tests.

For walking tests, desired torque was computed as a function of ankle angle and gait cycle phase. During stance, desired torque roughly matched the average torque-angle relationship of the ankle during normal walking using a control method described in detail in [35]. During swing, a small amount of slack was maintained in the Bowden cable, resulting in no applied torque.

3.2.3 Experimental methods

Torque sensors were calibrated by removing and securing the ankle lever upside down in a jig. Torque was incrementally increased by hanging additional weights of known mass from the Bowden cable. We computed root mean squared (RMS) error between applied and measured torque from the calibration set.

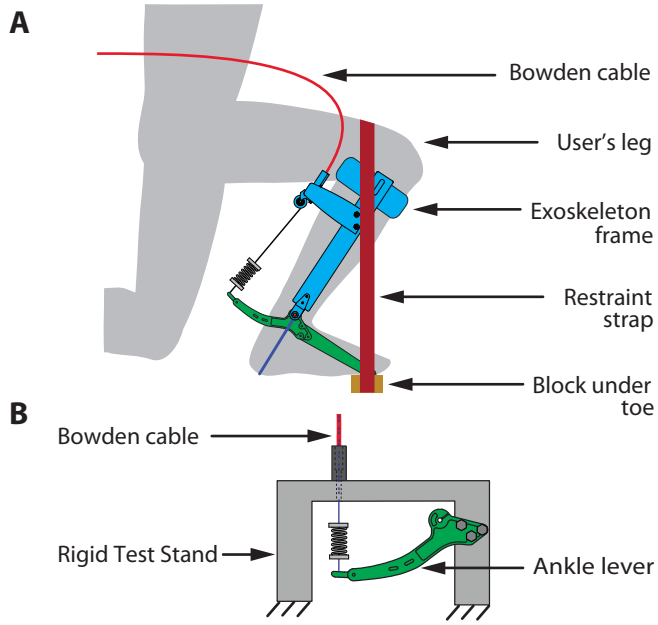

Figure 3.4: Bandwidth test setups. **A** The exoskeleton worn by a user. The leg was restrained using a strap that wrapped over the thigh and attached to a block beneath the toe segment. The exoskeleton acts in parallel with the user's leg. As such, the leg is part of the plant and may play a large role in determining the bandwidth of the device. It may be worth measuring the useful bandwidth of the device while worn by a user. **B** Bandwidth setup with the ankle lever attached to a rigid test stand.

We performed closed-loop torque bandwidth tests on the ankle exoskeleton while worn by a user. This captured the effects of compliance in soft tissues and exoskeleton strapping on torque control. The user's ankle was restrained by a strap that ran under the toe and over the knee (Fig. 3.4A). Linear chirps in desired torque were applied with a maximum frequency of 30 Hz over a 30 second period, and measured torque was recorded. Bode frequency response plots were generated using the Fourier transform of desired and measured torque signals. Tests were performed at two peak-to-peak amplitudes, 20 N·m and 50 N·m. An offset in desired torque was used to prevent the cable from going slack, such that the desired torque oscillated between 10 N·m and 30 N·m or 10 N·m and 60 N·m, respectively. Ten tests were performed at each amplitude and results were averaged. Bandwidth was calculated as the lesser of the -3 dB cutoff frequency and the 30° phase margin crossover frequency [95].

Bandwidth tests were then repeated with the Beta exoskeleton fixed to a rigid test stand, rather than worn on a person's leg. During these tests, the titanium ankle lever was re-

moved from the exoskeleton frame and mounted in a fixture (Fig. 3.4B).

Peak power was tested in a setup similar to that used in the bandwidth test with the user included as part of the plant. Two extension springs in parallel (9630k9, McMaster-Carr Cleveland, OH, USA) were added to the restraint strap to allow plantarflexion under application of high torques. A step in motor velocity of 105 rad·s^{-1} was commanded for a period of 0.039 s. Ankle angle was measured by the optical encoder at the mechanical joint, while torque was measured by the strain guages located on the ankle lever arm. Exoskeleton mechanical power was then calculated as the product of joint torque and joint velocity, and the peak value of power from each trial was identified and averaged.

Torque tracking performance was evaluated during walking trials with a single healthy subject (1.85 m, 82 kg, 36 yrs, male). Data were collected during 100 steady-state steps while walking on a treadmill at 1.25 m·s^{-1}. RMS error was calculated over the entire trial and for an average step.

Leg circumduction about the hip was measured online using a marker-based motion capture system. A seven camera system (Vicon, Oxford, UK) measured the position of reflective markers attached to the medial malleolus of both ankles. Circumduction was characterized by the horizontal distance between the markers at midstance, which was defined as the moment that the ankle marker of the swing foot passed the ankle marker of the stance foot in the sagittal plane. Clearance between the medial markers was calculated for each step and then averaged.

3.3 Results

Table 3.1: Mass breakdown (kg)

Assembly	Alpha	Beta
Lever Arm, Spring and Joint	0.256	0.315
Struts and Bowden Cable Support	0.258	0.312
Toe Plates	0.154	0.074
Straps	0.063	0.120
Wiring and Sensors	0.104	0.054
Total	**0.835**	**0.875**

The total mass of the Alpha and Beta exoskeletons were 0.835 and 0.875 kg, respectively (a mass breakdown is provided in Table 3.1). The peak plantarflexion velocities, limited by motor speed, of the Alpha and Beta devices are 30 rad·s^{-1} and 33 rad·s^{-1}, respectively. Both devices allow a range of motion of 30° plantarflexion to 20° dorsiflexion, with 0° corresponding to a natural standing posture.

Torque measurement accuracy tests demonstrated that the Alpha and Beta exoskeletons have RMS measurement error of 0.751 N·m and 0.125 N·m, respectively (Fig. 3.7A).

The gain-limited (-3 dB) closed-loop torque bandwidths of the Alpha device with 20 N·m and 50 N·m peak torques were 21.0 Hz and 13.2 Hz, respectively (Fig. 3.7B) while being worn by a user. The phase-limited (30° phase margin) bandwidths for the Beta device with 20 N·m and 50 N·m peak torques were 24.2 Hz and 17.7 Hz, respectively (Fig. 3.7B) while being worn by a user.

When the Beta device was tested while fixed in a rigid test stand, the -3 dB crossover frequencies were much higher. In 20 N·m amplitude bandwidth trials the -3 dB crossover was measured to be 34.4 Hz, and bandwidth was phase-limited at 23.6 Hz. In 50 N·m trials the -3 dB crossover was measured to be 34.1 Hz, and bandwidth was phase-limited at 22.0 Hz (Fig. 3.6).

In peak power tests on the Alpha device, the maximum peak power observed was 1138 W with an average peak power of 1068 W. The Beta device delivered a maximum observed power of 1000 W and an average peak power of 892 W (Fig. 3.7C).

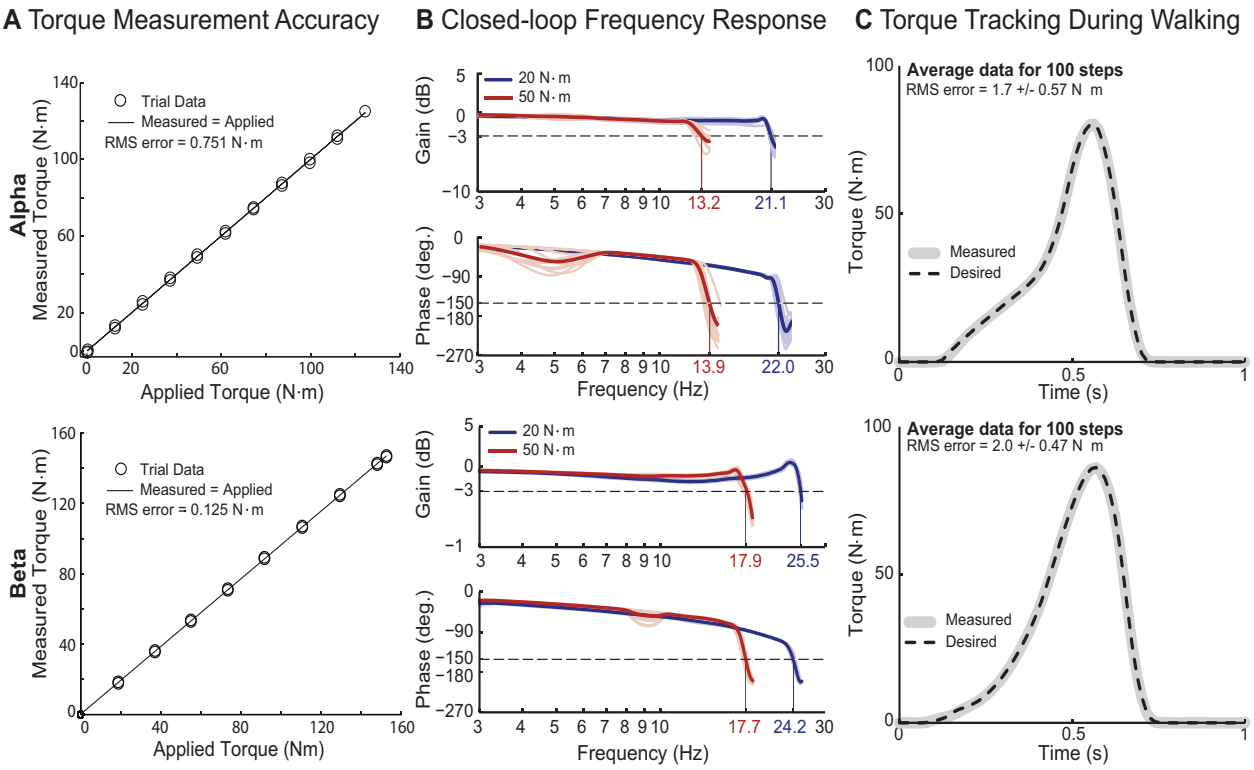

Figure 3.5: Experimental results from tests of the Alpha (top) and Beta (bottom) prototypes. **A** Torque measurement calibration results. **B** Bode plots depicting frequency response of the system with peak desired torques of 20 N·m (blue) and 50 N·m (red). Gain and phase crossings were very close for both devices indicating good controller tuning. All 10 indivicual trials shown in pale blue and red for 20 N·m and 50 N·m cases respectively. **C** Average desired and measured torque from 100 steady-state walking steps.

In walking trials with the Alpha device, the peak average measured torque was 80 N·m. The maximum observed torque was 119 N·m. The RMS error for the entire trial was 1.7 ± 0.6 N·m, or 2.1% of peak torque, and the RMS error of the average stride was 0.2 N·m, or 0.3% of peak torque (Fig. 3.7C). For the Beta device, the peak average measured torque was 87 N·m. The maximum observed torque was 121 N·m. The RMS error for the entire trial was 2.0 ± 0.5 N·m, or 2.4% of peak torque, and the RMS error of the average stride was 0.3 N·m, or 0.4% of peak torque (Fig. 3.7C).

The Alpha device resulted in much greater circumduction than the Beta device. Average ankle clearance at midstance with the Alpha and Beta devices were 0.118 m and 0.067 m, respectively. The Alpha device therefore required 76% greater ankle clearance than the Beta device (Fig. 3.8).

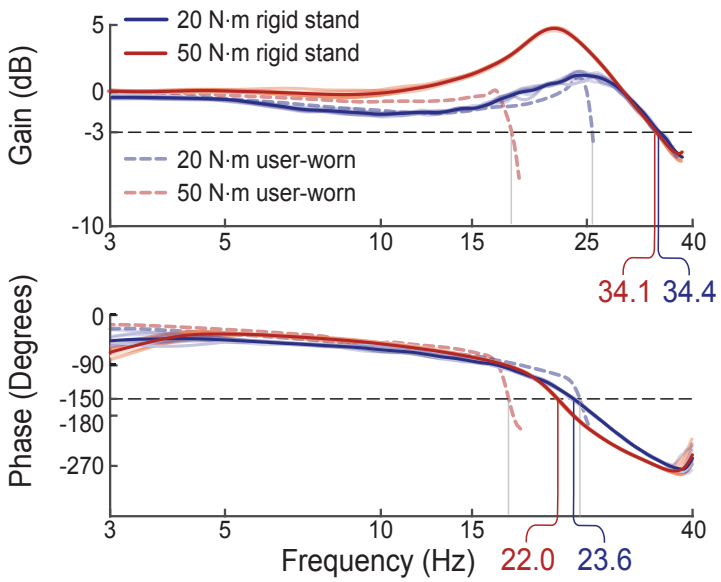

Figure 3.6: Bode Plot depicting frequency response of the Beta system when mounted on a rigid test stand. Results from frequency response tests with the exoskeleton worn on a user's leg are superimposed in dotted lines to show differences in performance. Large differences between gain-limited and phase-limited bandwidth may suggest that the system is less stable without the user. Similar bandwidth for both the 20 N·m and 50 N·m cases on the rigid test stand may indicate fewer non-linearities in the system without the user.

3.4 Discussion

Our primary aim was to design and characterize lightweight, modular ankle exoskeletons capable of a broad range of mechanical behaviors during interactions with humans. We designed two exoskeletons and characterized their performance in benchtop tests and walking trials. The results verified that both the Alpha and Beta exoskeletons were capable of comfortably and accurately applying torques and powers exceeding the values of the biological ankle during normal walking.

Our experimental results demonstrate that the performance of both exoskeletons compare favorably to similar devices. Weighing less than 0.88 kg, both exoskeletons are lighter than a tethered pneumatic device used for probing the biomechanics of locomotion [90] and an autonomous device for load carriage assistance [4]. A soft exoskeleton is lighter weighing in at 0.92 kg for bilateral ankle assistance (0.46 kg per ankle), but is designed to apply smaller loads on the order of 25 N·m with an impressively small overall envelope [53]. In walking tests with users of varying shank lengths (0.42 m to 0.50 m), we comfortably applied

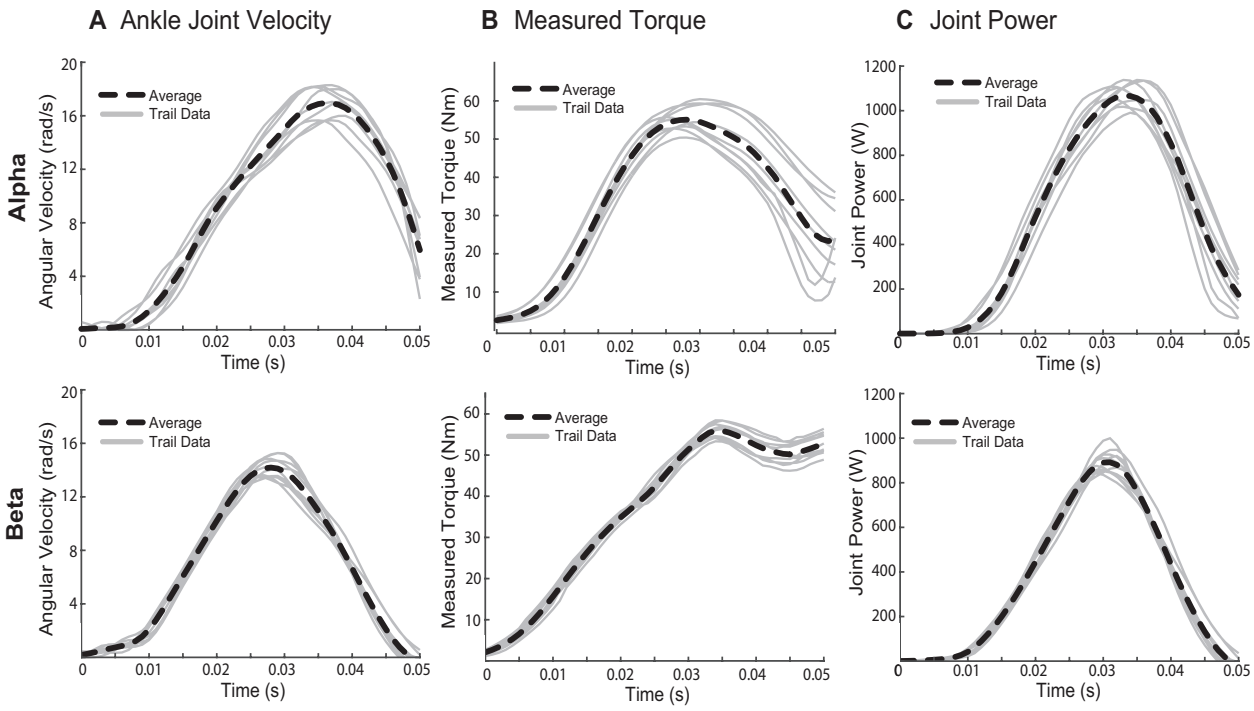

Figure 3.7: Results from power tests of the Alpha (top) and Beta (bottom) prototypes. **A** Ankle joint velocity. **B** Measured ankle torque. **C** Measured joint power. The average peak power was measured to be 1068 W for the Alpha exoskeleton and 892 W for the Beta exoskeleton.

peak torques of 120 N·m, comparable to values from similar devices [90, 1, 96].

Both exoskeletons tested here demonstrated six times the torque bandwidth of pneumatically actuated devices [1]. We found a force bandwidth similar to that of the actuator of a soft exoskeleton (20 Hz with 18 N·m peak-to-peak amplitude in [53]). However, comparing bandwidth to other similar devices is difficult due to inconsistency in testing and reporting. The experimental setup can have a strong effect on the measured usable bandwidth of the system. For example, bandwidth is usually tested using a single amplitude of force signal. In our experiments, bandwidth was measured to be about 7 Hz higher when commanded torque had an amplitude of 20 N·m compared to 50 N·m. If the system were linear, bandwidth would be independent of desired torque amplitude. However, nonlinearities in the system, such as motor saturation in series elastic actuators [97], can result in bandwidth that varies with torque magnitude.

Soft tissues are another source of nonlinearities that can affect bandwidth. The soft tissues of the user introduce non-linear changes in stiffness and damping. For this reason,

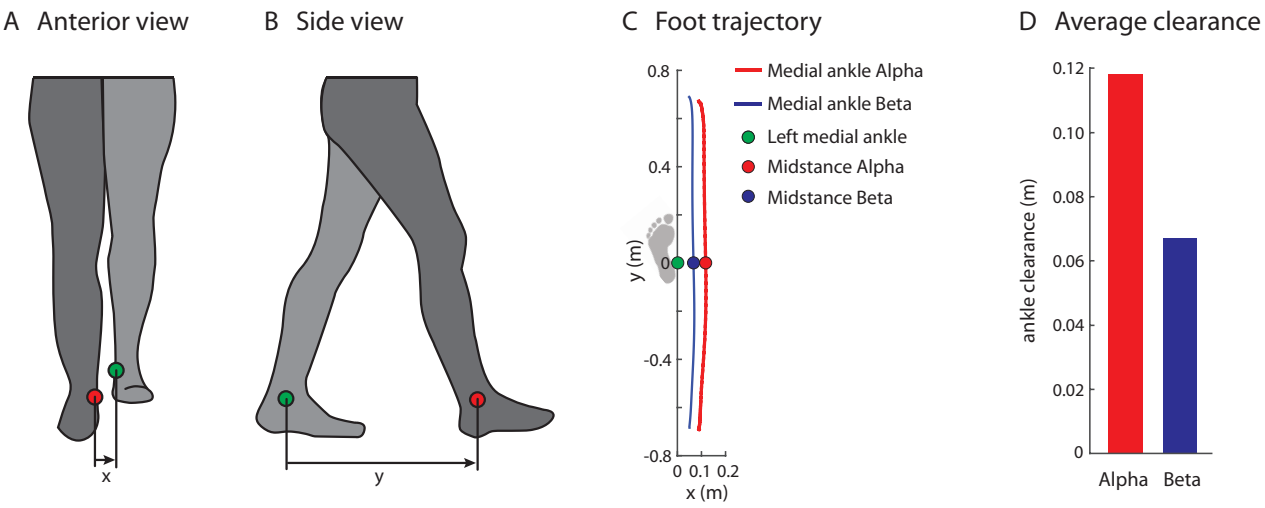

Figure 3.8: Foot tracking during zero impedance walking. **A** Posterior view depicting medial-lateral distance (x) between ankle markers. **B** Side view depicting fore-aft distance (y) between ankle markers. **C** Average motion capture data for 100 steps. The green dot represents the left medial ankle marker during stance. The red and blue lines represent the position of the right medial ankle marker from toe off to heel strike while walking with the Alpha and Beta exoskeletons, respectively. The dots represent the position of the right ankle marker during mid-stance at which point clearance was measured. **D** Average medial-lateral separation between the medial ankle markers at mid-stance.

it may be most useful to measure bandwidth for the device-user plant as a whole rather than for the actuator alone. Effects of the user on bandwidth were demonstrated by our comparison of performance both with a user and a without a user on a rigid test stand. The -3dB cuttoff frequency increased by about 40% when tested on a rigid test stand, and this value remained constant for both the 20 N·m and 50 N·m trials. This suggests that non-linearities that were present when worn by the user were absent on the rigid test stand. It was previously believed that non-linearities in the system such as motor velocity saturation and Bowden cable dynamics were responsible for the drop in bandwidth from high to low torque, but these dynamics remained unchanged in tests on the rigid test stand and cannot account for the difference in bandwidth. Instead, the user must be the main source of non-linearities in the system. Resonance caused more severe unwanted increases in applied torque at higher frequencies during testing on a rigid stand than on a user, suggesting that the user significantly increases damping in the system. While the phase-limited bandwidth and gain-limited bandwidth were similar for each condition when testing on a user, we found that the gain-limited bandwidth was greater than the phase limited bandwidth by

more than 10 Hz when tested on the rigid test stand. This may suggest that the system is less stable without the user as soft tissues add damping to the system resulting in less overshoot. These differences illustrate why it is important to report bandwidth as measured on a user as the useful dynamic range of the device may be overestimated or underestimated if only the bandwidth of the actuator is reported. Lastly, tuning of the motor should be performed with a user as part of the system when using closed loop control, because optimal proportional and damping gains may vary greatly between these conditions.

The high performance of these devices is largely enabled by powerful off-board motors, but many design choices also affected comfort and performance. Three-point contact with the user's leg implemented in both exoskeletons provided comfortable interfacing. Attachment point locations were chosen to provide a relatively stiff interface due to limited soft tissues and to maximize lever arms thereby minimizing the magnitude of forces applied to the body. Compliance in selected directions reduced interference with natural motions. Although differences in design led to more rigid struts in the Beta exoskeleton, compliance in the shoe and heel rope was sufficient to enable comfortable walking.

The heel rope was key to the low mass of these devices. It is an extremely simple and efficient method of applying an upward force to the heel that is easily adjustable, and has been used with success on other ankle exoskeletons [4, 98]. Instead of using a heel rope, several designs require an orthotist to fabricate custom heel cups for each user [99], which can improve fit, but requires substantially more time and adds to the cost of conducting an experiment. The easily manufactured modular components of the Alpha and Beta exoskeletons allow for accurate alignment of the mechanical joint with the human joint for a wide range of users. However, making components in a variety of sizes and exchanging these components is time consuming. An adjustable design may reduce these costs, but usually at the cost of added mass, which would increase discomfort for users. These devices are designed to be symmetric across their lateral center, but for many subjects, the calf protrudes much further from the leg center on the lateral side of the body than it does on the

medial side. This can shift the device signifcantly to the outside of the leg and can result in discomfort and undesireable loading. An additional degree of adjustability or modularity to account for leg asymmetry would be beneficial.

Medial-lateral foot displacement at mid-stance was almost twice as large with the Alpha exoskeleton as with the Beta exoskeleton. This was mainly due to the Beta device's smaller envelope, which was achieved through the manufacturing of more organically shaped components using additive manufacturing and lost-wax carbon fiber layups. This is beneficial because large envelopes may require users to increase step width and circumduction, resulting in higher metabolic energy consumption [33] and increased likelihood of collisions between the exoskeleton and the contralateral limb. However, the lost-wax carbon fiber layups require a wax casting of the part to be made, which is time consuming. Additionally, the wax casting can be extremely fragile and must be handled with care during the layup process. The electron beam sintered titanium heel lever allowed for hollow geometry, but access vents were required for the removal of titanium powder from the cavity. The unwanted titanium powder is partially sintered and must be forcibly removed. This requires the access vents to be large enough for dental tools to reach the entire cavity. These large vents reduce the strength of the component and limit the mass savings available through additive manufacturing. Additionally, post processing of the titanium component included drilling of all holes to specifications and surface finishing, both of which are challenging for this material. The component was more time consuming to produce and an order of magnitude more expensive than the equivalent Alpha structure.

Anthropomorphic joints used in the Alpha and Beta designs made measurement of ankle angle simple and accurate. Double shear connections at medial and lateral joints in the Beta design resulted in consistent shaft and encoder alignment. Co-axial single shear joints used in the Alpha design were less robust to loading out of the sagittal plane. Removing the explicit joint from an exoskeleton can reduce overall device weight and envelope while not compromising structural strength [4]. However, this approach complicates measurement of

the ankle angle, limiting the variety of control strategies that can be implemented. Removing the explicit joint also tends to yield structures with larger envelopes, which we have seen can increase circumduction.

Spring choice greatly affected overall mass, robustness, and device envelope. Leaf springs are theoretically much lighter than coil springs for a given stiffness, but increased size and additional hardware for improved robustness can limit mass savings. The Alpha lever arm assembly, including the two leaf springs, aluminum cross-bar, and connective hardware, was 19% lighter than the coil spring and titanium assembly of the Beta design. This comparison is confounded by the fact that the Beta exoskeleton was designed for larger loads than the Alpha design and the fact that the two devices have different spring stiffnesses. The Beta exoskeleton originally used a fiberglass leaf spring, which made the assembly 0.040 kg lighter and lengthened the ankle lever arm, thereby reducing torques at the motor. This leaf spring was prone to breaking, however and was replaced with a coil spring. The coil spring, though heavier, increased robustness and made interchanging springs of different stiffnesses easier and cheaper, because the fiberglass leaf springs had to be custom machined for each stiffness. If the optimal stiffness is unknown, it may be advisable to use a coil spring as it can be exchanged easily and inexpensively. If the optimal stiffness is known and the device is being used unilaterally, leaf springs may be advisable as they are lighter. If leaf springs are desired for bilateral use, a less boxy configuration than that shown on the Alpha device would be preferable.

Series elasticity plays a large role in torque tracking performance, but optimal spring stiffness may be a function of individual morphology, peak applied torques, and control strategies and might be difficult to predict. This makes adjustable or easily exchangeable springs advantageous. In pilot tests with the Beta device, we found that very stiff or very compliant elastic elements worsened torque tracking errors. This was not the case for a prosthetic device we developed [51], in which the Bowden cable itself provided sufficient series compliance. This may be because the prosthesis is in series with the limb, and therefore

receives more predictable loading. It would be useful to perform experiments characterizing the relationship between spring stiffness and torque tracking under a variety of conditions.

Tether dynamics play a large role in determining the bandwidth of the exoskeletons. Oscillations were present in the Bode plot phase diagram for the Alpha device at high torque and lower frequencies. It was considered that this may have been an artifact of the fast Fourier transform used to generate the plot due to insufficient data in the lower frequency range. However, we conducted bandwidth tests which included more data in the lower frequency range by commanding exponential rather than linear chirps, and the results were not significantly altered. We found that adjusting the routing of the Bowden cable had a large effect on the amplitude of the low frequency oscillations, suggesting the phenomena is a result of tether dynamics. It seems that minimizing the overall length and cumulative bending of the Bowden cable can reduce the amplitude of the oscillations. Therefore the routing of the Bowden cable should be carefully planned to maximize performance, and exploration of alternate transmission elements is warranted.

While both exoskeletons have high performance capabilities, we found the Beta design to be more suited to our purposes. The plate-like struts of the Alpha exoskeleton supply desirable compliance, but also a large envelope. This leads to wider steps and can cause collisions with the contralateral limb, which we anticipate would become a more serious issue if used bilaterally. The smaller envelope of the Beta device mitigated this issue. While the Beta design reduced compliance in directions orthogonal to the direction of the applied assistance, compliance in the shoe and strap seems to be sufficient to allow comfortable walking.

The use of a powerful, flexible testbed allowed these two designs to be implemented quickly and inexpensively. The development and testing of these devices has confirmed that widely spaced connections to the user, small overall device envelope, compliance in uncontrolled directions, series elasticity, and adjustability through modularity are desirable traits in lower-limb exoskeletons.

3.5 Conclusions

We designed, manufactured, and tested two ankle exoskeletons which proved to have high peak torque, peak power and closed-loop torque bandwidth and low torque tracking errors during walking. These devices allow accurate realization of a wide range of ankle exoskeleton behaviors, which will enable exploration of novel assistance strategies. Series elasticity, selective compliance, three-point attachment, form-fitting components, double-shear joints, and powerful off-board motors facilitate effective interactions between the exoskeleton and the user.

The Alpha exoskeleton features increased compliance in uncontrolled directions, inexpensive manufacturing, and lighter construction due to the use of leaf springs as both series elastic elements and lever arms. However, this design includes larger medial and posterior protrusions than the Beta device, which results in more circumduction and therefore less natural gait. The Beta device features strain gauges which proved to be lighter, more accurate, and less expensive than the load cell used on the Alpha device. The coil spring, while heavier than leaf springs, is more robust and allows stiffness to be adjusted easily. While the flowing three-dimensional carbon fiber forms of the Beta device allowed for a close fit, they were time consuming to construct. These illustrate some of the trade-offs to consider in exoskeleton design.

Differences between the results of bandwidth tests on a rigid fixture and those conducted while the exoskeleton was mounted to a user's leg demonstrate the importance of human compliance, damping and other dynamics when characterizing the dynamic response of wearable robots. High values of closed-loop exoskeleton bandwidth reported on the basis of benchtop tests alone likely overstate useful system performance.

The approaches demonstrated here could also be implemented in knee and hip exoskeletons, allowing researchers to explore biomechanical interactions across joints during locomotion as well as to analyze the effect of different assistance strategies.

Chapter 4

Design and characterization of knee exoskeletons

Abstract

Lower-limb exoskeletons show promise for improving gait rehabilitation for those with chronic gait abnormalities due to injury, stroke or other illness. We designed and built a tethered knee exoskeleton with a strong lightweight frame and comfortable, four-point contact with the leg. The device is structurally compliant in select directions, instrumented to measure joint angle and applied torque, and is lightweight (0.76 kg). The exoskeleton is actuated by two off-board motors. Closed loop torque control is achieved using classical proportional feedback control with damping injection in conjunction with iterative learning. We tested torque measurement accuracy and found root mean squared (RMS) error of 0.8 Nm with a max load of 62.2 Nm. Bandwidth was measured to be phase limited at 45 Hz when tested on a rigid test stand and 23 Hz when tested on a person's leg. During bandwidth tests peak extension torques were measured up to 50 Nm. Torque tracking was tested during walking on a treadmill at 1.25 m/s with peak flexion torques of 30 Nm. RMS torque

A manuscript presenting this chapter is in preparation. Portions of this chapter were presented in the proceedings of ICORR 2017 [100].

tracking error averaged over a hundred steps was 0.91 Nm. We intend to use this knee exoskeleton to investigate robotic assistance strategies to improve gait rehabilitation and enhance human athletic ability.

4.1 Introduction

Many lower-limb exoskeletons are under development and the potential for these devices is vast. They have been used to reduce the metabolic cost of normal [1, 21] and load-carrying walking [4]. They may be useful for aiding in rehabilitation for those with gait impairments [14, 101], and for improving stability in the elderly. Looking forward, we can imagine such scenarios as rescue workers using exoskeletons to carry victims to safety from disaster areas, or paralyzed individuals using exoskeletons for complex locomotor tasks such as hiking on uneven terrain.

While many possibilities exist for these devices, the best approaches to mechanical design, actuation and control are unknown. Human locomotion is a versatile and complex behavior and designing devices to interact usefully with humans during walking or running is a difficult task. Complex autonomous exoskeletons are often designed based on informed guesses as to what will be helpful. If these devices fail to interact usefully with a user, the design may be too complicated to easily adjust, so another prototype must be built before exploring the next candidate assistive strategy, which is time consuming and expensive.

Modular, high performance testbeds can be used to rapidly and inexpensively explore many design and control strategies for assisting gait, and the information gained can then be used to develop useful autonomous devices. Developing testbeds in which actuation and control are located off-board simplifies the process of designing, manufacturing and testing exoskeletons. Off-board power and actuation allows for large motors which can easily meet or exceed the peak torque, velocity and power naturally produced at the knee. High bandwidth enables testbeds to accurately render torque profiles to give the user the most

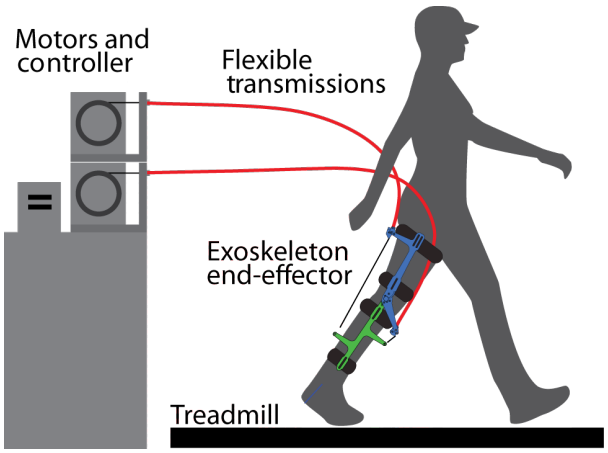

Figure 4.1: Emulator system and knee exoskeleton end-effector. Mechanical power is transmitted from powerful off-board motors to the end-effector via flexible Bowden cable transmissions (red). The end-effector can be divided into two major sections: the thigh section (blue) and the calf section (green). These are joined by an aluminum rotary joint approximately colocated with the center of rotation of the human knee. The device attaches to the user with four padded straps located at the top of the thigh, just above the knee, just below the knee, and above the ankle.

realistic experience of interacting with an emulated device. For example, it may be useful to give subjects the experience of wearing a passive exoskeleton to discover the most effective spring and clutch properties before developing new hardware. High performance capabilities of the testbed broaden the available experimental space without adding complexity to the exoskeleton design.

Highly capable testbeds may be used to discover the most useful controller settings for an individual using human-in-the-loop optimization. We recently used a testbed to apply a wide range of torque profiles generated using an evolutionary strategy to optimize an ankle exoskeleton controller for each individual subject. This strategy resulted in the greatest reductions in the metabolic cost of walking to date [2], which may not have been possible with a less capable system. Clinics may be able to use optimization strategies like this on testbeds for prescription of robotic devices such as exoskeletons and prostheses.

The mass and overall envelope of exoskeletons should be limited. End-effectors should have mass properties similar to the devices they are emulating. It is simple to add mass to match an emulated device, but difficult to remove it. Additionally recruitment for some protocols can be difficult if the task is excessively energetically taxing. For example, running

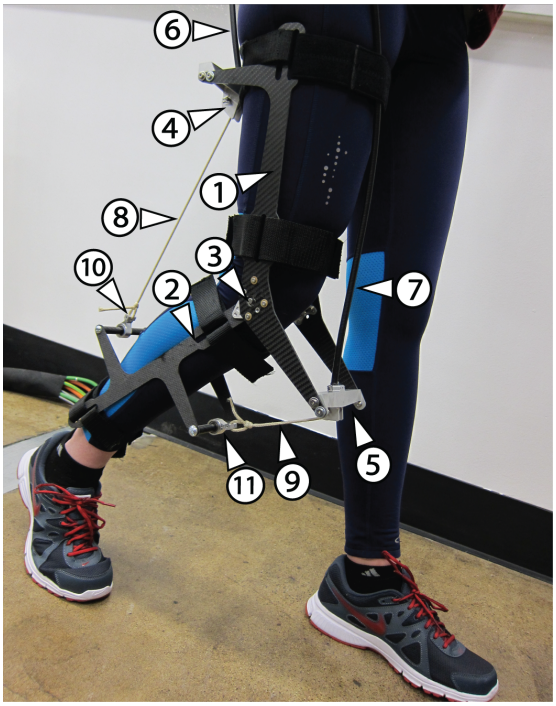

Figure 4.2: Large planar struts make up the frame of the exoskeleton. The thigh struts (1) are connected to the calf struts (2) by an aluminum rotary joint (3) approximately colocated with the center of rotation of the user's knee. Aluminum crossbars (4 and 5) connect the lateral and medial struts and include termination points for the Bowden cable housings (6 and 7) as well as pulleys for redirecting the inner Bowden cables (8 and 9) as the knee angle changes. The inner cables extend from the crossbars to aluminum cable anchors (10 and 11) which are mounted on bearings on the lower carbon fiber crossbars attached to the calf struts.

for any amount of time while wearing an exoskeleton with unoptimized settings may be exhausting. Energetic penalties incurred by wearing an exoskeleton can be reduced by minimizing mass and size of protrusions on the medial aspect of the leg as distal mass and increased circumduction for leg clearance are costly [31, 87, 56].

Even if an exoskeleton has high performance capabilities, its utility is limited if it is not comfortable. Comfort is maintained by applying forces normal to the user, achieving a good fit and accomodating the range of motion of the assisted joint. Forces should be applied normal to the skin as shear forces applied to skin cause discomfort, pain and increased risk of injury and occlusion [61]. Applying forces over large surface areas allows for greater magnitudes of applied force while maintaining comfort. Users may vary in anthropometry, such as body mass and leg length. Designing a new device for each user results in a comfortable fit [90], but at an additional expense. Adjustability or modularity [91] provide freedom to

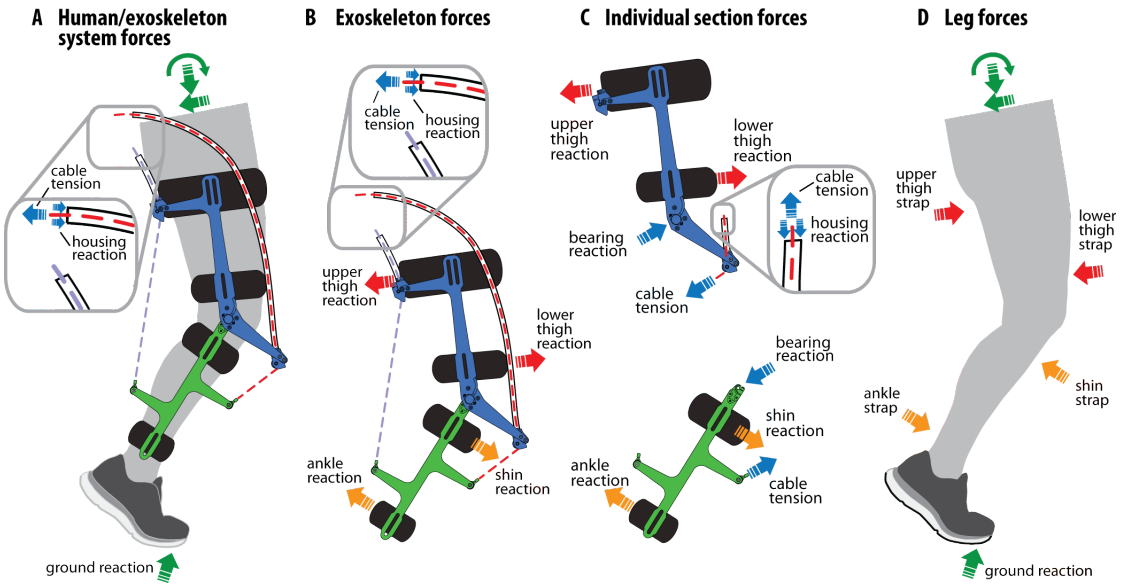

Figure 4.3: Free body diagrams of the exoskeleton structure. For the purposes of these diagrams, only knee extension torques are being applied. This means there is tension in the extension rope on the anterior side of the leg and the flexion rope is slack. **A** Resultant forces acting on the user's leg. The exoskeleton interacts with the user at four straps: At the top of the thigh, above the knee, above the calf muscle, and just above the ankle.**B** Forces in the Bowden cable conduit and inner rope (inset) are equal and opposite, producing no net external load on the leg. **C** The complete exoskeleton experiences external loads at each of the four straps. **D** Thigh section (blue) forces and calf section (green) forces. Cable tension and joint reaction forces are equal and opposite.

fit a range of users, but adjustability often adds mass by requiring additional components, and modularity may require bulky connective hardware to allow frequent reconfiguration. Designing for compliance in select directions can allow a better fit without added components by enabling the frame to act as a flexure to bend in and out to accommodate users of different shapes. Select compliance can also enable an exoskeleton to allow additional limited degrees of freedom that are not explicitly accounted for in the joint design.

A knee exoskeleton may make an interesting end-effector for a test bed as the human knee produces large peak torques and absorbs impact during walking and running [102]. A knee exoskeleton may also be useful in conjunction with an ankle exoskeleton in order to better assist the gastrocnemius muscle. When an ankle exoskeleton is used to aid walking, activity in the soleus and gastrocnemius muscle can decrease resulting in a reduction in metabolic energy consumption [103, 66, 104]. Assistance provided at the ankle alone is

limited as the gastrocnemius acts to both plantarflex the ankle and flex the knee during push off. An exoskeleton capable of assisting both the ankle and the knee may be most effective to target the gastrocnemius for assistance.

The human knee has six degrees of freedom including flexion and extension, external and internal rotation, varus and valgus rotation, and three degrees of translation, which must be accomodated either explicitly or through high compliance in order to maintain comfort. The knee is not well approximated by a rotary joint as the axis of rotation displaces between 8 and 20 mm as the joint flexes [105]. The knee also experiences between 5 and 10 degrees of external rotation automatically as the leg extends [106, 34]. The degree of varus or valgus rotation of the knee is nearly constant for each individual, but ranges across subjects. The last three degrees of freedom are translational, the largest of which is anterior/posterior sliding between the femur and the tibia which can be as much as 19 mm [34]. Compliance between the exoskeleton frame and the user's skeleton may be sufficient to accommodate these movements without bulky explicit degrees of freedom.

We aimed to develop a knee exoskeleton emulator that fits a wide range of subjects through modularity and compliance. Experiments presented here demonstrate the device is a useful tool for testing assistance strategies for rehabilitation or human performance augmentation.

4.2 Methods

We designed, built and tested a knee exoskeleton to be used as an end-effector in a tethered emulator system (Fig. 4.1). The prototype is designed to provide structural compliance in select directions and to provide torques similar to those observed in the biological knee during running. Benchtop tests were performed to determine force measurement accuracy, step response, and force bandwidth. Bandwidth was measured both on a human user and with the force sensor fixed in a rigid test stand. Walking tests were performed to quantify

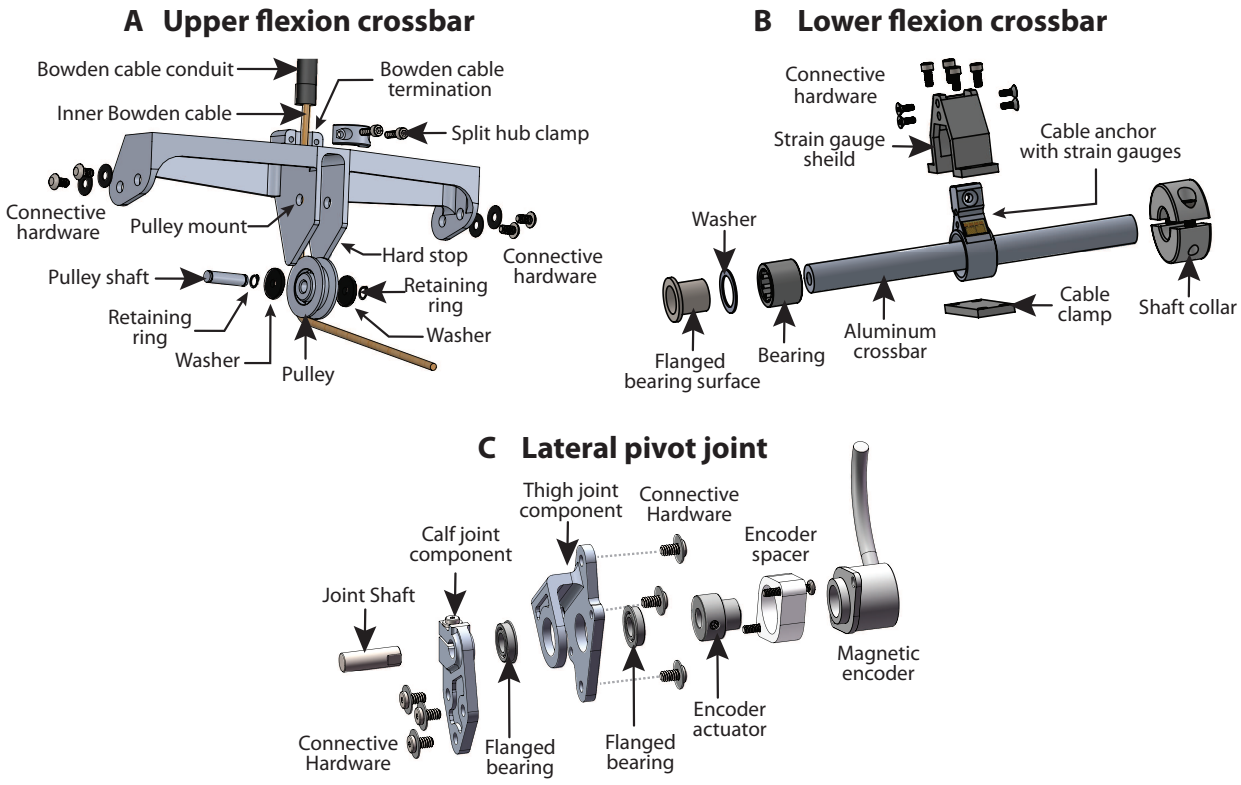

Figure 4.4: Exploded views of subassemblies: **A** The flexion crossbar connects the medial and lateral frame stays of the thigh section. The Bowden cable housing terminates in the center of the crossbar and is secured in a split hub clamp. The inner Bowden cable extends through the crossbar and is redirected with knee angle by a pulley. The extension crossbar has similar features. **B** The lower flexion crossbar connects the medial and lateral frame stays of the calf section. The inner Bowden cable is secured on the aluminum cable anchor. The cable anchor is instrumented with four strain gauges in a Wheatstone bridge configuration for sensing cable tension. The strain gauges are protected by a plastic shield that is secured to the cable anchor. The cable anchor is mounted on a bearing in order to prevent torsional load from being applied to the crossbar. The bearing sits on a steel bearing surface which is secured to the cross bar with epoxy. Translation of the bearing along the length of the crossbar is resisted by a flange on the steel bearing surface and by a shaft collar. **C** The pivot joint is composed of two aluminum components, the thigh joint fork and the calf joint clamp. The thigh joint fork connects to the thigh frame struts and provides a stable double shear connection with two ball bearings and a mounting point for the rotary encoder. The calf joint clamp connects to the calf frame and features a split hub clamp for rigidly attaching to the joint shaft.

the torque tracking capabilities of the system.

4.2.1 Mechanical design

The knee exoskeleton end-effector is actuated by two powerful off-board servo motors (AKM73P-ACCNR-00, Kollmorgen, Radford, VA, USA) and a real-time controller, with mechanical power transmitted through flexible Bowden cable tethers. The controller and tether elements of this system are described in detail in [35].

The frame of the exoskeleton consists of identical planar carbon fiber struts on the medial and lateral aspects of the leg (Fig. 4.2). The frame can be separated into thigh and calf sections, represented as blue and green, respectively, in Figs. 4.1 and 4.3. On the thigh section, the medial and lateral frame struts are connected by two aluminum crossbars with Bowden cable housing terminations (Fig. 4.4A). The inner Bowden cables extend from these cross bars to cable anchors mounted on the lower crossbars of the calf section (Fig. 4.4B). The aluminum anchors are mounted on bearings to prevent torsional loads on the crossbar. Tension in the cable located on the anterior side of the leg generates extension torques (Fig. 4.3) while tension in the posterior cable generates flexion torques. Pulleys mounted on the cross bar redirect the inner Bowden cable as the knee angle changes. The medial and lateral frames of the calf section are connected by tubular aluminum crossbars on which the inner Bowden cable anchors are mounted (Fig. 4.4B). The thigh and calf sections are connected via medial and lateral aluminum rotary joints (Fig. 4.4C). The shared axis of rotation of these joints is approximately colinear with the human knee joint.

The frame is connected to the user by four straps at the upper thigh, the lower thigh just above the knee, the calf, and the ankle. The ankle and knee strap locations are located as far from each other as possible, maximizing their leverage about the knee and minimizing forces applied to the user for a given knee torque. The same is true of the two thigh strap locations. The upper thigh strap can be connected to a belt at the waist or suspenders at the shoulders to prevent downward migration of the device.

Free body diagrams were analyzed assuming the axis of rotation of the knee joint is approximately aligned with that of the exoskeleton's joint and forces at the straps act normal to the user (Fig. 4.3D). Compression applied on the crossbar by the Bowden cable conduit and tension in the inner Bowden cable are equal and opposite resulting in a moment about the knee joint, but no net force on the leg in the world reference frame (Fig. 4.3A). A free body diagram of the upper section of the exoskeleton shows one possible set of reaction forces: the reaction force at the joint bearing acts opposite to the tension in the inner Bowden

cable and the forces applied by the exoskeleton straps are equal and opposite and act normal to the user's leg (Fig. 4.3C). The forces represented here are approximations; small shear forces at the straps are expected, but difficult to quantify.

The aluminum cross bars are of varying length with the longest at the thigh and the shortest above the ankle. Crossbars of different sizes can be exchanged to adjust the fit. The planar carbon fiber struts accommodate these changes in width with low stiffness in the frontal plane. The struts can be exchanged to fit users with shank lengths ranging from 0.42 to 0.50 m and thigh lengths ranging from 0.38 m to 0.46 m.

The exoskeleton accomodates knee angles ranging from straight leg to 120 degrees of flexion and can apply 120 Nm of exension torque and 75 Nm of flexion torque limited by frame strength. These values correspond to the range of motion and peak torques observed at the human knee during unaided running [107].

4.2.2 Fabrication

The exoskeleton frame struts were manufactured from plate carbon fiber on a water jet cutter. Aluminum tubes cut from stock lengths were used as crossbars for the lower lever arms. The ends of the tubes are threaded for attachment to the frame struts. The joint components and Bowden cable terminations and pulley mounts for the upper crossbars required more complex geometry achieved through CNC machining of 7075 aluminum.

Knee angle is sensed using a magnetic encoder (RM22I, Renishaw Inc., Hoffman Estates, IL, USA) and foot contact with heel switches (7692K3, McMaster-Carr, Cleveland, Ohio, USA) located inside the user's shoe. Tension in the Bowden cables is sensed using two sets of four strain gauges (KFH-3-350-D16-11L3M2S, OMEGA Engineering, Stamford, CT, USA) in Wheatstone-bridge configurations located on the aluminum rope anchors (Fig. 4.4 B). Bridge voltage is sampled at 5000 Hz and low-pass filtered at 200 Hz to reduce the effects of electromagnetic interference. Torque is geometry dependent and is calculated in real time using measurements of both cable tension and knee angle.

A combination of classical proportional control with damping injection and iterative learning is used to control exoskeleton torque [94].

4.2.3 Experimental methods

In tests of torque measurement accuracy, the aluminum cable anchors and supporting crossbars were removed from the exoskeleton and secured on a rigid test stand. Force was incrementally increased by hanging weights of known mass from the Bowden cable. We computed root mean squared (RMS) error between applied and measured force from the calibration set.

For the closed-loop bandwidth tests, steps in applied torque lasting 3 seconds were applied in both low (1745 N) and high force (436 N) settings. These forces are equivalent to the forces required to apply 20 Nm and 50 Nm of torque to the user's knee while wearing the device in a straight leg configuration.

In walking studies using an ankle exoskeleton we have demonstrated that providing positive work with large torques during walking can result in large metabolic reductions [2]. The magnitude of torques applied that resulted in the largest metabolic reductions corresponded to about 60 to 80% of the torque produced at the ankle during normal walking. Therefore, we are particularly interested in exploring torque at the knee at and above 20 Nm as it corresponds to approximately 65% of the peak torques produced at the knee during normal walking for an average-sized subject [108]. A 50 Nm benchmark was selected to allow for comparison to our ankle exoskeleton emulator [47].

4.2.4 Sensing and control

Closed-loop bandwidth tests were performed both while worn by a user and on the rigid test stand.Bandwidth tests were performed by applying a series of sinusoidal desired torque trajectories two seconds in length with a one second pause in between trials. The first sinusoidal signal for desired torque was commanded at 1.0 Hz and the frequency of each

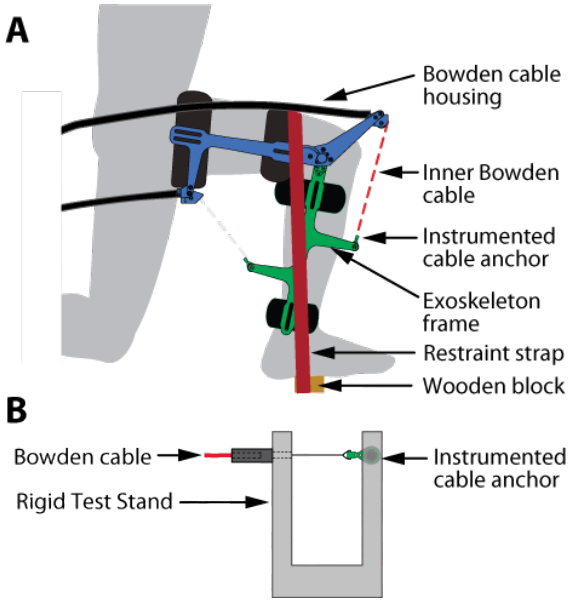

Figure 4.5: **A** Bandwidth test setup on human subject. The user's knee was restrained by a strap that wrapped over the user's thigh and attached to a block under the foot. This prevented the knee from extending during the test. **B** Bandwidth test setup on rigid test stand. An instrumented cable anchor and carbon fiber crossbar were removed from the exoskeleton and mounted on a rigid test stand.

successive trail was increased by 1.0 Hz until a frequency of 55 Hz was reached. For the low torque bandwidth test the desired sinusoidal signal had minimum and maximum values of 10 and 20 Nm. For the high torque trials the peak torque was 50 Nm with a minimum torque of 10 Nm. Each of these tests were performed ten times and the results were averaged. Bode plots were generated by fitting the applied and measured torque signals to sinusoids described by $A \cdot sin(B \cdot x + C)$ where A is the amplitude of the sine wave, B is the period, and C is the phase offset, assuming the frequency of the commanded and measured waves are equal. The magnitude of the frequency response was calculated in decibels as $20 \cdot log_{10}(\frac{A_m}{A_d})$ where A_m is the amplitude of the sinusoid fitted to the measured data and A_d is the amplitude of the desired torque signal. The phase shift between the desired and measured signals was calculated as $(C_d - C_m)$.

The same methods where applied for bandwidth tests performed on the exoskeleton while worn by a user. For the low torque bandwidth test, the maximum and minimum

values of the desired torque were 20 and 10 Nm. For high torque trials the peak torque was 50.0 Nm with a minimum of 20 Nm. These torques were commanded while the knee was positioned at roughly 90 degrees so that the force used to generate the torque was approximately the same as the force used in the bandwidth tests on the rigid test stand. The highest frequency tested while the exoskeleton was worn by a user was limited to 23 Hz by user comfort. During these tests the user's leg was restrained by a strap that wrapped over the knee and under the toe (Fig. 4.5). The high and low torque tests on a human user were each performed five times and the results averaged.

4.3 Results

The mass of the knee exoskeleton is 0.76 kg. The device allows a range of motion from straight leg at 0° to 120° of knee flexion. Force measurement accuracy tests showed RMS error of 6.14 N which corresponds to 0.78 Nm of torque with the exoskeleton in a straight leg configuration (Fig. 5.3 A). Step response tests showed a rise time of 0.023 s for the low torque (20 Nm) trials and 0.026 s for the high torque (50 Nm) trials (Fig. 5.3 B). The bandwidth of the combined exoskeleton and human system was phase limited at 23 Hz for both the low and high torque settings as measured by the -180° crossover (Fig. 5.3 D). The bandwidth of the motor with force sensor fixed on a rigid test stand was phase limited at 45 Hz in the high torque setting and gain limited at 52 Hz as measured by the -3 dB crossing in the low torque setting. Torque tracking was evaluated during 100 strides. The average RMS error over a stride was 0.91 Nm (Fig. 4.7).

4.4 Discussion

We have developed a comfortable knee exoskeleton which can supply high torque in both flexion and extension directions at high bandwidth. Its mass is low at 0.76 kg, which limits the metabolic cost incurred by adding distal mass to the user and allows for the device to be

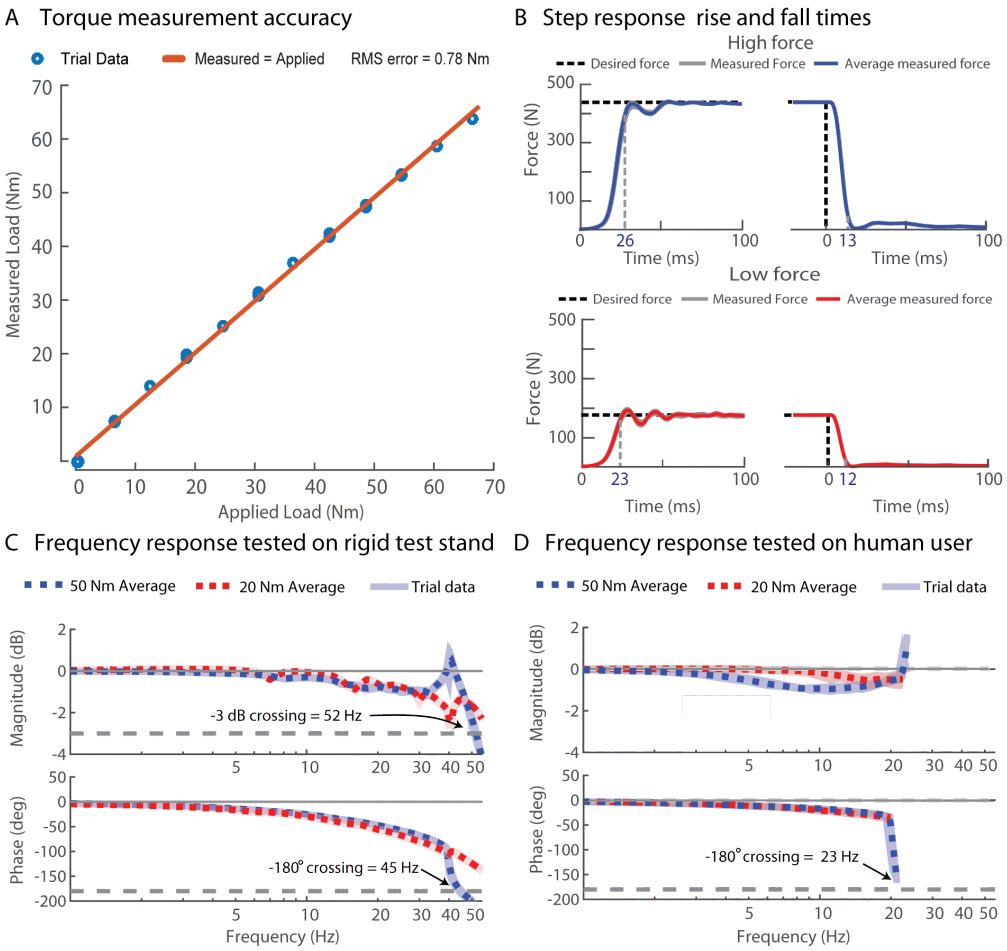

Figure 4.6: Experimental Results **A** Torque measurement calibration results demonstrate an RMS error of 0.78 Nm with a maximum load of 63 Nm. **B** Step response performed at both low and high force. The low force test was conducted at 175 N (corresponding to 20 Nm of torque on the knee exoskeleton in a 90° configuration.) with rise time of 0.023 seconds. The high force step response test was conducted at 436 N (corresponding to 50 Nm of torque on the knee exoskeleton in a 90° configuration) with a rise time of 0.026 seconds. **C** Bandwidth tested on a rigid test stand for both high (50 Nm maximum) and low torque (20 Nm maximum) settings. Bandwidth was phase limited at 45 Hz as measured by the -3 dB crossover. **D** Bandwidth tested on a human user for both high (50 Nm maximum) and low (20 Nm maximum) torque settings.

adjusted to approximate the mass properties of devices it may emulate. The bandwidth of the device is high compared to other tethered exoskeletons, which will enable researchers to accurately render desired torque profiles. The bandwidth measured on a human user was about half that measured on the rigid test stand. This suggests that performance of exoskeletons should be reported for the combined human/robot system as reporting the bandwidth of the actuator alone may overestimate the performance capabilities of the system as a whole.

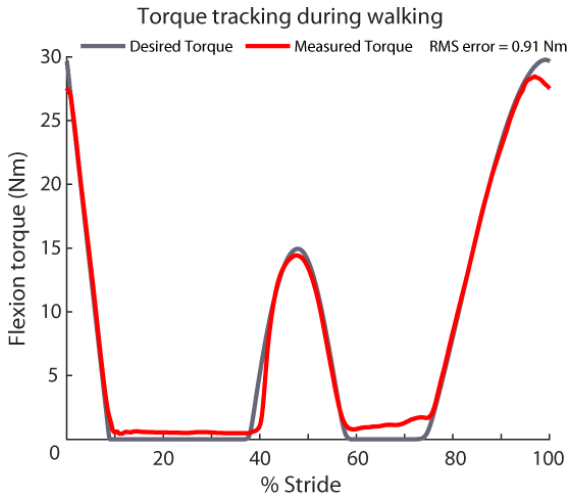

Figure 4.7: Average desired and measured flexion torque from 100 steps of walking at 1.25 m/s. The mean RMS torque error was 0.91 Nm.

The exoskeleton is comfortable with wide straps placed far apart to minimize forces on the body for a given applied torque. However, this wide spacing can become uncomfortable for some subjects as the upper thigh strap approaches the groin and the flexion lever arm prevents the user from easily sitting. In future designs lowering these components may be considered despite the corresponding increase in strap forces. Users report feeling mostly normal forces in the directions predicted by our free body diagrams (Fig. 4.3). However, no experiments have been conducted to confirm the direction of the reaction forces at the straps.

The four straps proved to be insufficient to prevent downward migration of the exoskeleton. Adding suspenders between the thigh strap and the shoulders or connecting to a belt at the waist were both effective methods of securing the exoskeleton. The waist belt is a common solution and was connected to the thigh strap with an additional length of webbing on the lateral aspect of the hip where the distance to the exoskeleton changed little during hip flexion and extension [109, 110]. Inextensible webbing was used for the leg straps and we found that the lower thigh strap and calf strap became too tight at large angles of flexion and too loose at straight leg due to changes in muscle volume. As a result, the calf strap needed to be loosened for comfort and was no longer sufficient to prevent downward

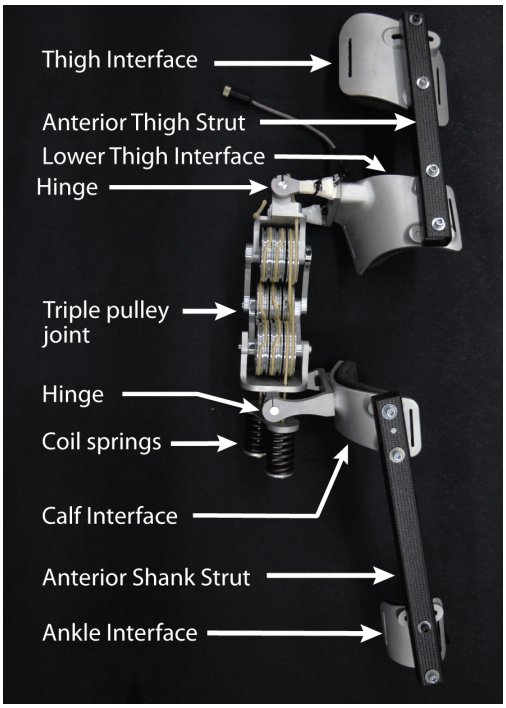

Figure 4.8: A five-degree-of-freedom exoskeleton developed to provide a pure moment to the knee joint. All rigid components are located on the lateral or anterior side of the leg. The exoskeleton consists of four aluminum strap interfaces at the upper thigh, lower thigh, calf, and ankle. The interfaces are connected by anterior struts formed of rectangular carbon fiber tubes. The joint is composed of two hinges and three sets of three pulleys which allow for five degrees of freedom. The three sets of pulleys are used for flexion, extension, and an adjustable safety hard stop. The inner Bowden cables used to apply extension and flexion torques wrap around these pulleys and terminate on compression coil springs for series elasticity.

migration. This was not the case for our ankle exoskeleton which has a single strap at the calf.

Many exoskeletons feature a series elastic element to improve torque control or to allow for smaller actuators [94, 111]. Adding series elasticity can help improve disturbance rejection usually at the cost of lower bandwidth. This exoskeleton was not originally designed for series elasticity as it was expected that compliance in the vectran cable and the user's soft tissues would be sufficient. However, it was found that a compliant elastic cord added on the device side of the Bowden cable helped to correct torque tracking errors caused by stiction in the Bowden cable.

The simple rotary joints of this exoskeleton make it lightweight, inexpensive and simple to design and manufacture. Flexion and extension is actively controlled by the exoskeleton

and is allowed by the explicit rotary joint. Small displacements in the other five degrees of freedom are allowed through high compliance in uncontrolled directions. The user's soft tissues are very compliant. The exoskeleton can be easily shifted by 30 mm up and down or twisted around the leg by about 8 degrees by lightly lifting with a single finger on each side of the exoskeleton before resistance increases significantly. The low stiffness of the knee exoskeleton frame in the varus/valgus direction allows for some variability, but the knee exoskeleton is difficult for individuals with a high degree of valgus rotation due to limited clearance between the exoskeleton and the contralateral limb. Adding asymmetric spacers between the leg and the frame struts to shift the exoskeleton medially or laterally can help with fitting. An explicit degree of freedom for varus/valgus rotation would make fitting the exoskeleton to users easier. Overall, high compliance in our exoskeleton allows for comfortable use.

Several more complicated exoskeleton designs address the multiple degrees of freedom of the knee. A four bar linkage has been developed to more closely approximate the moving center of rotation of the knee [109]. However, this solution faces the same issues as a revolute joint if the exoskeleton migrates down the leg and becomes misaligned with the human joint. A six degree of freedom knee exoskeleton that takes advantage of rotary joints and articulated parallelograms delivers a pure moment to the user [112]. This exoskeleton should be comfortable and fit a wide range of subjects, but at the cost of complexity and mass.

We previously developed a knee exoskeleton end-effector with a five degree of freedom joint to accommodate the multiple degrees of freedom of the human knee joint, but we found it to be heavy and the additional degrees of freedom unnecessary. It used a triple pulley configuration with double hinges that could accommodate any joint motion other than internal and external rotation (Fig.4.8). No rigid components were placed on the medial aspect of the leg, which reduced hip circumduction during walking. However, the large offset joint mass on the lateral side of the leg caused the exoskeleton to rotate relative to the human leg during walking. The joint was composed of three sets of three pulleys wrapped with inner

Bowden cables (Fig. 4.9), one set for extension, one for flexion, and another for a safety hard stop to prevent hyperextension. Stretch in the cables made measurement of joint angle difficult and reduced the effectiveness of the safety hard stop. While this joint configuration made fitting a wide range of leg shapes and sizes simpler, it was heavy, complicated and anecdotally less comfortable to walk in than our current simple pivot joint.

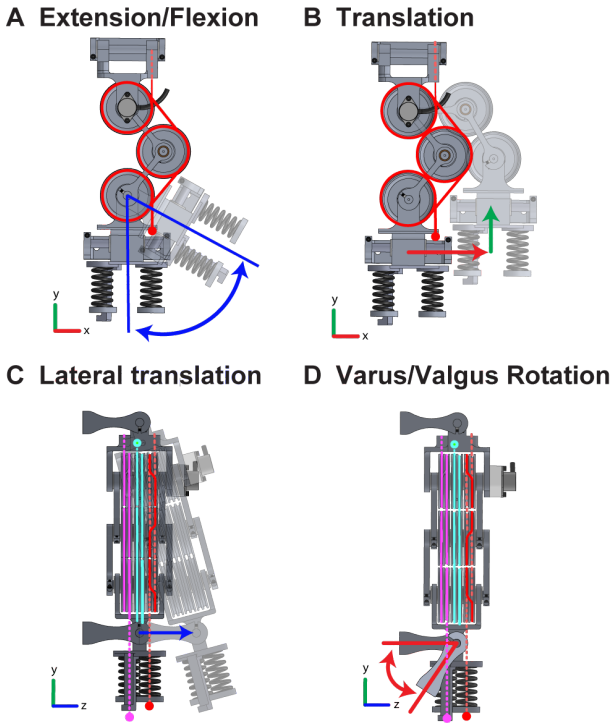

Figure 4.9: A five degree of freedom joint capable of producing pure extension and flexion moments in the flexion/extension degree of freedom while accommodating four other degrees of freedom. Internal and external rotation of the calf section relative to the thigh section is not supported. Two Bowden cables produce extension (red) and flexion (pink) moments while a cable of fixed length acts as a hard stop to prevent hyperextension (blue).

4.5 Conclusions

We have developed a tethered knee exoskeleton and demonstrated through benchtop tests that it is capable of applying high torque at high bandwidth and can apply torques to a user comfortably during walking. Measured bandwidth was greater in tests on a rigid test stand than in tests on a user's leg, but high in either case. The pivot joint does not explicitly accommodate all degrees of freedom of the human knee joint, but we found that compliance

in the frame, straps and soft tissues of the user allow it to be used comfortably. The simple plate carbon fiber frame allows for some compliance in order to accommodate varus/valgus rotation of the knee and is compliant enough to flex in and out to provide a good fit for legs of different diameters. A more form-fitting frame could improve comfort and likely mitigate increases in step width and circumduction. This device will enable researchers to apply desired torque profiles with high fidelity in order to probe the neuromuscular system, augment athletic performance and test strategies for gait rehabilitation.

Chapter 5

Experimental comparison of ankle exoskeleton assistance strategies for improved running economy

Abstract

Using exoskeletons to reduce the energetic cost of running may make running more enjoyable and increase participation in running for fitness, potentially leading to better health outcomes. Additionally, individuals who must walk or run great distances for work, such as soldiers, may benefit from such devices as they may reduce fatigue and the incidence of injury. Both powered and spring-loaded ankle exoskeletons have been successful in reducing the metabolic cost of walking and may each be a good approach for assisting running. An experimental comparison of these two strategies may provide insights into the best design approach for portable product-like exoskeletons. Human-in-the-loop optimization of exoskeleton settings can identify the best characteristics for a given assistance strategy and individual user, which enables a more accurate comparison. We used a tethered ankle exoskeleton emulator to optimize both powered and spring-like exoskeleton characteristics while participants ran on a treadmill. Optimal powered assistance improved energy econ-

omy by 24.7 ± 6.9% compared to zero-torque mode and 14.6 ± 7.7% compared to running in normal shoes, the greatest benefit demonstrated during running to date. The optimal powered torque patterns for individuals varied substantially, but all resulted in relatively high mechanical work input. Surprisingly, spring-like assistance was far less effective, improving energy economy by only 2.1 ± 2.4% compared to zero torque.

5.1 Introduction

Addressing potential obstacles to participation in running for fitness may improve general health. Running provides health benefits from improved cardiovascular health [9], to alleviated symptoms of depression [10, 11] and even drastically reduced risk of all-cause mortality [12]. While running has a low barrier to entry, several factors can prevent participation. In 2018, only about 25% of Americans between 18 and 29 reported going for a run or a jog at least once within a twelve month period and participation dropped to 20% for adults 30 to 49 years of age [113]. Time commitments and the internal belief that individuals are not athletic are the two greatest barriers to increasing physical activity [114]. Perceived exertion and activity intensity also have a negative association with frequency of exercise, while perceived ability, enjoyment and interest can increase activity levels and energy expenditure [114, 115, 116].

Outside of running for fitness, many individuals run for work and are at risk of injury due to fatigue. Fatigue has been shown to increase the incidence of injury during running due largely to increased impact acceleration at heel strike [8]. Military personnel and first responders often run as part of their job in environments where even minor injuries may have dire consequences. Using exoskeletons to reduce fatigue could result in fewer injuries in these high stakes environments.

Highly effective running exoskeletons could potentially lead to greater participation in physical activity by decreasing activity intensity and fatigue while simultaneously enhanc-

ing safety, perceived ability, interest and enjoyment. Exoskeletons could allow entry-level runners to match the pace of more fit friends, which could have a significant impact as motivation and adherence to exercise is improved when exercising with a partner [117, 118, 115]. Exoskeletons may even be used to allow fair and enjoyable competition between runners of disparate skill level much like a bowling handicap. Enabling challenge and competition in this way may further improve participation [116].

The potential impact of reducing the energetic cost of running with exoskeletons is clear, and several devices have already demonstrated success. Nike's Vaporfly marathon shoes have reduced the metabolic cost of running by 4% [39] and a passive hip exoskeleton has achieved metabolic energy reductions of 8% compared to running without the exoskeleton [6]. These devices have been successful without the need for motors or electrical power. A portable, powered hip exoskeleton has been used to reduce the cost of running by 8% [119]. While these results are exciting, and have potential to make significant differences for elite athletes, larger metabolic reductions may be needed to noticeably improve performance for amateur runners.

While specialized shoes and hip exoskeletons have assisted running, past results suggest powered ankle exoskeletons may be even more effective. Ankle exoskeletons have been used extensively during walking [103, 1, 4, 120, 104] and have produced the highest metabolic reductions (24%) to date [2]. Preliminary running tests of untethered devices developed in industry have shown small improvements [121], and a single subject experiment utilizing bilateral ankle exoskeletons demonstrated an impressive reduction in energy cost of 27% [2]. In addition to promising experimental findings, the ankle naturally provides more positive work than the hip or the knee [107] suggesting it may be a more effective location for applying assistance. However, the benefits ankle exoskeletons supply during running may not offset the high penalties associated with their mass and location on the user's legs. The cost of carrying mass increases as the mass is placed more distally [31], and the negative effect of added mass to the foot on running times and metabolic rate is well documented [122].

Due to the high cost of adding mass to the leg, spring-loaded exoskeletons that can operate without the mass of batteries, motors and complex transmissions may be a preferable method of assisting running compared to powered exoskeletons. Passive ankle exoskeletons have been used to reduce the cost of walking by loading a spring in parallel with the Achilles tendon [30]. Spring-based assistance may be easy for users to adapt to as legs naturally exhibit spring-like behavior during running [123, 124, 125]. While the hip, knee and ankle all contribute to the overall stiffness of the leg, the ankle has been shown to be the dominate factor in hopping experiments [126]. Prior results demonstrate that total knee stiffness remains constant with and without a parallel spring engaged [127] suggesting that a spring-loaded exoskeleton can effectively offload muscle forces to achieve similar overall behavior. However, it should be noted that the same study also revealed that adding mass to the knee changes the joint's overall stiffness. It is unknown how this change in stiffness may affect performance.

Prior attempts at assisting running with spring-loaded exoskeletons may have been unsuccessful due to added lower-limb inertia and interface compliance [128]. The added weight of devices that assist the entire leg incurs penalties that are large and hard to offset. Additionally, mechanical power can be dissipated in the compression of soft-tissues when exoskeletons interface in areas with large volumes of soft-tissue such as the thigh [62].

Lightweight ankle exoskeleton emulators can be combined with human-in-the-loop optimization to efficiently and accurately compare the relative performance of powered and spring-like ankle exoskeleton assistance. Powered exoskeleton emulators [47] are extremely lightweight and can be used to emulate the behavior of a wide variety of exoskeleton designs. For example, emulators can apply torque in a manner consistent with spring-and-clutch-based exoskeletons to allow researchers to explore energetically conservative assistance strategies without the need to manually adjust spring stiffness or clutch timing. Any spring-like behavior can be embedded in such a system and there are many possibilities to explore including linear, softening and stiffening springs. This flexibility is particularly

powerful when paired with human-in-the-loop optimization (HILO), which can systematically explore the vast space of possible assistance strategies.

Human-in-the-loop optimization can discover optimal device settings for individuals that outperform hand tuning [2, 131, 132]. Selecting the appropriate exoskeleton settings for each user is nontrivial as people are difficult to model or predict [129], often have different responses to the same exoskeleton assistance [104], and require guidance while learning to use exoskeletons effectively [130]. HILO may improve performance of running exoskeletons in general, and also allow better across-device comparisons as the best versions of each device type can be discovered and compared.

We have applied human-in-the-loop optimization using an ankle exoskeleton emulator testbed to compare the metabolic benefits of passive and powered ankle exoskeletons during running. HILO has enabled us to optimize each assistance strategy for each individual subject for a more objective comparison. We expect the results to influence the design of future products by revealing the feasibility of a passive spring-like approach and broad design requirements for powered exoskeletons.

5.2 Methods

The goal of this study was to assess the effectiveness of two ankle exoskeleton assistive strategies: passive spring-based and biologically-inspired powered assistance applied as a function of time. The main outcome of interest was the metabolic cost of running using each of the strategies as compared to running with the exoskeleton in zero-torque mode and running in normal shoes. Accurate comparison of these two strategies was enabled by using human-in-the-loop optimization to find the optimal settings for each controller for each individual subject. The experiment was conducted using a highly adaptable ankle exoskeleton emulator (Fig. 5.1 A) [47]. The use of the emulator system enabled rapid alteration of device settings and ensured that the two assistance strategies were compared in isolation

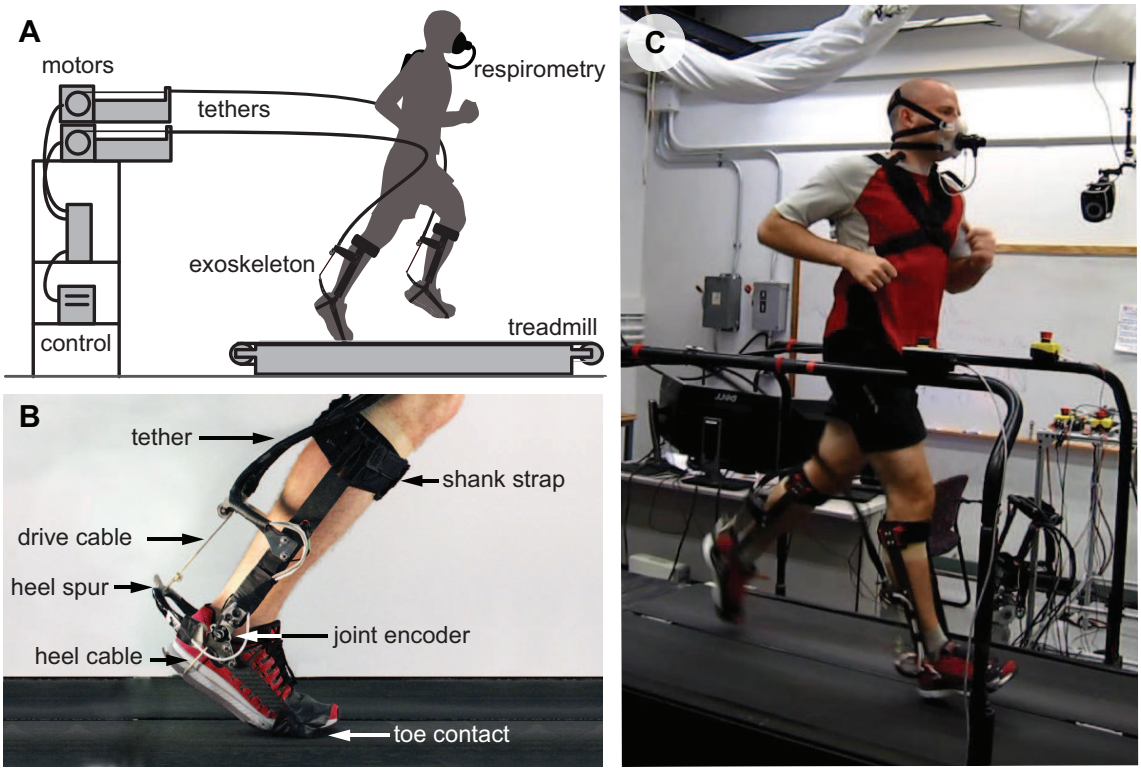

Figure 5.1: **Experimental Setup.** **A** Exoskeleton Emulator test-bed. A subject runs on a treadmill while wearing bilateral ankle exoskeletons actuated by motors located off-board with mechanical power transmitted through flexible Bowden cables. **B** Ankle exoskeleton. The ankle exoskeleton attaches to the user by a strap above the calf, a rope through the heel of the shoe, and a carbon fiber plate embedded in the toe of the shoe. The inner Bowden cable terminates on a 3D printed titanium heel spur that is instrumented with strain gauges for direct measurement of applied torque. A magnetic encoder measures ankle. **C** Participant running with exoskeletons. A subject runs on the treadmill while wearing bilateral ankle exoskeletons. Metabolics data is collected through a respiratory system.

with constant inertial properties and frame stiffness.

All subjects wore bilateral torque-controlled ankle exoskeletons (Fig. 5.1 B and C) [47] while running at a pace of 2.7 m/s. Twelve competitive runners were recruited for this study. Subjects were required to be natural heel strike runners between the ages of 18 and 40. Eleven subjects completed the protocol (Table 5.1), all of which had completed at least one marathon. One subject did not converge during the first optimization day and was not interested in participating further; this subject's data was discarded. Subjects experienced a separate day of optimization for each controller (section 5.2.2) followed by a day of validation

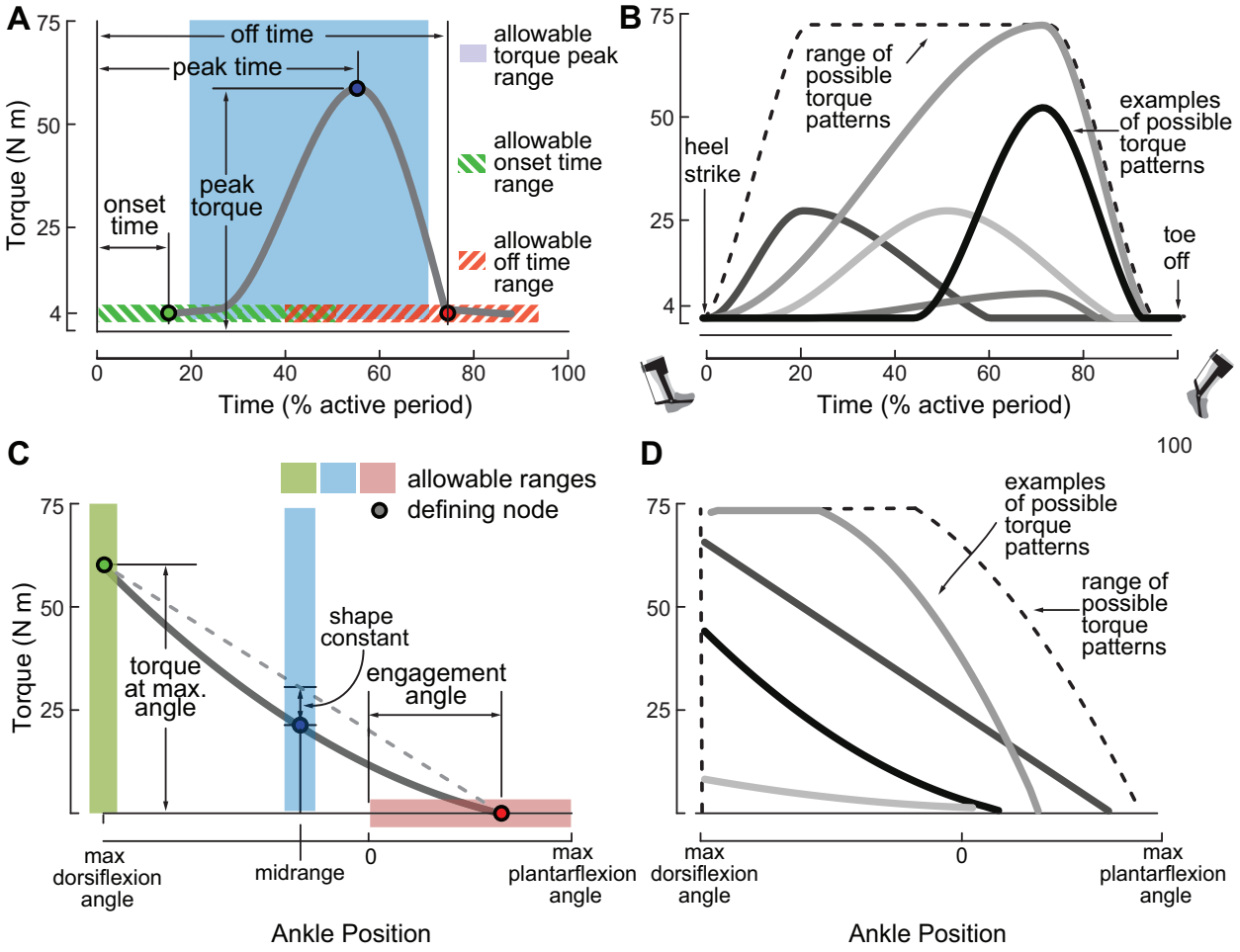

Figure 5.2: **Controller parameterization.** **A** Powered Parameterization. Three nodes define the pattern of torque control in the powered condition. These nodes are connected by sinusoids and defined by four parameters: magnitude of peak torque, peak time, on time, and off time. **B** Range and examples of possible powered torque patterns. A simple parameterization results in a wide range of possible torque patterns. **C** Spring-like parameterization. Three nodes fitted to a quadratic function define the relationship between ankle angle and applied torque. These nodes are defined by three parameters: the magnitude of torque applied at the maximum dorsiflexion angle, the ankle angle at which the spring engages, and a shape constant that determines whether the spring is linear, stiffening or softening. **D** Range and examples of possible passive torque patterns.

trials during which subjects ran in the following conditions: optimal spring-like, optimal powered, zero-torque, and normal shoes.

5.2.1 Controller parameterization

Powered assistance was inspired by a time-based approach used for walking assistance [2]. Desired torque patterns for the powered strategy were defined by four parameters: peak

torque magnitude and the timing of: peak torque (peak time), onset of torque (on time), and return to zero-torque (off time). These four parameters define three nodes connected by sinusoids shown in Figure (5.2 A). Maximum torque was allowed to vary between 4 and 60 Nm. With 4 Nm being the minimum torque setting that can be accurately tracked by the emulator system and 60 Nm being the maximum comfortable torque setting found during pilot testing. Maximum torque was adjusted to 75 Nm for two subjects who showed a preference for high torques during habituation. The timing of peak torque varied between 8.4% and 29.4% of average stride time. On-time was constrained to be between 0 and 21% of stride time with no less than 8.4% of stride time between the onset of torque and peak torque. Off-time ranged between 16.8% and 40.0% of stride time with no less than 8.4% of stride time between the peak-time and off-time. These ranges and constraints were set based on comfort in pilot tests.

Average stride time was calculated as a running average of the time between heel strikes of the same foot as detected by pressure switches in the heel of the shoe. Left and right ankle exoskeletons were controlled in isolation of each other, though controller settings were shared across both.

Passive spring-like assistance was applied as a function of ankle angle and was defined by three parameters: the torque experienced at the maximum expected dorsiflexion angle (maximum torque), the ankle angle at which the spring becomes engaged (engagement angle), and a shape constant that determines whether the spring is linear, stiffening or softening. These three parameters combined to define three nodes (Fig. 5.2). A quadratic function was fit to these three nodes to define torque as function of ankle angle. Maximum torque ranged from 0 to 60 Nm (or 75 Nm for two subjects). Engagement angle ranged between the maximum plantarflexion angle measured during running in zero-torque and the ankle angle half way between maximum expected dorsiflexion and maximum expected plantarflexion. The shape constant set the magnitude of torque experienced at an ankle angle midway between maximum expected dorsiflexion and maximum expected plantarflexion.

Maximum expected dorsiflexion angle was calculated as the 75th percentile of the maximum dorsiflexion angles measured over 32 strides. Maximum expected plantarflexion was set to the average of the maximum plantarflexion angles measured over 32 strides. This insured that the spring engaged and disengaged on every step despite small inter step variation.

Low-level torque control was enabled through a combination of proportional control, damping injection, and iterative learning [69].

5.2.2 Optimization strategy

Human-in-the-loop optimization [2] was applied to both assistance strategies using a covariance matrix adaptation evolutionary strategy (CMA-ES) [38]. Normal distributions for each parameter were created with means and variances defined as initial settings. Parameters were selected from these distributions to form a generation of trial controllers. The number of trial controllers included in a generation, λ, was calculated as a function of n, the number of parameters being optimized. The powered and passive controllers were optimized using generations of 8 and 7 trial controllers respectively as calculated in Equation 5.1.

$$\lambda = 4 + \lfloor 3 * ln(n) \rfloor \tag{5.1}$$

Each of the trial controllers was tested during two minutes of running. Steady state metabolic cost was estimated by fitting a first-order dynamical model [133] to the metabolic data collected using a respirometry system (Quark CPET: Cosmed). A covariance matrix adaptation was then performed to calculate new means and variances for each of the parameter distributions [38]. These new distributions were then used to select the trial controllers for the next generation. Each subject experienced four generations. The mean parameter values calculated for the fifth generation were considered the optimal controller settings. Refer to [2] for more details on this optimization approach.

5.2.3 Experimental protocol

Eleven male subjects completed the experimental protocol (age = 25.5± 6.1 yr.; mass = 75.4± 8.26 kg; height = 1.78 ± 0.05 m). Subject characteristics are shown in Table 5.1. The protocol consisted of habituation, optimization, and validation trials. Subjects ran on a treadmill at a speed of 2.7 m/s while wearing bilateral ankle exoskeletons [47].

Table 5.1: Subject characteristics

Subject	Mass (kg)	Age (yrs.)	Height (m)
1	76.0	24	1.77
2	83.9	36	1.83
3	72.6	24	1.80
4	63.5	22	1.75
5	79.4	21	1.84
6	79.4	30	1.83
7	77.1	21	1.80
8	59.4	20	1.75
9	70.3	23	1.73
10	83.5	37	1.70
11	84.4	21	1.80

Subjects experienced a day of habituation during which they were introduced to both controllers. Subjects were allowed five minutes of running in the exoskeletons in zero-torque mode followed by five minutes of running with the exoskeletons in one of the assistive modes. Next, one generation of trial controllers was experienced. The process was then repeated for the second assistive mode. The order in which the subject experienced the spring-like and powered assistive modes was randomized during habituation. Subjects then experienced optimization of powered and passive assistance on separate days in randomized order.

A day of validation trials was experienced after optimization of both controllers. The following conditions were tested: zero-torque, optimal spring-like, optimal powered, normal shoes and quiet standing. Validation trials were performed in randomized double reversed order (ABCDEEDCBA). The trials using normal shoes were predetermined to occur either as the first and last trials (A) or back-to-back (E) as the middle conditions to minimize the number of times the exoskeletons needed to be donned and doffed. The shoes utilized in

the normal shoes condition were identical to the shoes incorporated into the exoskeletons. Five minutes of rest were allowed between each validation trial. Validation trials were six minutes in length, with only the last three minutes of data utilized to calculate measured outcomes.

5.2.4 Measured outcomes

Net metabolic rate. Net metabolic rate was the primary outcome of this study. Volumetric carbon dioxide expulsion, oxygen consumption, and breath duration were measured using a breath-by-breath basis using respirometry equipment (Quark CPET: Cosmed). Data from the last three minutes of each validation trial were substituted into a commonly used equation [134] to calculate average metabolic rate. The net metabolic rate of running in each condition was calculated as the average metabolic rate minus the rate for quiet standing.

Average Exoskeleton Work. Mechanical work delivered by the exoskeleton was calculated for each step by integrating the exoskeleton torque over ankle angle during the stance period.

Average Exoskeleton Power. Exoskeleton power was calculated for each step by dividing the external work delivered during foot contact by stride time. Average power was calculated by summing the power delivered for all steps and dividing by the number of steps occurring in the last three minutes of data.

For purposes of comparison, all measured outcomes were normalized to body mass.

5.3 Results

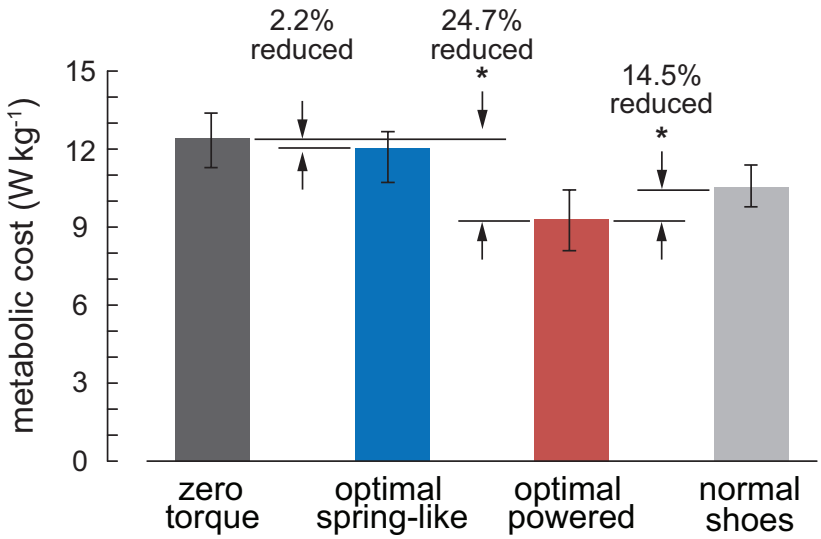

Figure 5.3: **Metabolic results.** Optimal spring-like and optimal powered assistance resulted in metabolic reductions of 2.2% and 24.7% respectively compared to running is a zero-torque mode. Optimal powered assistance resulted in an improvement in running economy of 14.5% compared to running in normal shoes, while spring-like assistance resulted in an increase in the cost of running.

5.3.1 Normal shoes and zero-torque

The average net metabolic rate measured for zero-torque and normal shoes were 12.23± 1.14 W kg^{-1} and 10.78 ± 0.97 W kg^{-1} respectively. The average mechanical work delivered by the exoskeletons per step in the zero-torque mode was negligible at -0.001 ± 0.003 Jkg^{-1}.

5.3.2 Optimal powered assistance

Moderately high peak torque was applied to all subjects in the powered setting with the peak occurring late in stance (Fig. 5.4 A). The optimal onset of torque occurred at or just after foot flat. The optimal timing of torque turning off occurred at toe off (97.2 ± 1.5 % of stance period) for all subjects.

The average net metabolic rate measured for the powered condition was 9.21 ± 1.15 W kg^{-1}. Powered assistance improved energy economy by 24.7% ± 6.9% (t-test, p = $1 * 10^{-6}$, n = 11) on average compared to running in the exoskeletons in zero-torque mode (Fig. 5.3).

Powered assistance improved running economy by 14.5% ± 7.66% compared to running in normal shoes (t-test, p = $1 * 10^{-4}$, n = 11).

Peak torque for the optimal powered assistance on the average step was 0.71 ± 0.14 Nm kg^{-1} (Fig. 5.4 A). Peak power for the average step was 0.48 ± 0.12 W kg^{-1}. The average mechanical work provided by an exoskeleton in a single step was 0.36 ± 0.09 J kg^{-1} in the optimal powered condition. Average work loops for each individual in the powered condition are shown in Figure 5.4 B.

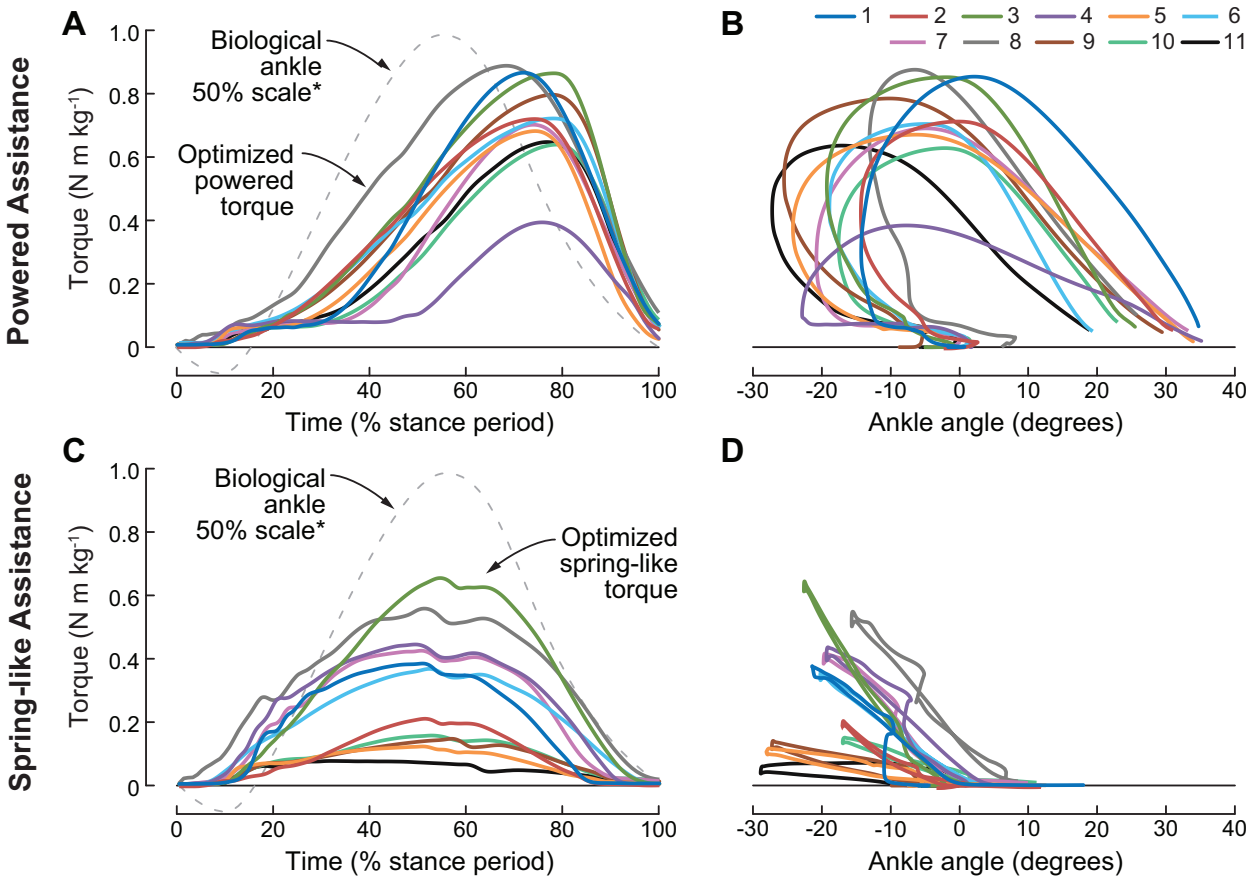

Figure 5.4: **Optimal assistance patterns.** **A** Optimized patterns of torque for the powered assistance strategy are shown as solid, colored lines for each subject. A 50% scale representation of the torque typically produced by the biological ankle during normal, unassisted running is shown as a dotted line [135]. **B** Torque vs. angle curves show large work injection for all subjects in powered condition. **C** Optimal torque patterns for spring-like assistance are shown as colored, solid lines. A 50% scale representation of the torque typically produced by the biological ankle during normal, unassisted running is shown as a dotted line [135]. **D** Torque vs. angle curves show minimal work injection for all subjects in passive spring-like condition.

5.3.3 Passive spring-like assistance

Average peak torque was lower for the passive spring-like condition compared to the powered condition (Fig. 5.4 C). No clear trends in stiffness or engagement angle were present. Participants experienced much lower dorsiflexion angles during stance compared to the powered condition (Fig. 5.4 D).

The average net metabolic rate measured for the spring-like condition was 11.96 ± 0.94. Optimized assistance for the spring-like controller improved energy economy by 2.2% on average (t-test, p = .014). Optimized spring-like assistance worsened running economy by 11.0% ± 2.84% compared to normal shoes (t-test, $p = 7 * 10^{-8}$).

Peak torque for the optimal passive condition was 0.32 ± 0.19 Nm kg^{-1} (Fig. 5.4 C). Average peak power provided during a stance period was -0.006 ± .012 W kg^{-1}. Average mechanical work applied during a stance period was -0.005 ± 0.009 J kg^{-1} in the optimal spring-like condition. Average work loops for each individual in the spring-like condition are shown in Figure 5.4 D.

5.4 Discussion

The powered torque strategy was much more effective than spring-like assistance, and outperforms any other running assistance strategy to date. Embedding the powered strategy into a mobile device could substantially increase speed and endurance, which could make running easier and more enjoyable.

Spring-like assistance was not as effective as expected. Its benefit was about half that of a specialized marathon shoe [39]. The magnitude of benefit was similar to that found for a passive ankle exoskeleton assisting walking [30], but represented a smaller percentage of the cost of locomoting without assistance. A small net benefit might be obtained by embedding the passive strategy into an exceptionally lightweight portable device with smaller overall envelope than that of the exoskeletons used in this study.

Powered assistance applied higher peak torques later in stance than the spring-like condition. As intended, large amounts of positive work were applied in the powered condition and a negligible amount of negative work was applied in the passive spring-like condition. This difference in work input does not necessarily explain the difference in performance. The optimal settings for the powered assistance did not maximize power or work input, and previous studies have demonstrated that that additional power is not always helpful [2, 136].

The peak torques applied by the optimal powered assistance were experienced significantly later than the peak torque typically supplied by the biological ankle during normal, unassisted running [135]. The shape of the torque applied by the spring-like controller is much more similar to that normally produced by the biological ankle during normal running, with the timing of peak torque well aligned (Fig. 5.4). It is possible that the powered assistance strategy is successful because it can supply torque late in stance when force production in the soleus muscle is limited [137], while the spring-like assistance strategy implemented here cannot produce late-stance torques.

Human-in-the-loop optimization appears to have found near optimal settings for each subject. All subjects converged after 64 minutes of running with one exception who didn't complete the protocol. The metabolic reductions achieved using the optimization were larger than those found using hand-tuning in pilot testing for both powered and spring-like strategies. Hand tuned spring-like assistance raised the metabolic cost of running.

The powered assistance strategy applied here is biologically inspired and the resulting torque patterns are not particularly different from those tried unsuccessfully in the past. It is suspected that this particular HILO method utilizing a covariance matrix adaptation evolutionary strategy (CMA-ES) is successful partly due to the customization of settings to fit individual needs, but also because it facilitates learning through forced exploration.

The results for the powered condition are similar to those found in a comparable study on walking assistance [2] with record setting metabolic reductions. Both studies took advan-

tage of human-in-the-loop optimization to discover that optimal peak torque occurs late in stance and optimal off-time occurs very close to toe off. These two studies combined provide strong evidence that this particular method of HILO is highly effective. It is expected that the performance of other existing exoskeletons can be enhanced by applying a similar HILO strategy.

Another suspected key to success is the fact that our ankle exoskeletons are lightweight and interface with the user in areas of low compliance (little soft-tissue). This reduces the initial penalties associated with wearing mass distally and allows for efficient transfer of mechanical power [62].

This experiment demonstrated that assisting the ankle joint with a powered strategy can be effective. The metabolic reductions achieved during this experiment exceed all previous approaches that assist the hips; however, too many confounding factors exist between studies to make a definite statement about which joints are most effective. The high metabolic reductions demonstrated here may be more a matter of optimization than the location of assistance. Assisting different joints or combinations of joints may be more effective. In particular, simulations suggest hip assistance may be most effective, particularly at high running speeds [138]. Future experiments comparing similarly optimized assistance strategies across joints would be interesting to pursue.

It is unclear why the spring-like assistance was less effective. Intuition and prior work created the expectation that spring-like assistance would be highly effective. Efficiency is maintained differently during walking and running as the center of mass exhibits fundamentally different behavior. Efficiency during walking is enabled by an exchange between potential and kinetic energy as the COM vaults over the leg like an inverted pendulum. In running, potential and kinetic energy are out of phase, and efficiency is maintained through the storage and return of elastic potential energy in tendons and the transfer of energy between body segments through biarticular muscles, resulting in spring-like mechanics [107]. It is therefore entirely surprising that passive assistance at the ankle is more effective dur-

ing walking [30] than during running. Additionally, prior work has demonstrated that overall knee stiffness while wearing an exoskeleton remains constant whether a spring in parallel with the knee is engaged or not [127], suggesting it is possible to use springs to reduce muscle forces without drastically altering kinematics. Lastly, a passive strategy at the hip has significantly reduced energy cost, which demonstrates that spring-like assistance can be helpful [6].

There may be a fundamental difference between the ankle and hip that limits benefits of spring-like assistance at the ankle. A greater balance between positive and negative work performed during the stance period may be needed. The ankle performs large net positive work during running. In contrast, the hip provides large amounts of both positive and negative work exhibiting more spring-like behavior. Along the same line of reasoning, running speed may affect the ability of spring-like assistance to benefit the user. The ankle performs larger amounts of negative work during sprinting than at slower paces [**?**], suggesting greater benefits may be possible at higher speeds.

It is possible that additional training or optimization time may improve the performance of the spring-like controller. We strongly suspect that additional training time is not helpful based on pilot tests involving a single subject, but given the results presented in chapter 6 additional exploration of the spring-like controller may yield better results. All else being equal, powered assistance is clearly more effective when training and optimization time is limited.

This experiment has significant implications for the design of portable exoskeleton systems: powered, single joint exoskeletons can be successful if they are sufficiently lightweight. It is difficult to anticipate a numeric value for the metabolic benefit of a mobile device as there are several factors to consider. Our optimization did not include a penalty on device torque or power, which are details that drive design and ultimately determine the mass of a portable system. A mobile device designed to meet the performance criteria implied by our results may not be optimal as the mass associated with the motors and power supply

may outweigh the added benefits. Additionally, other factors such as overall device envelope must be considered. The exoskeletons used in this study increase the effective volume of the user's leg substantially. A portable system may be designed to be more form fitting, which would have a positive effect on metabolic cost. All things considered, the design of assistive devices is a Pareto optimality problem with many competing factors. Considering all of these factors early in the design process and using emulator systems to evaluate options may well accelerate development [139].

5.5 Conclusions

This experiment demonstrates that powered assistance is much more effective than spring-like assistance in reducing the metabolic cost of running using ankle exoskeletons. Parameters defining applied torque patterns were optimized for each individual subject to allow for a fair comparison between the two assistance strategies. Powered assistance reduced the metabolic cost of walking by 24.7% compared to zero-torque mode and 14.5% compared to running in normal shoes, while spring-like assistance resulted in a 2.2% reduction compared to zero torque and increased the cost of running by 11.0% compared to normal running shoes. The powered ankle exoskeleton assistance strategy presented here outperforms any prior attempts at improving running economy and demonstrates the significance of human-in-the-loop optimization in meeting the needs of individuals and facilitating learning. The results have exciting practical implications suggesting that portable ankle exoskeletons may be capable of sharply improving running performance using a similar powered assistance strategy. Such devices may improve participation in running by decreasing the intensity of running and increasing enjoyment, interest, and perceived ability.

Chapter 6

Experimental comparison of high-level ankle exoskeleton controllers for walking assistance

Abstract

Time-based control used on ankle exoskeletons holds the record for the greatest metabolic energy reduction produced during walking, but it is unclear that time-based methods are fundamentally more effective than others. A paucity of experimental comparisons and confounding factors between experiments make it difficult to evaluate the relative benefits of different control architectures. Electromyographic (EMG) controllers are thought to be advantageous as they are controlled by the user's muscle activity and should be responsive to their changing needs. Muscle-tendon controllers that respond to EMG in a way that captures the dynamics of human muscle may be more intuitive. An experimental comparison of time-based, simple EMG, and EMG-based muscle-tendon controllers was performed to evaluate the relative benefits of each. Subjects walked on a treadmill while using tethered, bilateral ankle exoskeletons. Human-in-the-loop optimization allowed a more objec-

A manuscript presenting this chapter is in preparation.

tive comparison by customizing each controller to fit individual needs. Each subject experienced 240 minutes of optimization over three days. Two tailed, paired t-tests determined the significance of the difference between the assisted and unassisted trials and between metabolic reductions achieved by each controller type. Validation trials were performed at the beginning and end of each session of optimization to provide an indication of learning and adaptation over time. Optimal time-based, EMG, and muscle-tendon controllers produced statistically significant metabolic reductions of 17.8%, 15.1%, and 7.9%, respectively, compared to a zero-torque mode with statistical significance between the time-based and muscle-tendon controllers overall. The muscle-tendon controller failed to produce metabolic reductions below that of walking in normal shoes. Results demonstrate this implementation of virtual muscle-tendon control was not effective. While a time-based strategy was most effective on average, linear EMG was a close second with maximum metabolic reductions greater than those experienced in the time-based setting. The optimal settings for all controllers outperformed the initial settings, demonstrating that the optimization was beneficial in all conditions. Our results indicate the relative efficacy of different control architectures and highlight the importance of training and optimization in maximizing the benefits of exoskeleton assistance.

6.1 Introduction

Identifying the most effective qualitative assistive strategies to apply with exoskeletons should accelerate research by providing an indication of the most promising directions to take development. Many exoskeleton assistance strategies have been used to improve walking economy, but it is unclear which broad strategies are most effective due to confounding factors between studies. An experimental comparison between time-based, EMG based, and novel muscle-tendon based controllers could reveal which qualitative controllers are most promising.

Time-based and EMG based controllers have both been used on ankle exoskeletons to reduce the metabolic cost of walking. Time-based ankle assistance currently holds the record for the greatest metabolic energy reduction during walking [2], and has traditionally been a leading strategy in this field [20, 21, 4, 3]. Electromyographic (EMG) control has also been successful in reducing metabolic energy, though not to the same degree [40, 26, 27].

Time-based control of lower-limb exoskeletons has dominated the field mainly due to its simplicity. In general, time-based control involves first detecting some important indicator of gait phase, such as heel strike [1] or maximum hip flexion [22], and applying assistance accordingly as a function of time as a percentage of the anticipated duration of the step. This approach may depend on a single event for timing, or may apply assistance as a piece-wise function according to several gait events. It is very simple, but requires clever implementation to operate well under non-steady state conditions where estimation of step duration is not accurately achieved by a slow moving average.

The long term efficacy of time-based control is in question as accomplishing diverse tasks requires prediction of user intent through classifiers. Though there has been significant success in this area [23, 24, 25], incorrect classification of intent could have disastrous results. For example, mistaking stair descent for stair ascent could be life threatening. This highlights the need for classifiers capable of predicting user intent accurately with adequate time for the exoskeleton to apply appropriate assistance.

In contrast to time-based control, electromyographic (EMG) control should be highly responsive to inter-step variability and user intent. Surface electrodes adhered to the user's skin are used to measure electrical activity in underlying muscles. This electrical activity is indicative of muscle recruitment and should encode user intent. Using EMG signals to drive exoskeleton assistance should allow seamless transitions between different activities with little need for classifiers. Proportional EMG control [26] and variants involving adaptive gains [27] have been shown to significantly reduce metabolic cost during walking. Strategies that leverage measurement of antagonistic muscle activity to inhibit exoskele-

ton assistance have resulted in more natural kinematics than methods that utilize activity from a single muscle [28]. A potential disadvantage of EMG control is that high levels of torque assistance are not maintained if muscle activity drops. While adaptive EMG strategies may partially address this issue [27], time-based control may allow users to better take advantage of torque assistance by being insensitive to drops in muscle activity. Regardless of the optimality of the controller settings, EMG control may be limited as muscle activity does not entirely encode muscle force or joint torque. Due to the complexity of muscle dynamics, user intent may not be completely encoded in muscle activity alone. Muscle force is produced as a function of muscle activation, the length of muscle fascicles, and their contractile velocity [140]. Limits on muscle performance, such as force-length and force-velocity relationships, can drive muscle force production from its maximum to zero even if muscle activation, which is indicated by measured EMG, is held constant. Capturing these aspects of muscle dynamics may be crucial to improving the performance of EMG-based control. Unfortunately, it is not feasible to make real time measurements of muscle fascicle length or contractile velocity.

Neuromuscular controllers may provide a more intuitive mapping between measured EMG signals and exoskeleton assistance. Neuromuscular controllers contain a simulation of muscle dynamics to estimate muscle fascicle length and contractile velocity, which can be used to estimate muscle force and joint torque. Neuromuscular controllers have been used in robotic prostheses to create human-like joint torques [41, 141, 142] and have been used to reduce the metabolic cost of walking for amputees [29]. In the case of amputees, EMG signals may not be available as the muscles associated with the replaced joint may be missing or no longer have normal function. Neuromuscular controllers simulate not only muscle dynamics, but also muscle activation using reflex models [143]. Similar control has been implemented in exoskeletons for assisting individuals with spinal cord injury [144] and experiments evaluating its feasibility for assisting healthy individuals are underway at Georgia Tech's PoWeR lab [145], but no data is available on the metabolic effects of neuro-

muscular control of exoskeletons for healthy individuals.

No current exoskeleton control strategies both capture muscle dynamics and allow measured EMG as an input to allow high responsiveness to user intention with behavior similar to human muscle. Reducing a neuromuscular controller to a simpler muscle-tendon controller may be a good option for applications featuring exoskeletons on healthy individuals. A virtual muscle-tendon model could calculate joint torque using measured joint angle and measured EMG signals as a proxy for muscle activation. No data on this strategy exists as neuromuscular controllers are traditionally used in prostheses, in which case EMG signals are unavailable. A muscle-tendon model controller is being explored for prosthesis control for amputees whose EMG activity is preserved through experimental surgery [146, 147], but no data exists for an EMG driven, muscle-tendon-model-based exoskeleton controller for healthy individuals.

Confounding factors between studies make it difficult to ascertain the relative benefits of each qualitative strategy. Time-based controllers currently appear to outperform EMG based controllers, but the reason is unclear. Is time-based control a fundamentally more effective approach? Or is it a matter of implementation? Too many confounding factors such as device mass, training, presence of optimization, or hardware limitations exist between experiments exploring qualitatively different strategies to be certain of the relative benefits between them. Developing tools to enable fair comparisons of qualitatively different assistive strategies in isolation from other confounding factors may enable developers to make more informed choices, leading to more rapid development.

Experimental comparisons of qualitatively different strategies can provide more accurate representations of the relative benefits between strategies. Unfortunately very few experimental comparisons have been performed. Those that have been performed have made impactful discoveries, highlighting the need for more. For example, a first-of-its-kind comparison study recently showed that an EMG controller with an adaptive gain reduced energy cost by 19% [27]. The same study then compared the result to a mechanically in-

trinsic (time-based) controller that applied a torque profile derived from the average desired torque developed by the EMG controller. The time-based controller matched the performance of the EMG based controller. This suggests that the ability of proportional EMG controllers to react to inter-step variability does not intrinsically result in metabolic reductions during steady state walking. Questions still remain as to how well proportional EMG control compares to other patterns of time-based assistance.

Performing experimental comparisons of qualitatively different controllers can be difficult as exoskeleton users often exhibit different responses to the same exoskeleton assistance [148, 104], and each individual user can benefit from customized assistance [2, 132, 149]. The comparison of qualitatively different strategies is not accurate if each controller is not equally well customized to fit the needs of individual users.

We have performed an experimental comparison demonstrating the relative benefits of time-based control, simple EMG control, and a novel muscle-tendon controller in isolation of outside confounding factors. Subjects walked on a treadmill while wearing bilateral tethered ankle exoskeletons [47] and experienced all three control strategies in a nine day protocol.

Human-in-the-loop optimization (HILO) using a covariance matrix adaptation evolutionary strategy (CMA-ES) enabled better comparisons between controllers by ensuring the best possible versions of each controller were compared on an individual subject basis. Each subject experienced 240 minutes of optimization distributed over three days. Optimizing all three controllers for the same individual subjects resulted in a more objective comparison. The performance of each controller was tested immediately following the end of the optimization on the third day by comparing the metabolic cost of walking with optimized control to walking in zero-torque mode and normal shoes. The effectiveness of the optimization was assessed by comparing the metabolic cost of walking in the optimal controller to the cost of walking with the control settings used to initialize the optimization. A similar approach has been used to compare powered and passive strategies for assisting running with bilateral ankle exoskeletons (Chapter 5).

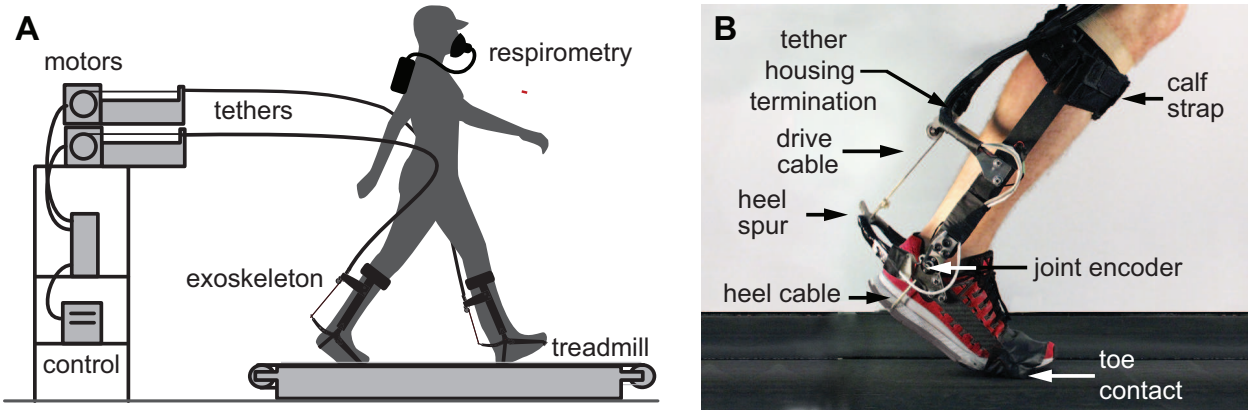

Figure 6.1: **Experimental setup.** **A** Participants walked on a treadmill while wearing bilateral ankle exoskeleton end-effectors actuated by off-board motors with mechanical power transmitted through flexible Bowden cables. A respirometry system recorded volumetric oxygen consumption and carbon dioxide expulsion data for the purpose of calculating metabolic rate. **B** The frames of the ankle exoskeletons were composed of plate carbon fiber. Joint angle was measured by a magnetic encoder and torque was measured directly by strain gauges located on the titanium heel spur. When the exoskeleton applied plantar flexion assistance, the calf strap applied pressure to the front of the shin and a force was applied to the heel using a heel cable. The line of action of the heel cable was approximately coincident with the biological ankle joint. A plate embedded in the toe of the shoe pressed down on the treadmill when the exoskeleton applied torque.

6.2 Methods

The goal of this study was to assess the relative benefits of three different high-level ankle exoskeleton control strategies: time-based, linear EMG, and a virtual muscle-tendon model based controller which used EMG measurements as input. We performed an experiment in which participants walked on a treadmill at 1.25 m/s while wearing bilateral ankle exoskeletons (Fig. 6.1) [47] connected to a universal exoskeleton emulator system [35]. Controller settings were optimized for each individual subject using a Covariance Matrix Adaptation Evolutionary Strategy (CMA-ES) [38]. Each subject experienced three days of testing for each controller for nine days in total. The main outcome of interest was the metabolic cost of walking using each of the three strategies as compared to walking with the exoskeleton in unassisted conditions: zero-torque mode and walking in normal shoes. Muscle activity in the medial and lateral aspects of the soleus muscles was also collected for comparison and as an input for two of the controllers. Speed trials were conducted to examine how well each of the optimized controllers performed at different speeds without adjusting settings.

6.2.1 Controller parameterizations

All three controllers utilized the same phase detection and swing behavior. The beginning of stance was detected by a heel switch in the toe of the shoe and a transition to swing could be triggered by four different criteria: plantarflexion beyond 110% of the maximum plantarflexion angle measured during walking in zero-torque mode, a zero crossing in ankle angular velocity after a minimum amount of time had passed after heel strike, vertical ground reaction forces dropping below a threshold, or if the first three criteria failed to detect the transition, a timer triggered a transition at 110% average stance time. Zero-torque mode was applied during the swing phase, in which the motor is position controlled to maintain a small amount of slack in the Bowden cable.

Time-based control

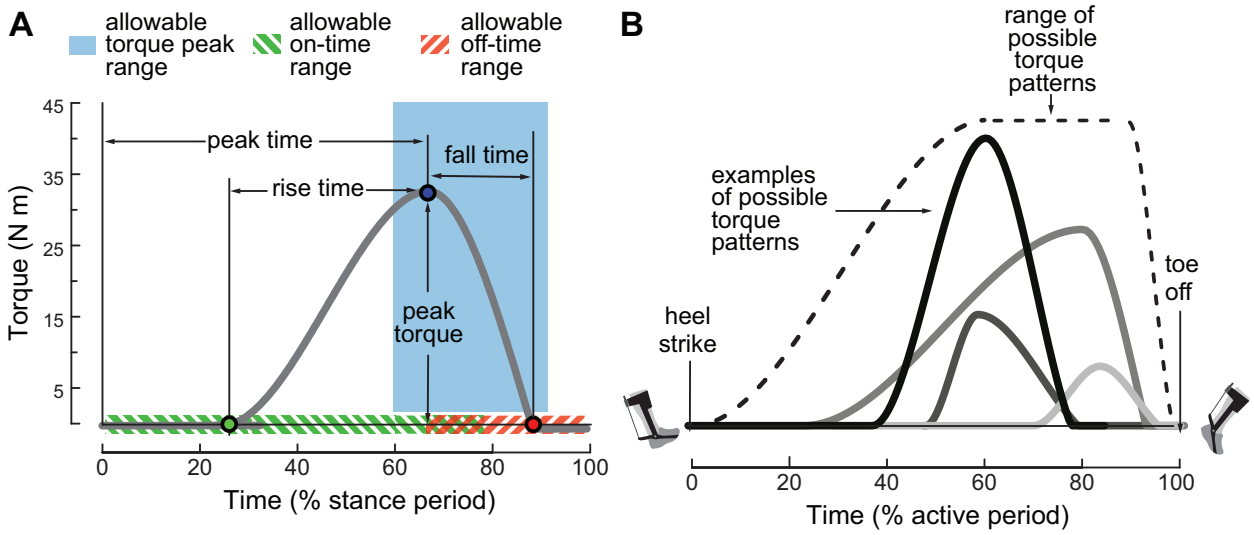

Figure 6.2: **Time-based control parameterization.** **A** The time based controller is defined by three nodes connected by sinusoids. These three nodes are defined by four parameters: rise time, t_r, peak time t_p, fall time t_f, and peak torque τ_p. 0% stance corresponds with heel strike. 100% stance corresponds with toe off. **B** The range of possible torque patterns is shown as the area enclosed by a dotted line. Several example torque patterns are shown.

The time-based controller was defined by three nodes connected by two sinusoids (Fig. 6.2). These three nodes were defined by four parameters: the magnitude of peak torque, the timing of peak torque relative to heel strike (peak time), the time required for torque

to increase from zero to peak torque (rise time), and the time required for torque to fall back to zero (fall time). Table 6.2 shows the initial settings, and maximum and minimum boundaries allowed for these parameters.

Table 6.1: Time-based controller parameters, initial settings, and boundaries.

Parameter	Units	Initial	Min.	Max.
peak torque	Nm	0.42m	0	45
peak timing	% stance	80	60	92
rise time	% stance	40	16	60
fall time	% stance	16	8	25

Linear EMG

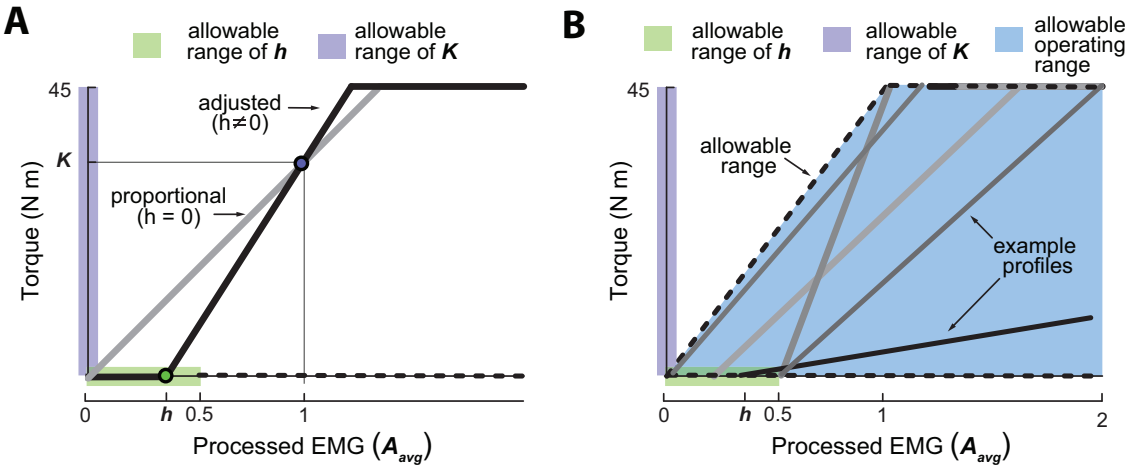

Figure 6.3: **Linear EMG parameterization.** **A** Torque is applied as a linear function of processed EMG signal. The x-intercept is set by the parameter, h and the slope of the curve is set by the gain, K. The controller is proportional when $h = 0$. **B** The range of possible relationships between torque and processed EMG signals.

The EMG controller calculated desired torque, τ_{exo}, by applying a gain, K, and threshold, h, to the processed EMG activity measured from the user's soleus muscle, A_{avg}. Raw EMG signals were high-pass filtered (Butterworth) with a cut-off frequency of 20 Hz, full wave rectified, and low-pass filtered with a cut-off frequency of f_{LPF}. Each EMG signal was normalized by the average peak EMG measurement recorded for each of 50 steps taken with the exoskeletons in zero-torque mode. This ensured that the calculated desired torque, τ_{exo}, exhibited peaks equal to the gain, K, on steps with average EMG signal. Lastly, any

EMG signal below a threshold cut-off, h, was set to zero to eliminate background noise. The relationship between A_{avg} and τ_{exo} was adjusted to ensure that a normalized average EMG signal of 1.0 would result in a torque equal to K and a signal of h would result in zero torque as shown in Equation 6.1 and Figure 6.3.

$$\tau_{exo}(t) = K * \Big(A_{avg}(t-d) - h\Big) * \frac{1}{1-h} \tag{6.1}$$

Where d is a delay applied to the processed EMG signal, A_{avg}. A_{avg} is calculated using the processed EMG signals from the medial and lateral aspects of the soleus muscle, A_{sm} and A_{sl} respectively.

$$A_{avg}(t) = \frac{A_{sl}(t) + A_{sm}(t)}{2} \tag{6.2}$$

The parameters included in the optimization for the Linear EMG controller were K, h, d and f_{lpf}.

The controller becomes a proportional EMG controller when h is set to 0. These parameters were selected because they are representative of the tunable settings applied to most EMG controllers, though no other research group has applied a delay. This delay was added to allow adjustment of the timing of torque application largely because muscle dynamics are slow and muscle force production is delayed in time with respect to electrical activity measured by EMG. Additionally, the low pass filter frequency has two unintended functions other than smoothing data: delaying signals and reducing peaks. The delay allows the optimizer to determine if torque patterns with higher frequencies that are also delayed are useful. This will help determine if smoothing is the main benefit of filtering as expected.

The torque produced by this controller can decrease substantially if subjects drastically reduce activity in the soleus muscle. Pilot testing suggested that subjects were not able to take advantage of very high torques while using this controller. For this reason the maximum bound on the gain was limited to 45 Nm per unit of normalized EMG.

Table 6.2: Linear EMG parameter initial settings and boundaries

Parameter	symbol	Units	Initial	Min.	Max.
Gain	K	Nm / unit EMG	0.4*m	0	45.0
Theshold	h	unit EMG	0.25	0	0.5
delay	d	s	0.02	0	0.10
low pass filter frequency	f_{LPF}	Hz	3.0	1.75	6.0

EMG with virtual muscle-tendon control

The virtual muscle-tendon controller was designed to function similarly to the soleus muscle in order to provide more intuitive exoskeleton control. The controller uses EMG signals and ankle position as inputs to a virtual model of a muscle-tendon unit to calculate exoskeleton torque (Fig. 6.4). The muscle-tendon model was a commonly used Hill-type muscle model which represents the muscle body as a contractile element (CE) connected to a series elastic element (SE), which represents the Achilles tendon, two additional elastic elements, HPE and LPE, act in parallel with the contractile element (Fig. 6.4) [143].

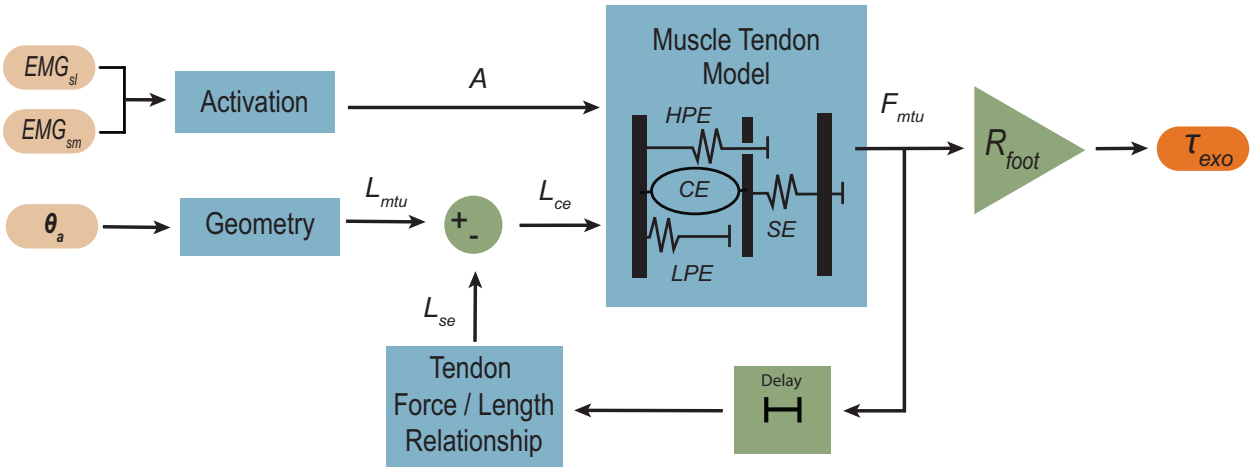

Figure 6.4: **The virtual muscle-tendon model.** Ankle angle, θ_a, and processed EMG signals, EMG_{sl} and EMG_{sm}, were used as inputs to the muscle tendon model. The model calculated the length of the series elastic tendon, L_{se}, and subtracted it from the total length of the virtual muscle tendon unit L_{mtu} in order to calculate the length of the contractile element, L_{ce}. The muscle model calculated the force produced by the virtual muscle, F_{MTU}, which was multiplied by a lever arm, R_{foot} to produce the torque applied by the exoskeleton,τ_{exo}. F_{MTU} was fed back into the model to resolve the inner degree of freedom L_{se}.

This controller was strongly based on the controller for a robotic prosthesis [41] with all model parameters matched with the exception of the parameters included in the opti-

mization. While muscle activity was simulated on the prosthesis, we used the average of the processed EMG signals from the medial and lateral aspects of the soleus as a proxy for muscle activation, A. Force in the virtual muscle tendon unit, F^{MTU}, was calculated as a shown in equation 6.3. Exoskeleton torque, τ_{exo}, was calculated as F^{MTU} multiplied by a a lever arm, R_{foot}, similar to the leverage of the soleus muscle about the ankle (Equation 6.4).

$$F^{MTU} = F_{max} * [A(t) * f_l(L_{ce}) * f_v(v_{ce})] + F_p(L_{ce}) \tag{6.3}$$

$$\tau_{exo} = F^{MTU} * R_{foot} \tag{6.4}$$

Where A is muscle activation estimated by low pass filtering measured EMG, v_{ce} is the contractile velocity of the contractile element, L_{ce} is the length of the contractile element and $f_l(L_{ce})$ is the force-length relationship of the contractile element (Equation 6.5), and $f_v(v_{ce})$ is the force-velocity relationship of the contractile element (Equation 6.7) and $F_p(L_{ce})$ is the parallel passive elastic muscle force.

$$f_l(L_{ce}) = e^{(c*|\frac{lce-lopt}{lopt*w}|^3)} \tag{6.5}$$

The width of the bell-shaped force-length relationship (Equation 6.5) is determined by w, and c is a constant that fulfills the relationship shown in Equation 6.6.

$$f_l(L_{opt} * (1 \pm w)) = 0.05 \tag{6.6}$$

Max contractile velocity, v_{max}, determined the contractile velocity at which the virtual muscle could no longer produce force as shown in Equation 6.7.

$$f_v(v_{ce}) = \begin{cases} (v_{max} - v_{ce})/(v_{max} + K * v_{ce}), & v_{ce} < 0 \\ N + (N-1) * \dfrac{v_{max} + v_{ce}}{7.56 * K * v_{ce} - v_{max}}, & \text{otherwise} \end{cases} \tag{6.7}$$

Note that $f_v(v_{ce})$ is reduced to zero when the velocity of the contractile element, v_{ce}, is equal to v_{max}, which results in zero force produced by the muscle. K is a curvature constant and N defines the dimensionless muscle force (normalized by F_{max}) produced during an eccentric contraction with a velocity of equal magnitude to v_{max} such that

$$N = f_v(v_{ce} = -v_{max}) \tag{6.8}$$

N is larger than one meaning that eccentric contractions can result in very high force output. Maximizing v_{max} should have the effect of both reducing the force typically available during eccentric contractions and reducing the limitations on muscle force experienced during concentric contractions with high velocity.

The virtual tendon behaved like a non-linear spring with reference strain, ϵ_{ref}, which indicated the length of the tendon when the virtual muscle was producing its max isometric force, F_{max}. The relationship between the length of the series elastic unit and tendon strain is shown below (Equation 6.9).

$$F_{se} = \begin{cases} F_{max}\left(\epsilon/\epsilon_{ref}\right)^2, & \epsilon > 0 \\ 0, & \text{otherwise} \end{cases} \tag{6.9}$$

The equations listed above are key to understanding the effects of the parameters optimized in this experiment, but do not represent a complete description of the virtual muscle tendon model. A more complete description can be found in [41].

The parameters included in the optimization of this controller were: F_{max}, v_{max}, ϵ_{ref}, and f_{LPF}, the low pass filter cut-off frequency applied to EMG measurements. Adjusting the level of F_{max} acted as a gain on muscle force. Increasing v_{max} relaxed the limitations

placed on muscle force applied by the force-velocity relationship while decreasing it reduced the ability of the virtual muscle to produce force at high contractile velocities. Adjusting the reference strain, ϵ_{ref}, adjusted the stiffness of the tendon with higher values of ϵ_r resulting in lower stiffness. This stiffness has a significant effect on force production as the length of the muscle determines force output due to the force-length relationship shown in Equation 6.5. f_{LPF} was the low pass filter cut-off frequency applied to EMG signals. Increasing this value essentially smoothed virtual muscle activation. The initial settings and boundaries of these parameters are shown in Table 6.3. The initial setting for F_{max} was dependent on the body mass of the user, m.

Table 6.3: Muscle-tendon controller parameters, initial settings, and boundaries

Parameter	Units	Initial	Min.	Max.
F_{max}	N	25*m	1000	3000
v_{max}	L_{opt}/s	6	12	0
ϵ_r	l/l	0.08	.035	0.2
f_{LPF}	Hz	4.0	1.75	6.0

6.2.2 Overall experimental protocol

Three ankle exoskeleton control strategies were compared experimentally after being optimized for minimal metabolic cost during walking. Each subject experienced a nine day protocol during which they walked on a treadmill at a pace of 1.25 ms^{-1} while wearing bilateral ankle exoskeletons. Three days were dedicated the optimization of each controller. Subjects were offered optional breaks after each generation of optimization, and four minute breaks were experienced between validation trials which were six minutes in length. See section 6.2.4 for more details on the optimization strategy. The three controllers were experienced in randomized order by each subject such that every permutation of the controllers was experienced by one subject.

Day 1

Subjects were first fitted for the exoskeletons. Modular components were replaced to account for leg length and calf diameter. After donning the exoskeletons, subjects were allowed five minutes of walking in zero-torque mode. A six minute trial of zero-torque mode was then recorded. The initial settings of the first randomly selected controller were applied and torque was slowly increased from 0 to the average setting over a duration of five to ten minutes depending on subject comfort. A six minute trial of the initial settings for generation 1 was then recorded. The subject then experienced four generations of optimization. The mean of the fifth generation was calculated and applied in a six minute trial immediately following the fourth generation (Gen5Imm). The subject then experienced a four minute break followed by validation trials. These trials included the following conditions: Generation 1 mean (Gen1), generation 5 mean (Gen5), zero-torque (ZT), and quiet standing (QS). Validation trials were completed in randomly assigned double reversed order (ABCDDCBA). Four minute breaks were experienced between each of these six minute trials.

Day 2

Day 2 of a given controller was similar to day 1. Six minute trials of zero-torque and the optimal settings from the prior day (Gen5) were experienced prior to continuing the optimization with generations 4 through 8. The mean calculated for the ninth generation was considered the optimal control law for the day (Gen9). A six minute trial of the optimal control law was performed immediately following the optimization (Gen9Imm). The subject then experienced eight validation trials of the following conditions in double reversed order: Gen5, Gen9, ZT, and QS.

Day 3

The pattern continued on day 3 with six minute trials of ZT and Gen9 followed by optimization. The mean calculated for the 13th generation was considered the optimal control

law. This optimal control law was tested immediately following the optimization. Twelve validation trials were then performed: Optimal, Gen9, Gen1, ZT, QS, and normal Shoes (NS). These conditions were performed in block randomized double reversed order such that walking in normal shoes either occurred first and last or back to back in the middle of the validation trials. This is a time saving measure that ensures that the exoskeletons only need to be donned and doffed twice. Placement of the normal shoes trials was occasionally adjusted (not random) to allow for convenient timing of restroom breaks. Optional speed trials were then performed. Subjects walked in four six-minute trials including ZT and Opt modes at both slow (1.0 m/s) and fast (1.5 m/s) speeds. All subjects opted to complete the speed trials. Due to the length of the protocol these trials were not repeated in double reversed order.

6.2.3 Measured outcomes

The main outcome of interest was the difference in net metabolic energy consumption between the zero-toque mode and the optimal controller settings for the purposes of comparing the three assistance strategies. The average metabolic rate was calculated for each condition in which the last three minutes of data from each six minute trial were collected. Volumetric oxygen consumption and carbon dioxide expulsion were used to calculate metabolic rate for each breath using a commonly used equation [134]. Combining this information with breath duration allowed the calculation of average metabolic rate over the course of the collection. Data from each matched pair of double reversed trials was averaged. Net metabolic rate was calculated as the difference between the average metabolic rate of each condition type and that of quiet standing, which was then normalized to body weight.

Additional outcomes included differences in metabolic rate measured between other test conditions. The initial settings used at the beginning of the optimization were used as the Gen1 condition and the metabolic rate was compared to that experienced in the optimal condition. This provided an indication of whether or not customization of device settings

was largely responsible for improved performance. It is possible that motor learning occurring over the course of the optimization may be the key factor in improved performance experienced after the optimization. Comparing the optimal control law to normal shoes provided some understanding of what benefits may be delivered by commercial devices with similar capabilities. Including the speed trials provided some indication of the flexibility of the controllers by assessing their ability to provide benefit under conditions dissimilar to those experienced during optimization. In addition to metabolic reductions, the optimized parameter values and their variance are of interest as they may provide insight for product design and future training protocols.

6.2.4 Optimization strategy

Human-in-the-loop optimization [2] was applied to all three assistance strategies using a Covariance Matrix Adaptation Evolutionary Strategy (CMA-ES) [38]. Normal distributions for each parameter were created with means and variances defined as initial settings. Parameters were selected from these distributions to form eight trial controllers. In contrast to our prior work [2] elitism was introduced by including two additional trial controllers in each generation: the mean of the current generation, and the best controller from the prior generation. While random selection of trial controllers facilitates robustness to drift, measurement noise, and changing behavior as the user learns [2], it is possible for a generation composed of outlier settings located far from the means to be generated. Testing the mean of the current generation ensured that the user experienced at least one controller in the direction that the optimizer was moving, and testing the best setting from the prior generation helped the optimizer to converge if a good strategy was discovered. The remaining 8 randomly selected trials allowed an appropriate amount of exploration as recommended when optimizing four parameters [38].

Each trial controller was tested for two minutes. Steady state metabolic cost was estimated by fitting a first-order dynamical model [133] to the metabolic data collected using a

respiratory system (Quark CPET: Cosmed). A covariance matrix adaptation was performed after each generation of ten controllers to calculate new means and variances for the parameter distributions. These distributions were then used to sample ten new trial controllers for the following generation. The mean parameter values calculated for the thirteenth generation on the third day of optimization were considered the optimal control law.

The initial settings for the means of the controller parameters were discovered during pilot testing as a result of hand tuning and several days of optimization for a single pilot subject. The maximum and minimum boundaries for each parameter were selected during pilot testing as the bounds comfort would allow.

6.2.5 Participants

Seven subjects were recruited for the study. One subject completed three days, but dropped out due to time commitments. This subject's data was discarded. Six subjects completed the protocol (5 male, 1 female, Age = 27.8 ± 4.3 yrs, mass = 77.1 ± 10.1 kg). These subjects represented a variety of levels of fitness and ages (Table 6.4).

Table 6.4: Subject characteristics

Subject	Sex	Age (yrs)	Mass (kg)	Height (m)
1	m	35	82.3	1.82
2	m	23	80.0	1.77
3	f	28	61.7	1.78
4	m	30	80.7	1.78
5	m	25	68.4	1.83
6	m	26	89.5	1.83

6.3 Results

6.3.1 Metabolic results

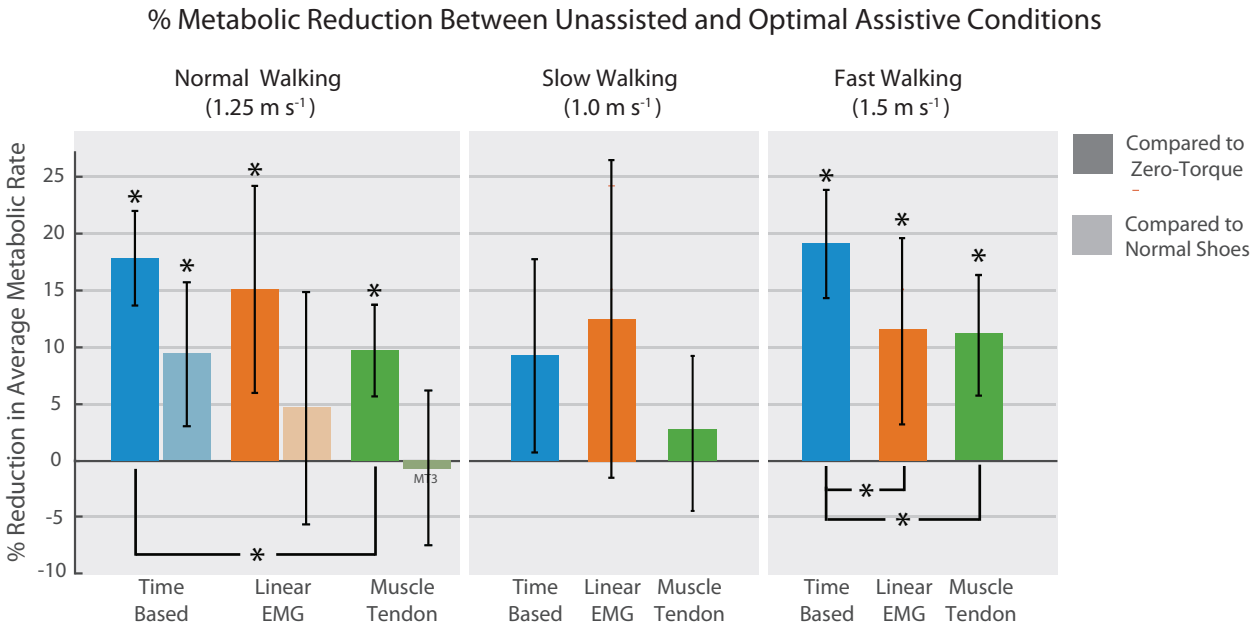

Figure 6.5: **Percent reductions in average net metabolic rate between assisted and unassisted conditions.** Net metabolic reductions were calculated between the optimal settings and the unassisted conditions including zero-torque mode (dark bars) and normal shoes (light bars). Single speed trials (not double reversed) compared the performance of the controllers at slow (1.0 ms^{-1}.) and fast (1.5 ms^{-1}.) paces to zero-torque mode at the same pace. Controller settings were applied as optimized for normal walking in both the slow and fast trials. Asterisks indicate that the differences between the assisted and unassisted trials were statistically significant as tested by a two tailed, paired t-test. Brackets and asterisks indicate a statistically significant difference between the percent metabolic reductions achieved by each controller.

A summary of the average net metabolic reductions produced in each of the validation conditions for all subjects and controllers can be seen in (Table 6.5).

Time-based control

Time-based control resulted in the greatest metabolic reductions compared to zero-torque mode at 1.25 ms^{-1} (17.8% ± 4.16%) (Fig.6.5). This translated to a metabolic benefit of about 9.5% compared to normal shoes. Time-based control produced a smaller reduction (9.26% ± 8.44%) than linear EMG during slow walking, but far outperformed the EMG controllers at

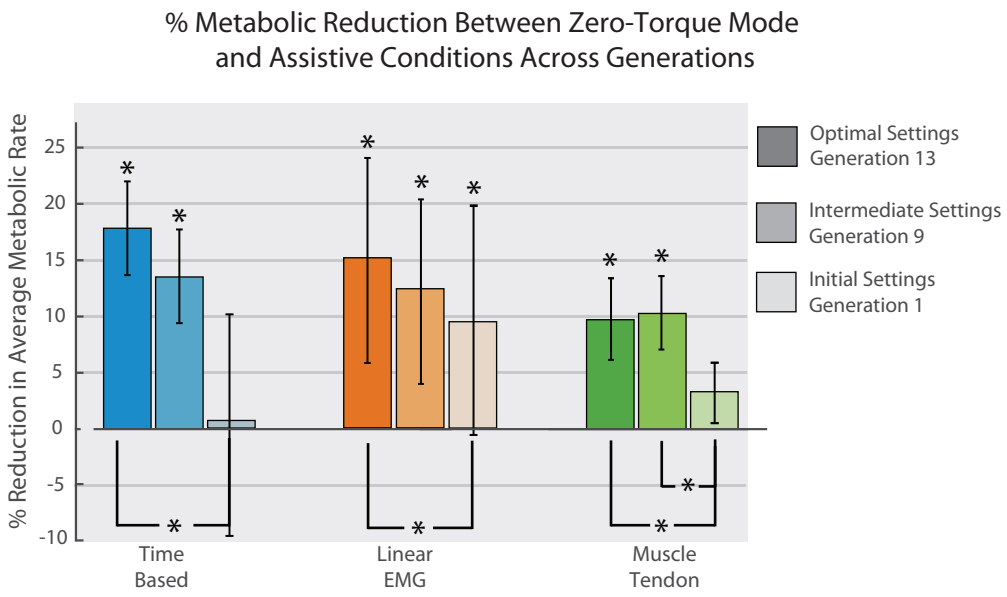

Figure 6.6: **Metabolic reductions achieved after optimization for optimal and intermediate settings.** Net metabolic reductions were calculated for validation trials following optimization. The conditions included the initial settings from generation 1, intermediate settings calculated as the mean of generation 9, and the optimal settings calculated as the mean of generation 13 at the end of the optimization. An upward trend is evident as the settings from more recent generations outperform earlier generations for the time-based and linear EMG controllers. Trends are less clear for the muscle tendon controller. Asterisks above bars indicate that the differences between the assisted and zero-torque trials were statistically significant as tested by a two tailed, paired t-test. Brackets and asterisks indicate a statistically significant difference between the percent metabolic reductions achieved by each condition as tested by a two tailed, paired t-test.

the fast pace with an average reduction nearly double that of the other controllers (18.9% ± 4.75%). A benefit was observed for additional customization as evidenced by the fact that reductions achieved by the optimal settings calculated for the 13th generation significantly outperformed those measured for the Gen1 (0.64% ± 9.76%) settings (Fig. 6.6). This demonstrates that the optimizer was effective at least partly due to customization and not only facilitating learning through practice and forced exploration. The optimal settings also outperformed the Gen9 settings (14.0% ± 5.8%), but the difference was not significant ($p = 0.20$).

Linear EMG control

Optimal linear EMG assistance resulted in a metabolic reduction of (15.1% ± 9.1%) compared to zero-torque at normal speed (Fig. 6.5). The metabolic reduction compared to nor-

mal shoes was not statistically significant. The reductions achieved in the optimal condition were greater than those produced in the Gen1 condition (9.82% ± 8.43%) by a statistically significant margin (p = 0.004). Again, suggesting that the customization of device settings was largely responsible for the reductions achieved in the optimal condition. The average metabolic reduction for the linear EMG optimal settings was higher than the other two controllers during slow walking (12.8% ± 15.5%), but the variance was also much higher than the other controllers in all test conditions suggesting that subjects may have had unequal ability to adapt to the linear EMG controller. While the average metabolic reductions for torque time were greater for normal and fast paces, the maximum reductions achieved by the optimal controller settings compared to zero-torque were nearly equivalent between the torque time (25.26%) and proportional EMG controllers (25.54%).

Muscle-tendon control

The muscle-tendon controller placed last in every condition: normal (7.9% ± 4.0%) , slow (2.9% ± 7.0%) and fast (11.3% ± 5.2%). The muscle tendon controller even increased metabolic cost compared to normal shoes by 0.79% though the finding was not significant. It did not produce statistically significant reductions in the normal or slow walking conditions. Though the muscle tendon controller's average reduction was lower, the variance was smaller than that of the linear EMG controller suggesting that subjects could take advantage of it more equally well.

The optimal condition calculated for the 13th generation did not outperform the settings from generation 9 for the muscle tendon controller. Both generation 9 settings and optimal settings did perform better than the initial settings by a statistically significant amount (p = .002 and p = .010 respectively).

Table 6.5: **Average net metabolic reductions compared to zero-torque condition.**

Time Based							
Subject	Opt13	Gen1	Gen9	Gen9Pre	slowOpt	fastOpt	OptImm
1	14.36%	6.89%	6.46%	-2.75%	16.85%	17.37%	21.77%
2	15.72%	3.86%	13.49%	6.16%	3.35%	19.49%	16.30%
3	19.99%	-17.65%	22.24%	7.22%	-4.81%	15.61%	29.86%
4	25.36%	8.35%	11.20%	19.29%	15.49%	26.72%	30.95%
5	16.38%	-2.79%	19.27%	13.38%	10.28%	13.14%	13.65%
6	15.25%	5.19%	11.26%	3.90%	14.39%	21.10%	2.00%
average	17.84%	0.64%	13.99%	7.87%	9.26%	18.91%	19.09%
std	4.16%	9.76%	5.80%	7.65%	8.45%	4.75%	10.89%
Linear EMG							
Subject	Opt13	Gen1	Gen9	Gen9Pre	slowOpt	fastOpt	OptImm
1	24.54%	16.46%	23.25%	19.95%	18.35%	16.35%	22.50%
2	8.66%	0.68%	11.96%	11.83%	40.00%	9.34%	18.77%
3	25.54%	21.43%	23.02%	16.24%	6.83%	5.10%	16.24%
4	19.00%	13.36%	17.93%	22.41%	12.22%	24.91%	21.93%
5	8.61%	4.18%	-0.65%	20.16%	4.19%	-0.41%	-0.62%
6	4.25%	2.83%	-0.27%	4.82%	-5.01%	13.93%	-9.72%
average	15.10%	9.82%	12.54%	15.90%	12.76%	11.54%	11.52%
std	9.11%	8.43%	10.88%	6.58%	15.48%	8.91%	13.43%
Muscle Tendon							
Subject	Opt13	Gen1	Gen9	Gen9Pre	slowOpt	fastOpt	OptImm
1	8.37%	3.73%	8.14%	5.18%	9.59%	15.74%	10.67%
2	5.99%	1.23%	8.14%	6.06%	-7.73%	7.44%	7.38%
3	6.77%	5.57%	8.86%	3.01%	1.71%	11.78%	4.90%
4	17.23%	7.36%	17.51%	8.84%	4.37%	19.12%	16.33%
5	9.64%	1.88%	10.04%	6.04%	-1.55%	7.74%	9.76%
6	10.30%	-2.25%	7.75%	17.35%	11.05%	6.02%	17.18%
average	9.72%	2.92%	10.07%	7.75%	2.91%	11.31%	11.04%
std	4.03%	3.41%	3.73%	5.06%	7.04%	5.23%	4.87%

6.3.2 Values of optimized parameters and resulting torque profiles

Time-based control

All subjects converged to the minimum allowable fall time (8.08% ± 0.07% of the stance period) and within 1.5% of the stance period of the latest possible peak time of 92% of stance period (91.4%stance ± 0.55% of the stance period). There was much higher variation in rise time (37.8% ± 13.4% of the stance period) (Fig. 6.7). Though most peak torque settings were high, only two subjects converged to the maximum allowable torque, and subjects did not reach these high levels of torque until the third day of testing. The resulting torque profiles can be seen in Figure 6.7 A.

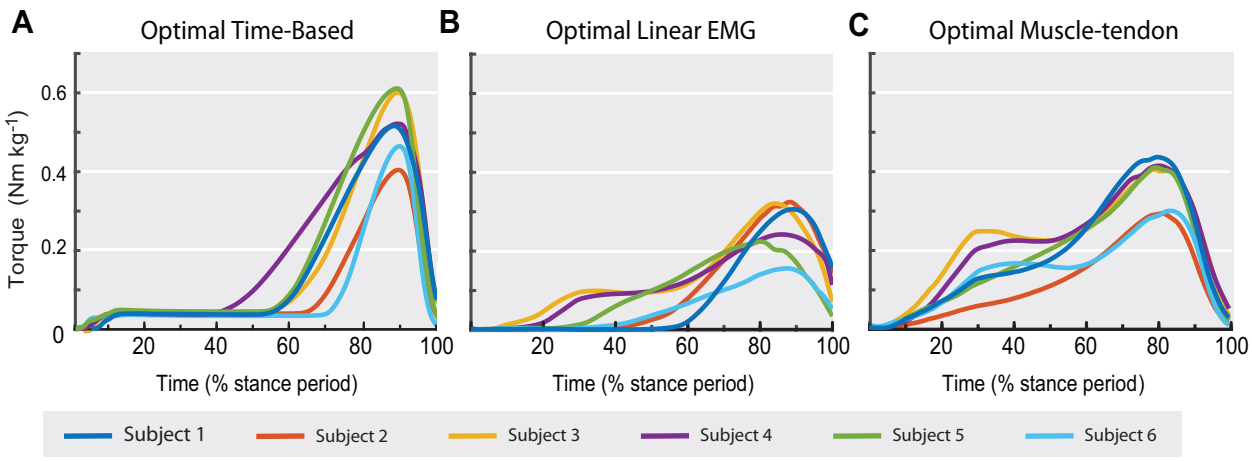

[h]

Figure 6.7: **Average torque produced by optimal settings (Gen13) for each controller.** **A** The time-based controller produced the highest peak torques of any of the optimal control laws. With peak torque closely grouped near 92 % stance, which was the maximum allowable setting. All subjects converged to the minimum setting for fall time. There was higher variability in the ranges of optimal rise times. **B** Torques were generally lower for the proportional EMG controller. Subjects did not reach the boundaries of any of the parameters, though all seemed to benefit from lower settings for the low-pass filter frequency which resulted in smooth curves. **C** Optimal control laws for the muscle-tendon controller resulted in higher early torque and earlier peak torque compared to the other controllers. Timing of peak torque is closely grouped for all three controllers.

Linear EMG

Optimal linear EMG control resulted in much lower torques (Fig. 6.7 B) and higher overall variability in parameter settings (Table 6.6). All subjects benefited from lower settings of the low-pass filter frequency, f_{lpf},(f_{LPF} = 2.15 ± 0.37 Hz). Most subjects also benefited from small delays.

Muscle-tendon control

The torque profiles created by the muscle tendon controller contained higher early stance torques than those produced by the other controllers (Fig 6.7 C).

Trends were not obvious in the maximum isometric force (F_{max} = 2201.3 ± 566.5). Four subjects converged to maximum contractile velocities in a very small range (between 4.36 and 4.98 $lopts^{-1}$, representing 5 percent of the total available range), while two subjects (subjects 4 and 6) converged to noticeably higher values (8.32 and 7.1) and experienced higher metabolic reductions for this controller compared to the other two subjects in the Opt,

OptImm, and slow conditions. All subjects benefited from lower filter frequency settings for both the linear EMG and muscle tendon controllers (f_{LPF} = 2.98 ± 0.51 Hz).

Table 6.6: **Optimal control law settings calculated for the 13th generation.** The settings calculated for the optimal condition are shown for each subject as well as the average value across subjects. The standard deviation is also presented both as an absolute value and as a percentage of the total available range. Also presented are the average net metabolic reductions calculated between the zero-torque and the optimal conditions for each subject.

	Torque Time					Linear EMG					Muscle Tendon				
Subject	Peak Torque (Nm)	Peak time (% stance)	Rise Time (% stance)	fall time (% stance)	% reduction	K (Nm/unit EMG)	h (unit EMG)	d (s)	flpf (Hz)	% reduction	Fmax (N)	vmax (lopt/s)	e dl/lo	flpf (Hz)	% reduction
1	45.00	91.606	43.909	8.197	14.36%	42.46	0.46	0.022	1.78	24.54%	2829.144	4.98	0.121	2.688	8.37%
2	33.82	91.607	28.553	8.105	15.72%	34.34	0.21	0.012	2.51	8.66%	1533.06	4.885	0.169	3.441	5.99%
3	39.65	92	35.907	8	19.99%	35.42	0.14	0.002	2.60	25.54%	1962.083	4.362	0.132	2.404	6.77%
4	45.00	91.783	58.525	8	25.36%	32.98	0.10	0	2.32	19.00%	2929.7	8.319	0.111	2.586	17.23%
5	43.13	90.529	38.784	8.073	16.38%	28.36	0.16	0	1.89	8.61%	1782.437	4.698	0.104	3.117	9.64%
6	43.78	90.968	21.968	8.081	15.25%	33.88	0.27	0	1.81	4.25%	2171.5389	7.068	0.174	3.667	10.30%
Average	**41.73**	**91.42**	**37.94**	**8.08**	**17.84%**	**34.57**	**0.22**	**0.01**	**2.15**	**15.10%**	**2201.33**	**5.72**	**0.14**	**2.98**	**9.72%**
Sd	4.34	0.55	12.71	0.07	4.16%	4.57	0.13	0.01	0.37	9.11%	566.54	1.59	0.03	0.51	4.03%
Sd (%)	9.66%	1.73%	25.93%	0.61%		10.17%	25.88%	9.12%	12.31%		28.33%	14.49%	18.02%	11.88%	

6.4 Discussion

The clearest result of this experiment is that time-based control outperforms the muscle-tendon controller by a statistically significant margin (p = .001) with three days of optimization allowed for each controller. The benefits of the time based controller are not statistically greater than the linear EMG controller (p = 0.46). Though the average performance of the time-based controller at normal speed was greater than that of the linear-EMG controller, there was significant overlap in the ranges of the two controllers with the two greatest reductions being produced by the linear EMG controller.

Differences between the optimal condition and the initial settings were significant for the time based, linear EMG, and muscle tendon controllers with p values equal to 0.012, 0.004, and 0.010 respectively. This demonstrates that the optimizer was successful in customizing the settings of each controller to improve performance. Motor learning could not have been mainly responsible for reductions as both conditions were tested in double reversed order at the end of day 3. This result suggests that this implementation of HILO with CMA-ES was

applicable across all three controllers.

It is suspected that metabolic benefits are achieved through two mechanisms. First, the exoskeleton may replace some of the function of the calf muscles. Second, the exoskeletons may produce beneficial joint torques at times that human muscle is limited by the force-length or force-velocity relationships. Simulations leveraging experimental data suggest that as net exoskeleton work increases, both soleus muscle force and mechanical work are reduced when using a similar time-based controller with unilateral ankle exoskeleton assistance [150].

All subjects converged to the minimum fall time and maximum peak times for the time-based controller. This suggests that additional metabolic benefits may be possible if the bounds were expanded. It also suggests that users may have adopted a similar strategy for interacting with the time-based controller, though there was significant variation in rise time and the magnitude of peak torque.

Though three days of optimization were allowed, it is possible that not all subjects achieved expertise in the use of the proportional EMG and muscle-tendon controllers. Subjects seemed more equally capable of taking advantage of the time-based controller as evidenced by the narrow spread of optimal parameters and net metabolic reductions in the optimal condition combined with smaller step sizes between generations of optimization. This was less true for the linear EMG controller and muscle tendon controller. It is possible that more time may have allowed subjects to discover better strategies for interacting with the linear EMG and muscle-tendon controllers.

The parameterization of the linear EMG controller limited the torque available to subjects who reduced their soleus activity below their normal levels. The allowable bounds of the linear EMG parameters were selected as the limits of the range of settings that pilot subjects could successfully and comfortably negotiate on the first day of testing. It is not suspected that the bounds on the gain, K, reduced the effectiveness of the linear EMG controller. It appears that subjects prefer lower torques in general for the linear EMG controller

as demonstrated by the fact that all but one subject converged to a gain significantly lower than the maximum allowable setting. All controller parameter distributions were initialized with the same variance calculated as a percentage of the range of allowable settings. It is possible that different methods of initializing the variance of parameter distributions or creating moving boundaries would have allowed for more gradual increases in the gain over the course of the optimization. This may have better facilitated learning as results from other work suggest that gradually increasing gains is beneficial [27].

It is important to note that only in special cases is it possible for the linear EMG and muscle-tendon controllers to provide torque patterns similar to those produced by the time-based controller. This requires the correct combination of controller settings, muscle activity, and ankle angle, and is not expected in general. There are constraints on the shape of the time-based torque patterns that do not exist for the other two controllers, which make it unlikely for the same torque patterns to be generated by each of the three controllers.

The parameterization of the linear EMG controller was selected so that it would be possible in some cases to reproduce the torque patterns created by the time-based controller with little or no change in the subjects' normal EMG activity. Higher settings for the threshold, h, would result in low or no torque during early and midstance, and the increased sensitivity in the higher range of EMG measurements should produce high peaks in late stance. Adding the ability to adjust the delay also allowed the timing of the torque peak to be adjusted. Only one subject discovered this strategy as their optimal settings by converging to a very high threshold (almost double the average) and the maximum allowable delay. The resulting average net metabolic reduction was nearly the highest reduction measured over the course of this study. It is interesting that metabolic reductions for this subject were higher for the optimal linear EMG condition than for the time-based condition (25% vs 14%) despite having lower net work input from the exoskeletons. Torque applied by the linear EMG controller for this subject was essentially a scaled version of that applied by the time-based controller (compare blue torque profiles for Subject 1 in Figure 6.7 A and B). This

trend was true in both double reversed trials.

Subject 3 also achieved high reductions for the linear EMG controller, but had a very different torque profile that did not capture the same features as the time-based controller. This subject also developed an asymmetric compensatory behavior with higher torques applied to the left ankle than the right that persisted for all three days of testing (average peak torques of 22 Nm/kg on the left and 14 Nm/kg on the right). Some of the other subjects exhibited asymmetric patterns during the first day of the EMG protocol, but all other subjects developed symmetric behaviors by the end of day 2. It is possible that subject 3 may have developed more symmetric assistance with more time.

The differences in the strategies used by Subjects 1 and 3 to interact with the linear EMG controller highlight the fact that users experience exoskeleton assistance differently and may have variable methods of adaptation. These subjects had drastically different strategies as evidenced by EMG activity and by optimal controller settings, but achieved similar levels of metabolic reductions of 25% which were the two highest reductions recorded in this experiment.

It is unknown why five of the subjects did not develop the high threshold strategy for the linear EMG controller. It is possible that 2 minute trials during optimization are not long enough for subjects to learn how to best interact with randomly selected device settings. It is also possible that the high threshold strategy may never be effective for some subjects. More work investigating methods of providing forced exploration for improved adaptation times may answer these questions.

While it is clear that the optimization improved performance in this study, another experiment involving an EMG controller with an adaptive gain on bilateral ankle exoskeletons has produced higher average metabolic reductions (19%) [27]. The gain was adjusted as the user adapted such that the average peak EMG signal measured within a step resulted in peak torques of consistent value even if subjects gradually reduced overall soleus activity. This study included three days of training and a fourth day of collections, similar

to our three days of experimentation per controller. However, subjects experienced greater metabolic benefits with 60% less time spent walking overall. This raises important questions. What is most crucial for enabling metabolic reductions? It is possible the adaptive gain made the difference, but once again too many confounding factors exist to make a clear comparison. Another experiment comparing these two strategies directly would be interesting and perhaps reveal guiding principles for facilitating useful human-robot interaction. Interestingly, the same study demonstrated that time-based control that produced the average torque commanded by the EMG controller was equally capable of reducing metabolic cost (but with different effects on soleus muscle activity). This demonstrated that EMG control provided no metabolic benefit as a direct result of being responsive to inter-step variability. It may be time to take EMG experiments off of the treadmill in order to assess whether responsiveness to changing behavior is truly useful.

The muscle-tendon controller was the least effective controller with the greatest variability in optimized settings. The most obvious difference between the muscle-tendon controller and the other controllers is the presence of high torques in early stance. No ankle exoskeleton assistance strategy providing high torque in early stance has succeeded in producing metabolic reductions [104, 20] and prior EMG studies have shown that users reduce soleus activity in early stance when recieving EMG based ankle exoskeleton assistance to reduce negative work produced by the exoskeleton [40]. Additionally, simulations driven by measured EMG demonstrate that tendon recoil can be limited by supporting torques in early stance, which results in increased metabolic cost [150]. It was surprising that subjects did not converge to high settings for the maximum contractile velocity, v_{max} as this would result in lower torques in early stance and provide greater ability to produce torque late in stance. The two subjects with the highest optimal settings of v_{max} did achieve the highest reductions in the optimal condition. The same two subjects did not achieve the greatest maximum reductions in the initial settings condition, suggesting that this difference played a key role in the success of these subjects. While the muscle-tendon controller was hypothesized to

be intuitive to use, it may be that assistance strategies should complement the biological system by providing torques when human-muscle is naturally limited. The muscle-tendon model may be too similar to the human system to be useful in its current parameterization.

The optimized parameters for the muscle-tendon controller were selected because they were expected to have the greatest effect on torque production during walking based on the results of altering these values in simulation. F_{max} affects the total amount of available torque similar to the gain in the linear EMG controller. v_{max} determined the sensitivity of the muscle tendon controller to the contractile velocity of the contractile element, which limited torque production late in stance in simulated tests. The stiffness of the tendon also had a very large effects on torque production by both smoothing applied torque and influencing the values of f_l, the force-length relationship, and f_v, the force-velocity relationship. The filter frequency applied to the measured EMG signal also had a significant effect on developed torque patterns, and was included for comparison to the linear EMG controller settings. Moving forward, it would be interesting to replace the filter frequency with values that affect the force-length relationship such as w or c in Equation 6.5. Adjusting these values along with v_{max} could potentially drive the muscle-tendon controller to behave like a proportional EMG controller.

The time based controller may have resulted in greater reductions overall because it is easy to learn. It provides repeatable behavior with low inter-step variability. Trials of randomly selected controllers were experienced for only two minutes during the optimization. This may be enough time to adjust to new patterns of time-based torque, but not enough time for subjects to ascertain the relationship between their behavior and exoskeleton torque while optimizing the linear EMG and muscle-tendon controllers. This seems to be especially true of the muscle tendon model as there is very high variability in optimal parameter settings across subjects compared to the other two controllers. The average optimal settings for the muscle tendon model did not vary far from the means of the initial controller settings applied in the first generation. The only parameter that changed significantly on

average was tendon stiffness, which mainly resulted in smoother and later development of torque. The more compliant virtual tendon resulted in greater values of f_v late in stance by allowing the contractile element to behave more isometrically. This is consistent with simulation studies investigating the effect of tendon compliance on the cost of running [151].

The most surprising outcome of this study is the fact that average reductions for the time-based controller on bilateral exoskeletons in this study were *significantly lower* (p = .03 by two tailed t-test assuming unequal variances) at 17.8% than the average 24% reductions measured for a similar controller in a study on unilateral assistance [2]. This comparison is confounded by the fact that different subjects completed the two studies. However subjects 3 and 4 completed both studies. Subject 3 performed much worse in the bilateral study (19.9% bilaterally vs 27.7% unilaterally) while subject 4 performed about equally well in the bilateral study compared to the unilateral study (25.36% bilaterally vs 26.6% unilaterally) despite having *three times* as much time dedicated to the optimization. Anecdotally, the two subjects with prior experience reported that walking with two ankle exoskeletons was much more difficult than walking with only one. This is counter-intuitive as it is expected that symmetric assistance should be easier to adapt to. Perhaps having one leg under the complete control of user allows a greater measure of stability as the unassisted leg may be more responsive. The largest difference in implementation between our two studies was that the controller was defined in terms of stance time for this study and stride time in the unilateral study. This change was made to ensure that torques would return to zero before toe-off even if subjects experienced a change in duty factor (the percent of a stride spent in stance). This may have resulted in torques being applied earlier to less effect. In contrast to our findings, a controlled study which explored bilateral and unilateral ankle assistance demonstrated higher reductions for the bilateral conditions compared to the unilateral conditions [152]. This suggests that our observations between bilateral and unilateral assistance may be a result of differences in implementation or differences between subjects.

The relative benefits of these controllers may not exhibit the same patterns during non-

steady state locomotion. Time based control produced large metabolic reductions in the normal and fast settings, but this is not surprising as assistance was applied based on an estimate of stance time derived from a moving average of measured stance time. This means torques were still applied in close proximity to toe-off. It is not expected that the time-based controller will perform well in non-steady state conditions when there is large variation in stance duration and the timing of peak torque may not be well aligned with respect to toe-off. Additional classifiers and locomotion-mode identification methods might be used to provide better estimates of gait phase [23, 24, 25]. Such tools may extend the usefulness of time-based controllers to some non-steady state activities. In contrast, EMG based controllers have potential to be useful in general non-steady state applications without the need for classifiers or mode identification. Linear EMG control outperformed time based control in the slow condition using the optimal settings for normal walking. Users can even comfortably stand and step in place when using the linear EMG control mode, which is not currently possible with this version of time-based control. In general, the motivation for using EMG based control is that it should be responsive to changing conditions and effective in diverse activities without significant modification or the need for classifiers. It would be interesting to test the capabilities of linear EMG-based control in non-steady state conditions. What is more, recording and reporting the time and resources required to prepare time-based and EMG-based controllers for discrete steady state behaviors or non-steady state behaviors would be an interesting measure of the suitability of the controllers for general assistance.

Prior to completing this experiment, pilot studies were conducted with treadmill speed that varied sinusoidally in time to better compare the ability of the three controllers to operate during non-steady state use. However, metabolic measurements were not repeatable even across trials using only normal shoes. It seems that treadmill walking at changing speed is difficult and may require training even before implementing exoskeleton assistance. Tethered exoskeletons may not be adequate tools for exploring non-steady state behaviors. Fully portable devices may be needed for an accurate comparison of these methods during

non-steady state locomotion.

6.5 Conclusions

This experiment allowed a comparison of the metabolic benefits of three qualitatively different control strategies with as few confounding factors as was feasible to produce within constraints. This study demonstrates that time-based control produces significantly greater metabolic reductions on average compared to the muscle-tendon controller with equal amounts of training. This particular implementation of a muscle-model based controller with EMG input is not effective and was not able to reduce the cost of walking below that of normal shoes. It is not advised to implement a similar controller on exoskeletons for assisting healthy individuals without significant modification or inclusion of different parameters in an optimization. While it is suspected that subjects may not have fully adapted to the linear EMG controller, the linear EMG controller was not significantly outperformed by the time-based controller. The wide spread in metabolic reductions for the linear EMG controller demonstrates that subjects have unequal ability to benefit from linear EMG control. It is possible that more than three days of optimization or a different training strategy is needed to improve performance for some subjects. While time-based control was better on average, two subjects experienced significantly higher reductions using the linear EMG controller compared to the time based controller. This demonstrates that inter subject variability may not allow for a one-strategy-fits all approach. All subjects did experience higher metabolic reductions for the optimal control conditions compared to the initial settings, which demonstrates the effectiveness of the optimization strategy across all three controllers.

Treadmill testing at constant speed does not take advantage of the responsiveness of EMG based controllers. While time-based control was better on average, two subjects experienced significantly higher reductions using the Linear EMG controller compared to the time based controller. This demonstrates that inter subject variability may not allow for a

one-strategy-fits-all approach. While time-based control was better on average, two subjects experienced significantly higher reductions using the Linear EMG controller compared to the time based controller. This demonstrates that inter subject variability may not allow for a one-strategy-fits all approach. Moving forward, experimental comparisons of EMG and time-based controllers should be performed. This will allow a better assessment of the ability of each strategy to be generally useful as part of commercial devices.

Exoskeletons have great potential to augment ability and aid individuals with disabilities. Reductions in metabolic cost on the levels reported in this and other studies have the potential to be life changing for populations with a high cost of transport such as stroke patients or the elderly. Reducing the energy required to walk will increase independence and quality of life. This experiment, though extremely time consuming to perform, provided convincing data to demonstrate that the muscle-tendon controller is not as effective as other strategies. Separate experiments exploring each of these controllers in isolation would not be as convincing as this study in comparing the performance of each of these controllers under the same conditions on the same subjects. Placing more emphasis on relative benefits of strategies rather than raw, record-breaking magnitudes may accelerate progress by quickly determining which qualitatively different approaches are most effective.

Chapter 7

Conclusions

Lower-limb exoskeletons have potential to improve the enjoyment of physical activity, increase endurance, reduce incidence of injury, aid rehabilitation and prolong independence. We are far from achieving these goals with affordable, portable systems, but the findings of this thesis will act as important steps towards the realization of exoskeletons as life changing tools. Principles of exoskeleton design were developed in the process of designing and characterizing ankle and knee exoskeletons. The implementation of these tools in human-subject experiments leveraging both universal exoskeleton emulator systems and human-in-the-loop optimization enabled objective comparisons to be made between qualitatively different assistance strategies. These experimental comparisons resulted in the greatest metabolic reductions measured during running to date, and revealed that a passive, spring-like strategy for assisting the ankle is unlikely to result in significant metabolic reductions. A similar experimental comparison revealed that time-based and linear EMG controllers may be equally well suited to assisting walking while a novel muscle-tendon controller appears to be less effective when implemented under similar conditions. The findings of this thesis will likely proliferate useful tools that will accelerate research, impact the design of lower-limb exoskeletons, and influence the direction of the development of high-level exoskeleton assistance strategies.

7.1 Summary of findings

First, I developed and characterized exoskeleton end-effectors that outperform all similar devices to date in terms of maximum torque, peak power, and torque bandwidth. Decisions made early in the design process of these devices enabled impactful exoskeleton experiments. Placing interfaces far apart maximized leverage about the joint, which resulted in smaller, more comfortable forces being applied to the user. Carefully selecting the locations in which the device contacted the user resulted in mostly normal forces being applied to the user, which improved comfort and prevented migration of the devices. Utilizing selective compliance resulted in lightweight exoskeletons that allowed relatively uninhibited, natural motion. The process of designing and implementing these tools lead to the development of several principles of exoskeleton design. These principles of design will aid developers in producing effective devices mainly by providing insight into the evaluation of candidate exoskeletons early in the design process, encouraging the use of simple safety mechanisms, providing guidance in the selection of materials and manufacturing processes, and introducing the concept of selective compliance which enables simpler and lighter frames and joints.

These exoskeleton end-effectors were then used to perform an experiment comparing passive, spring-like exoskeleton assistance to a powered assistance strategy with high work input. Human-in-the-loop optimization using a covariance matrix adaptation evolutionary strategy as the optimizer customized device settings for individuals to enable an objective comparison. The responsiveness of the ankle exoskeleton end-effectors produced accurate emulations of passive, spring-loaded exoskeletons. These emulations revealed that passive ankle exoskeletons have little capacity to produce metabolic reductions. In comparison, the powered condition produced the greatest metabolic reductions ever demonstrated during running.

An experimental comparison of high-level control strategies provided a first evaluation of a muscle-tendon controller in comparison to two other established controllers. The muscle-

tendon controller was created by reducing an existing neuromuscular controller developed for prostheses to a simpler muscle-tendon controller that accepted ankle angle and measured electrical activity in muscles as inputs. This controller addressed a possible limitation of proportional EMG control by better capturing the dynamics of human muscle. The experiment demonstrated that muscle-tendon control performed less well than time-based control by a statistically significant margin, while linear EMG control could potentially perform on the same level as time-based control. Interestingly, the time based controller in this study using bilateral ankle exoskeletons produced far lower reductions than expected based on prior work using a unilateral exoskeleton with a similar controller and optimization strategy. This was true despite allowing three days of optimization compared to only one in the unilateral study. This comparison is confounded by several small differences in the protocol, primarily the use of different subjects, but the results suggest, counterintuitively, that bilateral ankle assistance may be more difficult for users to learn to take advantage of than unilateral assistance.

7.2 Implications

The principles of design developed in the course of creating and implementing the ankle and knee exoskeletons will help designers produce more effective exoskeletons for years to come. The results of the running experiment will influence the direction that developers will take commercial devices. Time and effort developing passive, spring-loaded ankle exoskeletons for running will be saved by our efficient demonstration of the ineffectiveness of the strategy using an emulator system. The outstanding performance of the powered controller in producing metabolic reductions during running will encourage developers to create powered mobile exoskeletons. This result will also proliferate the use of exoskeleton emulators and human-in-the-loop optimization by highlighting the power of these strategies when used in combination.

The results of the controller comparison should discourage further exploration of the muscle-tendon controller without significant modification to either the controller itself or the training and optimization process applied to it. The results should also encourage further development of the linear EMG controller and other similar variations as they may perform as well as time-based controllers without many of the innate limitations of time-based control.

7.3 Making strides in the future

The greatest gap in lower-limb exoskeleton research remains the development of assistive strategies for non-steady state behaviors. EMG based controllers are theorized to be more effective during non-steady state and should not require the need for classifiers to predict user intent as intent should be encoded in muscle activity. However, this has not been sufficiently tested. Our experimental comparison of assistance strategies did not demonstrate that EMG control is significantly worse than time-based control during steady-state walking. It is expected that EMG control will be significantly better during non-steady state activities due to the inability of time-based controllers to respond to inter-step variability and transitions between activities. Developing classifiers to predict user intent may enable time-based strategies to be generally useful, but more research must be done.

The development of portable ankle exoskeletons is needed as treadmill testing using emulators is not well suited to testing real world non-steady state behaviors. The majority of exoskeleton research has centered on the ankle for the past five years and a sufficient understanding of ankle assistance has developed to warrant development of autonomous devices. Ankle exoskeleton assistance during walking or running should feature relatively high torque late in stance with little or no assistance applied in early stance. Effective design of portable devices will not be simply achieved by using the experimental results presented here as design requirements and selecting motors accordingly. The design of

portable exoskeletons is a Pareto optimality problem with many conflicting factors. For example, higher torque capabilities may require larger motors, thus adding mass. The resulting trade-off in metabolic cost (a likely decrease for added torque versus a likely increase for added mass) is unclear. Performing human-in-the-loop optimization of candidate portable designs using an emulator system would be an efficient way of going about the selection of a final design. Torque could be applied as a result of a simulation of a proposed motor, driver and transmission and the mass of the exoskeleton end-effectors could be adjusted to approximately match that of the proposed design. This process should result in a final product with a high probability of success.

In the process of answering one question we often open the door to many more. This is at once the wonderful and infuriating nature of research. The poorer performance of the time-based controller on bilateral ankle exoskeletons compared to a prior study with unilateral assistance should highlight the possibility that symmetric assistance may not always be the best and that learning and adaptation may be more difficult as the number of assisted joints increases. This highlights the need for developing a better understanding of human-exoskeleton interaction in hopes of better facilitating human adaptation to exoskeletons and accelerating the process of optimizing assistance through human-in-the-loop optimization.

Reducing the metabolic cost of walking and running is a worthwhile goal. Reducing the cost of transport experienced by individuals such as soldiers who travel great distances may improve their productivity and enhance their safety. Expanding exoskeleton research including patient populations such as the elderly or individuals who have experienced stroke could be life changing by improving quality of life and prolonging independence. The biomechatronics community is focused on these important issues and will continue to make progress in this area, but very little research is being done on other outcomes of interest. In particular, human-in-the-loop optimization may be used to boost performance in ways that are immediately obvious and visible. For example, improving top speed for the elderly would help them to keep pace with grandchildren and reduce the stress of crossing the street. Ex-

oskeletons could also augment athletic ability by improving peak running speed or vertical jump height for healthy individuals. We could also potentially use exoskeletons to get injured athletes back in the game by reducing internal joint loads. The potential of this field is vast, and the tools and methodologies we have developed will hopefully accelerate research, bringing exoskeletons one step closer to being life-changing products that can make us generally more capable: stronger, faster and better than we were before.

Bibliography

[1] P. Malcolm, W. Derave, S. Galle, and D. De Clercq, "A simple exoskeleton that assists plantarflexion can reduce the metabolic cost of human walking," vol. 8, no. 2, p. e56137, 2013.

[2] J. Zhang, P. Fiers, K. A. Witte, R. W. Jackson, K. L. Poggensee, C. G. Atkeson, and S. H. Collins, "Human-in-the-loop optimization of exoskeleton assistance during walking," *Science*, vol. 356, no. 6344, pp. 1280–1284, 2017.

[3] K. Seo, J. Lee, and Y. J. Park, "Autonomous hip exoskeleton saves metabolic cost of walking uphill," in *Rehabilitation Robotics (ICORR), 2017 International Conference on*. IEEE, 2017, pp. 246–251.

[4] L. M. Mooney, E. J. Rouse, and H. M. Herr, "Autonomous exoskeleton reduces metabolic cost of human walking during load carriage," *J. Neuroeng. Rehabil.*, vol. 11, p. 80, 2014.

[5] G. Lee, J. Kim, F. Panizzolo, Y. Zhou, L. Baker, I. Galiana, P. Malcolm, and C. Walsh, "Reducing the metabolic cost of running with a tethered soft exosuit," *Sci. Robot.*, vol. 2, p. eaan6708, 2017.

[6] R. Nasiri, A. Ahmadi, and M. N. Ahmadabadi, "Reducing the energy cost of human running using an unpowered exoskeleton," *IEEE Transactions on Neural Systems and Rehabilitation Engineering*, 2018.

[7] W. He, D. Goodkind, and P. R. Kowal, *An aging world: 2015*. United States Census Bureau Washington, DC, 2016.

[8] J. Mizrahi, O. Verbitsky, E. Isakov, and D. Daily, "Effect of fatigue on leg kinematics and impact acceleration in long distance running," *Human movement science*, vol. 19, no. 2, pp. 139–151, 2000.

[9] D.-c. Lee, R. R. Pate, C. J. Lavie, X. Sui, T. S. Church, and S. N. Blair, "Leisure-time running reduces all-cause and cardiovascular mortality risk," *Journal of the American College of Cardiology*, vol. 64, no. 5, pp. 472–481, 2014.

[10] C. R. Richardson, G. Faulkner, J. McDevitt, G. S. Skrinar, D. S. Hutchinson, and J. D. Piette, "Integrating physical activity into mental health services for persons with serious mental illness," *Psychiatric services*, vol. 56, no. 3, pp. 324–331, 2005.

[11] E. J. Doyne, D. J. Ossip-Klein, E. D. Bowman, K. M. Osborn, I. B. McDougall-Wilson, and R. A. Neimeyer, "Running versus weight lifting in the treatment of depression." *Journal of consulting and clinical psychology*, vol. 55, no. 5, p. 748, 1987.

[12] D.-c. Lee, A. G. Brellenthin, P. D. Thompson, X. Sui, I.-M. Lee, and C. J. Lavie, "Running as a key lifestyle medicine for longevity," *Progress in cardiovascular diseases*, vol. 60, no. 1, pp. 45–55, 2017.

[13] E. Guizzo and T. Deyle, "Robotics trends for 2012," pp. 119–123, 2012.

[14] D. Aoyagi, W. E. Ichinose, S. J. Harkema, D. J. Reinkensmeyer, and J. E. Bobrow, "A robot and control algorithm that can synchronously assist in naturalistic motion during body-weight-supported gait training following neurologic injury," vol. 15, no. 3, pp. 387–400, 2007.

[15] M. Watch. Exoskeleton market is expected to be worth us $ 2.5 billion by 2024. [Online]. Available: https://www.marketwatch.com/press-release/exoskeleton-market-is-expected-to-be-worth-us-25-billion-by-2024-2018-05-14

[16] S. Francis. Fast-growing exoskeeleton market set to exceed $5 billion in annnual revenue, says report. [Online]. Available: https://roboticsandautomationnews.com/2018/10/25/fast-growing-exoskeleton-market-set-to-exceed-5-billion-in-annual-revenue-says-report/19525/

[17] L. Greenemeier, "Trouble walking? try hondaâĂŹs new exoskeleton legs," *Sci Am*, 2008.

[18] H. K. Ko, S. W. Lee, D. H. Koo, I. Lee, and D. J. Hyun, "Waist-assistive exoskeleton powered by a singular actuation mechanism for prevention of back-injury," *Robotics and Autonomous Systems*, 2018.

[19] T. G. Sugar, S. Redkar, and J. K. Hitt, "Wearable robots for worker assistance–17464."

[20] S. Galle, P. Malcolm, S. H. Collins, and D. De Clercq, "Reducing the metabolic cost of walking with an ankle exoskeleton: interaction between actuation timing and power," *Journal of neuroengineering and rehabilitation*, vol. 14, no. 1, p. 35, 2017.

[21] B. Quinlivan, S. Lee, P. Malcolm, D. Rossi, M. Grimmer, C. Siviy, N. Karavas, D. Wagner, A. Asbeck, I. Galiana *et al.*, "Assistance magnitude versus metabolic cost reductions for a tethered multiarticular soft exosuit," *Science Robotics*, vol. 2, no. 2, p. eaah4416, 2017.

[22] S. Lee, N. Karavas, B. T. Quinlivan, D. LouiseRyan, D. Perry, A. Eckert-Erdheim, P. Murphy, T. G. Goldy, N. Menard, M. Athanassiu *et al.*, "Autonomous multi-joint soft exosuit for assistance with walking overground," in *2018 IEEE International Conference on Robotics and Automation (ICRA)*. IEEE, 2018, pp. 2812–2819.

[23] H. Huang, F. Zhang, L. J. Hargrove, Z. Dou, D. R. Rogers, and K. B. Englehart, "Continuous locomotion-mode identification for prosthetic legs based on neuromuscular–mechanical fusion," *IEEE Transactions on Biomedical Engineering*, vol. 58, no. 10, pp. 2867–2875, 2011.

[24] L. H. Smith, L. J. Hargrove, B. A. Lock, and T. A. Kuiken, "Determining the optimal window length for pattern recognition-based myoelectric control: balancing the competing effects of classification error and controller delay," *IEEE Transactions on Neural Systems and Rehabilitation Engineering*, vol. 19, no. 2, pp. 186–192, 2011.

[25] H. A. Varol, F. Sup, and M. Goldfarb, "Multiclass real-time intent recognition of a powered lower limb prosthesis," *IEEE Transactions on Biomedical Engineering*, vol. 57, no. 3, pp. 542–551, 2010.

[26] C. R. Kinnaird and D. P. Ferris, "Medial gastrocnemius myoelectric control of a robotic ankle exoskeleton," *IEEE Transactions on Neural Systems and Rehabilitation Engineering*, vol. 17, no. 1, pp. 31–37, 2009.

[27] J. R. Koller, C. D. Remy, and D. P. Ferris, "Comparing neural control and mechanically intrinsic control of powered ankle exoskeletons," in *Rehabilitation Robotics (ICORR), 2017 International Conference on*. IEEE, 2017, pp. 294–299.

[28] G. S. Sawicki and D. P. Ferris, "A pneumatically powered knee-ankle-foot orthosis (kafo) with myoelectric activation and inhibition," *Journal of neuroengineering and rehabilitation*, vol. 6, no. 1, p. 23, 2009.

[29] H. M. Herr and A. M. Grabowski, "Bionic ankle–foot prosthesis normalizes walking gait for persons with leg amputation," *Proc. R. Soc. B*, vol. 279, no. 1728, pp. 457–464, 2012.

[30] S. H. Collins, M. B. Wiggin, and G. S. Sawicki, "Reducing the energy cost of human walking using an unpowered exoskeleton," *Nature*, vol. 522, pp. 212–215, 2015.

[31] R. C. Browning, J. R. Modica, R. Kram, and A. Goswami, "The effects of adding mass to the legs on the energetics and biomechanics of walking," vol. 39, no. 3, pp. 515–525, 2007.

[32] A. Grabowski, C. Farley, and R. Kram, "Independent metabolic costs of supporting body weight and accelerating body mass during walking," vol. 98, pp. 579–583, 2005.

[33] J. M. Donelan, R. Kram, and A. D. Kuo, "Mechanical and metabolic determinants of the preferred step width in human walking." vol. 268, pp. 1985–1992, 2001.

[34] M. Lafortune, P. Cavanagh, H. Sommer Iii, and A. Kalenak, "Three-dimensional kinematics of the human knee during walking," *Journal of biomechanics*, vol. 25, no. 4, pp. 347–357, 1992.

[35] J. M. Caputo and S. H. Collins, "A universal ankle-foot prosthesis emulator for experiments during human locomotion," vol. 136, p. 035002, 2014.

[36] W. C. Flowers and R. W. Mann, "An electrohydraulic knee-torque controller for a prosthesis simulator," *Journal of biomechanical engineering*, vol. 99, no. 1, pp. 3–8, 1977.

[37] G. S. Sawicki and D. P. Ferris, "Mechanics and energetics of level walking with powered ankle exoskeletons," *Journal of Experimental Biology*, vol. 211, no. 9, pp. 1402–1413, 2008.

[38] N. Hansen, "The cma evolution strategy: a comparing review," in *Towards a new evolutionary computation*. Springer, 2006, pp. 75–102.

[39] W. Hoogkamer, S. Kipp, J. H. Frank, E. M. Farina, G. Luo, and R. Kram, "A comparison of the energetic cost of running in marathon racing shoes," *Sports Medicine*, vol. 48, no. 4, pp. 1009–1019, 2018.

[40] K. E. Gordon and D. P. Ferris, "Learning to walk with a robotic ankle exoskeleton," *Journal of biomechanics*, vol. 40, no. 12, pp. 2636–2644, 2007.

[41] M. F. Eilenberg and H. Geyer, "Control of a powered ankle-foot prosthesis based on a neuromuscular model," vol. 18, no. 2, pp. 164–173, 2010.

[42] K. A. Witte and S. H. Collins, "Design of lower-limb exoskeletons and emulator systems," in *Wearable robotics: systems and applications*, J. Rosen, Ed. Amsterdam: Elsevier, 2019.

[43] A. Roy, H. I. Krebs, S. L. Patterson, T. N. Judkins, I. Khanna, L. W. Forrester, R. M. Macko, and N. Hogan, "Measurement of human ankle stiffness using the anklebot," 2007, pp. 356–363.

[44] H. Lee, E. J. Rouse, and H. I. Krebs, "Summary of human ankle mechanical impedance during walking," *IEEE journal of translational engineering in health and medicine*, vol. 4, pp. 1–7, 2016.

[45] J. M. Caputo and S. H. Collins, "An experimental robotic testbed for accelerated development of ankle prostheses," 2013, pp. 2630–2635.

[46] J. Caputo and S. Collins, "Prosthetic ankle push-off work reduces metabolic rate but not collision work in non-amputee walking," *Scientific reports*, vol. 4, p. 7213, 2014.

[47] K. A. Witte, J. Zhang, R. W. Jackson, and S. H. Collins, "Design of two lightweight, high-bandwidth torque controlled ankle exoskeletons," in *ICRA*, 2015.

[48] M. Kim, T. Chen, T. Chen, and S. H. Collins, "An ankle–foot prosthesis emulator with control of plantarflexion and inversion–eversion torque," *IEEE Transactions on Robotics*, no. 99, pp. 1–12, 2018.

[49] Y. Ding, I. Galiana, A. T. Asbeck, S. M. M. De Rossi, J. Bae, T. R. T. Santos, V. L. de Araújo, S. Lee, K. G. Holt, and C. Walsh, "Biomechanical and physiological evaluation of multi-joint assistance with soft exosuits," *IEEE Transactions on Neural Systems and Rehabilitation Engineering*, vol. 25, no. 2, pp. 119–130, 2017.

[50] P.-C. Kao, C. L. Lewis, and D. P. Ferris, "Invariant ankle moment patterns when walking with and without a robotic ankle exoskeleton," *Journal of biomechanics*, vol. 43, no. 2, pp. 203–209, 2010.

[51] S. H. Collins, M. Kim, T. Chen, and T. Chen, "An ankle-foot prosthesis emulator with control of plantarflexion and inversion-eversion torque," 2015, pp. 1210–1216.

[52] D. P. Ferris, G. S. Sawicki, and A. R. Domingo, "Powered lower limb orthoses for gait rehabilitation," vol. 11, no. 2, pp. 34–49, 2005.

[53] Y. Ding, I. Galiana, A. T. Asbeck, B. Quinlivan, S. M. De Rossi, and C. Walsh, "Multi-joint actuation platform for lower extremity soft exosuits," in *Robotics and automation (ICRA), 2014 IEEE international conference on*. IEEE, 2014, pp. 1327–1334.

[54] J. Lee, K. Seo, B. Lim, J. Jang, K. Kim, and H. Choi, "Effects of assistance timing on metabolic cost, assistance power, and gait parameters for a hip-type exoskeleton," in *Rehabilitation Robotics (ICORR), 2017 International Conference on*. IEEE, 2017, pp. 498–504.

[55] F. A. Panizzolo, I. Galiana, A. T. Asbeck, C. Siviy, K. Schmidt, K. G. Holt, and C. J. Walsh, "A biologically-inspired multi-joint soft exosuit that can reduce the energy cost of loaded walking," *Journal of neuroengineering and rehabilitation*, vol. 13, no. 1, p. 43, 2016.

[56] J. M. Donelan, Q. Li, V. Naing, J. A. Hoffer, D. J. Weber, and A. D. Kuo, "Biomechanical energy harvesting: Generating electricity during walking with minimal user effort," *Science*, vol. 319, no. 5864, pp. 807–810, 2008.

[57] A. Esquenazi, M. Talaty, A. Packel, and M. Saulino, "The rewalk powered exoskeleton to restore ambulatory function to individuals with thoracic-level motor-complete spinal cord injury," *American journal of physical medicine & rehabilitation*, vol. 91, no. 11, pp. 911–921, 2012.

[58] C. Meijneke, W. van Dijk, and H. van der Kooij, "Achilles: An autonomous lightweight ankle exoskeleton to provide push-off power," in *Proceedings of International Conference on Biomedical Robotics and Biomechatronics (BioRob)*, 20014.

[59] W. van Dijk, C. Meijneke, and H. Van Der Kooij, "Evaluation of the achilles ankle exoskeleton," *IEEE transactions on neural systems and rehabilitation engineering*, vol. 25, no. 2, pp. 151–160, 2017.

[60] A. Ruina, J. E. A. Bertram, and M. Srinivasan, "A collision model of the energetic cost of support work qualitatively explains leg sequencing in walking and galloping, pseudo-elastic leg behavior in running and the walk-to-run transition," vol. 237, pp. 170–192, 2005.

[61] J. E. Sanders, B. S. Goldstein, and D. F. Leotta, "Skin response to mechanical stress: adaptation rather than breakdown-a review of the literature," *Journal of rehabilitation research and development*, vol. 32, pp. 214–214, 1995.

[62] M. B. Yandell, B. T. Quinlivan, D. Popov, C. Walsh, and K. E. Zelik, "Physical interface dynamics alter how robotic exosuits augment human movement: implications for optimizing wearable assistive devices," *Journal of neuroengineering and rehabilitation*, vol. 14, no. 1, p. 40, 2017.

[63] K. A. Shorter, A. Wu, and A. D. Kuo, "The high cost of swing leg circumduction during human walking," *Gait & posture*, vol. 54, pp. 265–270, 2017.

[64] S. D. Potter, C. E. Thorne, and M. P. Murphy, "Brace system," May 10 2016, uS Patent 9,333,107.

[65] A. Schiele, P. Letier, R. Van Der Linde, and F. Van Der Helm, "Bowden cable actuator for force-feedback exoskeletons," in *Intelligent Robots and Systems, 2006 IEEE/RSJ International Conference on*. IEEE, 2006, pp. 3599–3604.

[66] D. P. Ferris and C. L. Lewis, "Robotic lower limb exoskeletons using proportional myoelectric control," in *Engineering in Medicine and Biology Society, 2009. EMBC 2009. Annual International Conference of the IEEE*. IEEE, 2009, pp. 2119–2124.

[67] G. Pratt and M. Williamson, "Series elastic actuators," 1995.

[68] J. Zhang and S. H. Collins, "The passive series stiffness that optimizes torque tracking for a lower-limb exoskeleton in human walking," *Frontiers in neurorobotics*, vol. 11, p. 68, 2017.

[69] J. Zhang, C. C. Cheah, and S. Collins, "Torque control in legged locomotion," in *Bio-inspired legged locomotion: models, concepts, control and applications*, M. Sharbafi and A. Seyfarth, Eds. Butterworth-Heinemann, 2017.

[70] T. A. Book and M. D. Sangid, "Strain localization in ti-6al-4v widmanstätten microstructures produced by additive manufacturing," *Materials Characterization*, vol. 122, pp. 104–112, 2016.

[71] S. Oh and K. Kong, "High-precision robust force control of a series elastic actuator," *IEEE/ASME Transactions on Mechatronics*, vol. 22, no. 1, pp. 71–80, 2017.

[72] A. Calanca and P. Fiorini, "A rationale for acceleration feedback in force control of series elastic actuators," *IEEE Transactions on Robotics*, vol. 34, no. 1, pp. 48–61, 2018.

[73] ——, "Understanding environment-adaptive force control of series elastic actuators," *IEEE/ASME Transactions on Mechatronics*, vol. 23, no. 1, pp. 413–423, 2018.

[74] M. F. Eilenberg, J.-Y. Kuan, and H. Herr, "Development and evaluation of a powered artificial gastrocnemius for transtibial amputee gait," *Journal of Robotics*, vol. 2018, 2018.

[75] A. R. Wu, F. Dzeladini, T. J. Brug, F. Tamburella, N. L. Tagliamonte, E. Van Asseldonk, H. Van Der Kooij, and A. J. Ijspeert, "A versatile neuromuscular exoskeleton controller for gait assistance: a preliminary study on spinal cord injury patients," in *Wearable Robotics: Challenges and Trends*. Springer, 2017, pp. 163–167.

[76] G. Aguirre-Ollinger, J. E. Colgate, M. A. Peshkin, and A. Goswami, "Active-impedance control of a lower-limb assistive exoskeleton," in *Rehabilitation Robotics, 2007. ICORR 2007. IEEE 10th International Conference on*. IEEE, 2007, pp. 188–195.

[77] J. F. Veneman, R. Kruidhof, E. E. Hekman, R. Ekkelenkamp, E. H. Van Asseldonk, and H. Van Der Kooij, "Design and evaluation of the lopes exoskeleton robot for interactive gait rehabilitation," *IEEE Transactions on Neural Systems and Rehabilitation Engineering*, vol. 15, no. 3, pp. 379–386, 2007.

[78] A. Q. Keemink, H. van der Kooij, and A. H. Stienen, "Admittance control for physical human–robot interaction," *The International Journal of Robotics Research*, p. 0278364918768950, 2017.

[79] S. H. Collins, "Toward tip top testbeds: Biomechatronics for accelerated development of assistive devices," 2012.

[80] K. E. Gordon, G. S. Sawicki, and D. P. Ferris, "Mechanical performance of artificial pneumatic muscles to power an ankle-foot orthosis," vol. 39, pp. 1832–1841, 2006.

[81] C. Ong, J. Hicks, and S. Delp, "Simulation-based design for wearable robotic systems: An optimization framework for enhancing a standing long jump," pp. 894–903, 2014.

[82] K. W. Hollander, R. Ilg, T. G. Sugar, and D. Herring, "An efficient robotic tendon for gait assistance," *Journal of biomechanical engineering*, vol. 128, no. 5, pp. 788–791, 2006.

[83] D. A. Winter, *The Biomechanics and Motor Control of Human Gait: Normal, Elderly and Pathological*. Waterloo, Canada: Waterloo Biomechanics, 1991.

[84] R. W. Jackson and S. H. Collins, "An experimental comparison of the relative benefits of work and torque assistance in ankle exoskeletons," vol. 119, pp. 541–557, 2015.

[85] S. Galle, P. Malcolm, J. Speeckaert, S. H. Collins, and D. De Clercq, "Reducing the metabolic cost of walking with an ankle exoskeleton: Interaction between actuation timing and power."

[86] Y. Ding, I. Galiana, A. Asbeck, S. De Rossi, J. Bae, T. Santos, V. Araujo, S. Lee, K. Holt, and C. Walsh, "Biomechanical and physiological evaluation of multi-joint assistance with soft exosuits," 2016.

[87] D. P. Ferris, G. S. Sawicki, and M. A. Daley, "A physiologist's perspective on robotic exoskeletons for human locomotion," vol. 4, no. 3, pp. 507–528, 2007.

[88] A. Young and D. Ferris, "State-of-the-art and future directions for robotic lower limb exoskeletons," 2016.

[89] M. B. Yandell and K. E. Zelik, "Transforming how we physically integrate exoskeletons with the human body to augment movement," in *American Society of Biomechanics (ASB),40th annual meeting of the*, 2016.

[90] D. P. Ferris, K. E. Gordon, and G. S. Sawicki, "An improved powered ankle-foot orthosis using proportional myoelectric control," vol. 23, pp. 425–428, 2006.

[91] R. Vertechy, A. Frisoli, A. Dettori, M. Solazzi, and M. Bergamasco, "Development of a new exoskeleton for upper limb rehabilitation," in *Rehabilitation Robotics, 2009. ICORR 2009. IEEE International Conference on*. IEEE, 2009, pp. 188–193.

[92] M. P. Kadaba, H. K. Ramakrishnan, and M. E. Wootten, "Measurement of lower extremity kinematics during level walking," *Journal of Orthopaedic Research*, vol. 8, pp. 383–392, 1990.

[93] T. M. Owings and M. D. Grabiner, "Variability of step kinematics in young and older adults," *Gait and Posture*, vol. 20, pp. 24–29, 2004.

[94] J. Zhang, C. C. Cheah, and S. H. Collins, "Experimental comparison of torque control methods on an ankle exoskeleton during human walking," 2015.

[95] "Telecommunications: Glossary of telecommunication terms," *Federal Standard 1037C*, Aug. 1996.

[96] G. S. Sawicki and D. P. Ferris, "Powered ankle exoskeletons reveal the metabolic cost of plantar flexor mechanical work during walking with longer steps at constant step frequency," *The Journal of Experimental Biology*, vol. 212, pp. 21–31, Jan. 2009.

[97] J. Pratt, B. Krupp, and C. Morse, "Series elastic actuators for high fidelity force control," vol. 29, pp. 234–241, 2002.

[98] A. T. Asbeck, S. M. M. De Rossi, K. G. Holt, and C. J. Walsh, "A biologically inspired soft exosuit for walking assistance," vol. 34, no. 6, pp. 744–762, 2015.

[99] K. E. Gordon, D. P. Ferris, and A. D. Kuo, "Metabolic and mechanical energy costs of reducing vertical center of mass movement during gait," vol. 90, pp. 136–144, 2009.

[100] K. A. Witte, A. M. Fatschel, and S. H. Collins, "Design of a lightweight, tethered, torque-controlled knee exoskeleton," in *ICORR*, 2017.

[101] S. K. Banala, S. H. Kim, S. K. Agrawal, and J. P. Scholz, "Robot assisted gait training with active leg exoskeleton (alex)," *IEEE Transactions on Neural Systems and Rehabilitation Engineering*, vol. 17, no. 1, pp. 2–8, 2009.

[102] A. G. Schache, N. A. Brown, and M. G. Pandy, "Modulation of work and power by the human lower-limb joints with increasing steady-state locomotion speed," *Journal of Experimental Biology*, vol. 218, no. 15, pp. 2472–2481, 2015.

[103] G. S. Sawicki and D. P. Ferris, "Mechanics and energetics of level walking with powered ankle exoskeletons," vol. 211, no. 9, pp. 1402–1413, 2008.

[104] R. W. Jackson and S. H. Collins, "An experimental comparison of the relative benefits of work and torque assistance in ankle exoskeletons," vol. 119, pp. 541–557, 2015.

[105] V. Cai, B. Bru, P. Bidaud, V. Hayward, F. Gosselin, and V. Pasqui, "Experimental evaluation of a goniometer for the identification of anatomical joint motions," in *Proceedings of the Thirteenth International Conference on Climbing and Walking Robots and the Support Technologies for Mobile Machines, CLAWAR*, 2010.

[106] M. P. Kadaba, H. Ramakrishnan, and M. Wootten, "Measurement of lower extremity kinematics during level walking," *Journal of orthopaedic research*, vol. 8, no. 3, pp. 383–392, 1990.

[107] T. F. Novacheck, "The biomechanics of running," *Gait & posture*, vol. 7, no. 1, pp. 77–95, 1998.

[108] M. Whittle, *Gait Analysis: An Introduction*. Oxford, United Kingdom: Butterworth-Heinemann, 1996.

[109] C. Billings, John Scott (Vancouver, "Steady ratio four-bar linkage for genuflective energy harvesting," Patent 20 170 110 937, April, 2017.

[110] S. Potter, C. Thorne, and M. Murphy, "Brace system," Feb. 19 2015, uS Patent App. 13/967,541.

[111] J. E. Pratt, B. T. Krupp, C. J. Morse, and S. H. Collins, "The roboknee: An exoskeleton for enhancing strength and endurance during walking," New Orleans, LA, 2004, pp. 2430–2435.

[112] L. Saccares, I. Sarakoglou, and N. G. Tsagarakis, "it-knee: An exoskeleton with ideal torque transmission interface for ergonomic power augmentation," in *Intelligent Robots and Systems (IROS), 2016 IEEE/RSJ International Conference on*. IEEE, 2016, pp. 780–786.

[113] S. Survey. (2018) Share of people who went jogging or running in the united states in 2018 by age. [Online]. Available: https://www.statista.com/statistics/227423/number-of-joggers-and-runners-usa/

[114] H.-J. F. Zunft, D. Friebe, B. Seppelt, K. Widhalm, A.-M. R. de Winter, M. D. V. de Almeida, J. M. Kearney, and M. Gibney, "Perceived benefits and barriers to physical activity in a nationally representative sample in the european union," *Public health nutrition*, vol. 2, no. 1a, pp. 153–160, 1999.

[115] R. K. Dishman, R. W. Motl, R. Saunders, G. Felton, D. S. Ward, M. Dowda, and R. R. Pate, "Enjoyment mediates effects of a school-based physical-activity intervention." *Medicine and science in sports and exercise*, vol. 37, no. 3, pp. 478–487, 2005.

[116] C. M. Frederick and R. M. Ryan, "Differences in motivation for sport and exercise and their relations with participation and mental health," *Journal of sport behavior*, vol. 16, no. 3, p. 124, 1993.

[117] S. T. Forlenza, N. L. Kerr, B. C. Irwin, and D. L. Feltz, "Is my exercise partner similar enough? partner characteristics as a moderator of the köhler effect in exergames," *GAMES FOR HEALTH: Research, Development, and Clinical Applications*, vol. 1, no. 6, pp. 436–441, 2012.

[118] L. M. Wankel, "Decision-making and social-support strategies for increasing exercise involvement," *Journal of Cardiac Rehabilitation*, vol. 4, no. 4, pp. 124–135, 1984.

[119] J. Kim, R. Heimgartner, G. Lee, N. Karavas, D. Perry, D. L. Ryan, A. Eckert-Erdheim, P. Murphy, D. K. Choe, I. Galiana *et al.*, "Autonomous and portable soft exosuit for hip extension assistance with online walking and running detection algorithm," in *2018 IEEE International Conference on Robotics and Automation (ICRA)*. IEEE, 2018, pp. 1–8.

[120] L. M. Mooney and H. M. Herr, "Biomechanical walking mechanisms underlying the metabolic reduction caused by an autonomous exoskeleton," *Journal of neuroengineering and rehabilitation*, vol. 13, no. 1, p. 4, 2016.

[121] S. Sovero, N. Talele, C. Smith, N. Cox, T. Swift, and K. Byl, "Initial data and theory for a high specific-power ankle exoskeleton device," in *International Symposium on Experimental Robotics*. Springer, 2016, pp. 355–364.

[122] W. Hoogkamer, S. Kipp, B. A. Spiering, and R. Kram, "Altered running economy directly translates to altered distance-running performance," *Med Sci Sports Exerc*, vol. 48, no. 11, pp. 2175–80, 2016.

[123] C. T. Farley and O. Gonzalez, "Leg stiffness and stride frequency in human running," *Journal of biomechanics*, vol. 29, no. 2, pp. 181–186, 1996.

[124] A. Seyfarth, H. Geyer, M. Günther, and R. Blickhan, "A movement criterion for running," *Journal of biomechanics*, vol. 35, no. 5, pp. 649–655, 2002.

[125] F. Iida, J. Rummel, and A. Seyfarth, "Bipedal walking and running with spring-like biarticular muscles," *Journal of biomechanics*, vol. 41, no. 3, pp. 656–667, 2008.

[126] C. T. Farley and D. C. Morgenroth, "Leg stiffness primarily depends on ankle stiffness during human hopping," *Journal of biomechanics*, vol. 32, no. 3, pp. 267–273, 1999.

[127] G. Elliott, G. S. Sawicki, A. Marecki, and H. Herr, "The biomechanics and energetics of human running using an elastic knee exoskeleton," in *Rehabilitation Robotics (ICORR), 2013 IEEE International Conference on*. IEEE, 2013, pp. 1–6.

[128] M. S. Cherry, S. Kota, A. Young, and D. P. Ferris, "Running with an elastic lower limb exoskeleton," *Journal of applied biomechanics*, vol. 32, no. 3, pp. 269–277, 2016.

[129] M. L. Handford and M. Srinivasan, "Energy-optimal human walking with feedback-controlled robotic prostheses: A computational study," *IEEE Transactions on Neural Systems and Rehabilitation Engineering*, vol. 26, no. 9, pp. 1773–1782, 2018.

[130] J. C. Selinger, S. M. OâĂŹConnor, J. D. Wong, and J. M. Donelan, "Humans can continuously optimize energetic cost during walking," *Current Biology*, vol. 25, no. 18, pp. 2452–2456, 2015.

[131] Y. Ding, M. Kim, S. Kuindersma, and C. J. Walsh, "Human-in-the-loop optimization of hip assistance with a soft exosuit during walking," *Science Robotics*, vol. 3, no. 15, p. eaar5438, 2018.

[132]

[133] J. C. Selinger and J. M. Donelan, "Estimating instantaneous energetic cost during non-steady-state gait," *Journal of Applied Physiology*, vol. 117, no. 11, pp. 1406–1415, 2014.

[134] J. Brockway, "Derivation of formulae used to calculate energy expenditure in man." *Human nutrition. Clinical nutrition*, vol. 41, no. 6, pp. 463–471, 1987.

[135] M. S. Orendurff, T. Kobayashi, K. Tulchin-Francis, A. M. H. Tullock, C. Villarosa, C. Chan, and S. Strike, "A little bit faster: Lower extremity joint kinematics and kinetics as recreational runners achieve faster speeds," *Journal of biomechanics*, vol. 71, pp. 167–175, 2018.

[136] R. E. Quesada, J. M. Caputo, and S. H. Collins, "Increasing ankle push-off work with a powered prosthesis does not necessarily reduce metabolic rate for transtibial amputees," *Journal of Biomechanics*, vol. 49, no. 14, pp. 3452–3459, 2016.

[137] E. M. Arnold, S. R. Hamner, A. Seth, M. Millard, and S. L. Delp, "How muscle fiber lengths and velocities affect muscle force generation as humans walk and run at different speeds," *Journal of Experimental Biology*, pp. jeb–075 697, 2013.

[138] T. K. Uchida, A. Seth, S. Pouya, C. L. Dembia, J. L. Hicks, and S. L. Delp, "Simulating ideal assistive devices to reduce the metabolic cost of running," *PloS one*, vol. 11, no. 9, p. e0163417, 2016.

[139] M. L. Handford and M. Srinivasan, "Robotic lower limb prosthesis design through simultaneous computer optimizations of human and prosthesis costs," *Scientific reports*, vol. 6, p. 19983, 2016.

[140] J. M. Winters, "Hill-based muscle models: a systems engineering perspective," in *Multiple muscle systems*. Springer, 1990, pp. 69–93.

[141] J. Markowitz, P. Krishnaswamy, M. F. Eilenberg, K. Endo, C. Barnhart, and H. Herr, "Speed adaptation in a powered transtibial prosthesis controlled with a neuromuscular model," *Philosophical Transactions of the Royal Society of London B: Biological Sciences*, vol. 366, no. 1570, pp. 1621–1631, 2011.

[142] N. Thatte and H. Geyer, "Toward balance recovery with leg prostheses using neuromuscular model control," *IEEE Transactions on Biomedical Engineering*, vol. 63, no. 5, pp. 904–913, 2016.

[143] H. Geyer and H. Herr, "A muscle-reflex model that encodes principles of legged mechanics produces human walking dynamics and muscle activities," *IEEE Transactions on neural systems and rehabilitation engineering*, vol. 18, no. 3, pp. 263–273, 2010.

[144] A. R. Wu, F. Dzeladini, T. J. Brug, F. Tamburella, N. L. Tagliamonte, E. H. Van Asseldonk, H. Van Der Kooij, and A. J. Ijspeert, "An adaptive neuromuscular controller for assistive lower-limb exoskeletons: A preliminary study on subjects with spinal cord injury," *Frontiers in neurorobotics*, vol. 11, p. 30, 2017.

[145] G. Sawicki, "Personal communication," october, 2018. Interanational Conference on Intelligent Robots and Systems.

[146] S. Srinivasan, M. Carty, P. Calvaresi, T. Clites, B. Maimon, C. Taylor, A. Zorzos, and H. Herr, "On prosthetic control: A regenerative agonist-antagonist myoneural interface," *Science Robotics*, vol. 2, no. 6, p. eaan2971, 2017.

[147] H. Herr. (2018) How we will become cyborgs and expand human potential. [Online]. Available: https://www.ted.com/talks/hugh_herr_how_we_ll_become_cyborgs_and_extend_human_potential?language=en#t-879903

[148] K. E. Zelik, S. H. Collins, P. G. Adamczyk, A. D. Segal, G. K. Klute, D. C. Morgenroth, M. E. Hahn, M. S. Orendurff, J. M. Czerniecki, and A. D. Kuo, "Systematic variation of prosthetic foot spring affects center-of-mass mechanics and metabolic cost during walking," *IEEE transactions on neural systems and rehabilitation engineering: a publication of the IEEE Engineering in Medicine and Biology Society*, vol. 19, no. 4, p. 411, 2011.

[149] M. Kim, Y. Ding, P. Malcolm, J. Speeckaert, C. J. Siviy, C. J. Walsh, and S. Kuindersma, "Human-in-the-loop bayesian optimization of wearable device parameters," *PloS one*, vol. 12, no. 9, p. e0184054, 2017.

[150] R. W. Jackson, C. L. Dembia, S. L. Delp, and S. H. Collins, "Muscle-tendon mechanics explain unexpected effects of exoskeleton assistance on metabolic rate during walking," *Journal of Experimental Biology*, pp. jeb–150 011, 2017.

[151] T. K. Uchida, J. L. Hicks, C. L. Dembia, and S. L. Delp, "Stretching your energetic budget: how tendon compliance affects the metabolic cost of running," *PloS one*, vol. 11, no. 3, p. e0150378, 2016.

[152] P. Malcolm, S. Galle, P. Van den Berghe, and D. De Clercq, "Exoskeleton assistance symmetry matters: unilateral assistance reduces metabolic cost, but relatively less than bilateral assistance," *Journal of neuroengineering and rehabilitation*, vol. 15, no. 1, p. 74, 2018.